ČESKÉ VYSOKÉ UČENÍ TECHNICKÉ V PRAZE

FAKULTA JADERNÁ A FYZIKÁLNĚ INŽENÝRSKÁ
KATEDRA FYZIKY

DIPLOMOVÁ PRÁCE

Alternativní metody přípravy permeačních bariér

Autor:	Bc. Jakub Veverka
Vedoucí práce:	Ing. Jiří Matějíček PhD.

Praha, 2017

CZECH TECHNICAL UNIVERSITY IN PRAGUE

Faculty of Nuclear Sciences and Physical Engineering
Department of Physics

DIPLOMA THESIS

Alternative Methods of Permeation Barrier Preparation

Author: Bc. Jakub Veverka
Supervisor: Ing. Jiří Matějíček PhD.
Prague, 2017

Název práce: **Alternativní metody přípravy permeačních bariér**

Autor: Bc. Jakub Veverka
Obor: Fyzika a technika termojaderné fúze
Druh práce: Diplomová práce
Vedoucí práce: Ing. Jiří Matějíček, PhD., Ústav fyziky plazmatu AV ČR v Praze

Abstrakt: Permeační bariéry jsou jednou z nejdůležitějších částí materiálového výzkumu v oblasti řízené termojaderné fúze. Jejich primárním účelem je minimalizovat unikání (permeaci) izotopů vodíku (který jinak proniká strukturními materiály velmi snadno) z budoucích fúzních zařízení, sekundárním pak snížení množství těchto izotopů, trvale zachycených v materiálu (snížení retence). Uvažované provozní podmínky kladou vysoké nároky jak na samotný materiál, tak na vlastnosti vyrobených vrstev. Základní hledisko je snížení permeace tritia. Dalšími kritickými požadavky na permeační bariéry jsou absence povrchových defektů (zejména prasklin), stabilita při vysokých teplotách a v korozním prostředí, a kompatibilita se strukturními materiály (zejména feriticko-martensitické oceli). V práci byly provedeny experimenty s přetavováním plasmového nástřiku Al_2O_3 za účelem dosáhnutí požadovaných vlastností. Dále byly připraveny PVD povlaky nitridů, identifikovaných jako perspektivní pro permeační bariéry (CrN, ZrN...), jejich charakterizace (tloušťka, homogenita, adheze...) a bylo provedeno měření snížení permeace.

Klíčová slova: permeační bariéry, přetavování elektronovým svazkem, Al_2O_3, nitridy, měření permeace

Title: **Alternative methods of permeation barrier preparation**

Author: Bc. Jakub Veverka

Abstract: Permeation barriers represent one of the crucial fields in material development for thermonuclear fusion. Primary objective of the barriers is to suppress the permeation of hydrogen isotopes (mainly tritium) from future thermonuclear fusion facilities. Secondary objective is to reduce their retention in structural materials. Expected reactor conditions put high demands on the material, as well as on the final barrier quality. Key properties are tritium permeation reduction, defect-free barrier surface (especially cracks), high-temperature and corrosive stability and compatibility with structural materials (mostly ferritic-martensitic steels). In this thesis, remelting experiments with plasma sprayed Al_2O_3 were performed, in order to reach the desired characteristics. In addition, thin nitride layers, identified as promising as permeation barriers (CrN, ZrN...), were deposited by PVD and characterized (layer thickness, homogeneity, adhesion...). Ultimately, measurements of permeation reduction were performed.

Key words: permeation barriers, electron beam remelting, Al_2O_3, nitride layers, permeation measurement

Acknowledgements

I would like to thank Ing. Jiří Matějíček, Ph.D., for supervision of my thesis, for helping with samples preparation for experimental part and evaluating of the results, for language correction, numerous advices and extra questions. I would also like to thank Ing. Jan Čížek, Ph.D. and Bc. Jan Kouřil for valuable help during experiments on NETME facility and evaluating the remelting results.

And I would also like to thank Ing. Ladislav Cvrček, Ph.D., for help with nitride samples deposition and assistance during post-investigation of the samples at ICDAM. Last, but not least, I would like to thank Dr. Vincenc Nemanič for the permeation measurements.

Contents

List of Figures

List of Tables

1 INTRODUCTION

Satisfying of the energy demands of the mankind has always been important issue, influencing the quality of life and the evolution of the society. Since the Industrial revolution, the energy consumption increased furiously and facing the inevitable exhaustion of fossil fuels, importance of alternative energy sources has been rising. Replacement of the fossil fuels with renewable energy while maintaining current consumption already proved to be impossible, therefore entirely new means of energy production are needed. Harnessing of the thermonuclear fusion is expected to be the solution. Significant ambitions are put mostly on magnetically confined fusion, whereas inertial fusion is foreseen for different applications than energy production.

Indeed, since the discovery of nuclear fusion, scientists all over the world considered it appealing - inexhaustible source of clean energy, without major operational hazards. Success of early experiments from 1950s and 1960s supported this idea and scientists were eager to harness the new power. However, difficulties based on the physical background emerged soon and major breakthroughs were (and are) expected from international collaborations capable of constructing facilities with the necessary parameters - for enabling the hydrogen fusion, extreme temperatures of several hundred million Kelvin need to be reached. For sufficient confinement of the plasma and energy, magnetic fields up to 10 T are required. For maximizing the reaction probability and gain, the greatest possible plasma volume is advised. Thermonuclear fusion and fusion facilities are described in more detail in section 2. Enormous complexity and demands (technological, as well as economical) on large fusion facilities are the main issues for not yet harnessing fusion as for example fission. Crucial components of the facilities have to withstand enormous mechanical and heat loads and neutron fluxes which have never been experienced in any facility so far.

International efforts resulted in the construction of Joint European Torus (JET) and, more importantly, International Thermonuclear Experimental Reactor (ITER), described in section 3. Until the construction of ITER is finished, JET is the largest tokamak built, the first tokamak having conducted tritium experiments and reaching $Q = 0.65$, which is the record value (65% of power delivered to the plasma was replenished by thermonuclear fusion). The main objective of ITER is to demonstrate the feasibility of energy production by thermonuclear fusion, reliability of all components including in-situ production of tritium (tritium is a radioactive isotope and therefore is not present in nature) and to broaden our knowledge concerning fusion. Next step will be the construction of demonstrational powerplant DEMO - facility oriented primarily on electricity production, not science programme. Feasibility of the reaction refers not only to tritium production but also to maintaining sufficient fuel density in the reactor for sufficient time at sufficient temperature. This is the essential condition for sustaining the reaction, expressed by the famous Lawson criterion (also mentioned in section 2). However, most structural materials are highly permeable for hydrogen isotopes, which would result in fuel loss, termination of the reaction and in case of tritium also in the contamination of the facility. Therefore, special materials are involved in suppression of these phenomena, referred to as "permeation barriers". These components of fusion facilities are also exposed to high neutron fluxes, temperatures reaching up to 600 °C and the surrounding environment may be highly corrosive. Therefore, the material selection or development is a key task, as the replacement would be demanding and self-healing possibility is limited.

Issues concerning hydrogen transport and permeation barriers are discussed in section 4. This topic is also covered in the experimental part of the thesis, section 5. First part consists of experiments on electron beam remelting of plasma sprayed oxidic ceramic coatings. Properties of these coatings were recently identified as promising for their use as a permeation barriers and even though the deposition by plasma spraying is advantageous in many ways, the resulting coating is very porous. Therefore, post-treatment providing smooth and non-porous coating is needed, for example the remelting. The latter part deals with permeation measurements of thin ceramic layers deposited on structural material intended for the ITER construction. Not only oxidic ceramics but also other compounds, namely nitrides and carbides, were researched for the use as a permeation barriers. An attempt was made to identify perspective, less known materials, to deposit and to characterize the coatings. Finally, permeation measurements of the chosen coatings were performed.

2 THERMONUCLEAR FUSION

Thermonuclear fusion is a promising mean of energy production that is predicted to satisfy growing energy demand of the mankind. The process involves fusing several nuclei of lighter elements to produce heavier nucleus. This process is unfortunately naturally opposed by coulombic interaction – all nuclei are charged positive, ergo they repel each other. In order to fuse, the nuclei have to overcome this "coulombic barrier" and get to a distance close enough for the strong nuclear force to prevail. The heavier nucleus formed during the reaction has lower binding energy than the sum of the binding energies of initial reactants, which enables energy gain from the reaction. However, because the distances are of the order of femtometer (10^{-15} m), the matter needs to be heated to temperatures of several million degrees Kelvin. At these temperatures, so called fourth state of matter is reached – the plasma and particles from fast ends of Maxwell-Boltzmann distribution achieve sufficient energy to the overcome Coulombic forces. Due to quantum tunnelling effects, the process is feasible at lower temperatures too, but the reaction rates would be lower. Originally, thermonuclear fusion was discovered as the mechanism of energy production in stars. First theory from Arthur Eddington (1920, [104]) proposed fusion of hydrogen to helium as the basic reaction to generate energy of the stars. Hans Bethe (1939, [16]) later defined two reaction cycles for stars of different mass – proton-proton chain for Sun-like stars and CNO cycle for heavier stars. Since this discovery, substantial effort was put into facilitating fusion for energy production on Earth. However, the above mentioned reactions are not suitable for early attempts on reaching nuclear fusion. The stars retain enormous mass, which is strongly confined by gravitational force. This kind of confinement is not feasible in terrestrial conditions. Moreover, the cross sections of these reactions are so small, that the size of the reactor would have to be technically unreachable. Other reactions needed to be explored, especially those with best achievable conditions. Research of controlled thermonuclear fusion started in 1950s. Several concepts emerged simultaneously, differing in the means of plasma confinement.

- Magnetic confinement
    - Toroidal facilities
    - Tokamaks
    - Stellarators
    - Fusors
- Linear facilities
    - Linear Z-pinch

    - Reversed field pinch
- Inertial confinement
    - Ignitors

2.1 Lawson criterion

Conditions required for reaching fusion were mathematically derived by John D. Lawson in 1955. His famous criterion introduced the triple product – most useful figure of merit for fusion devices, combining density of matter, temperature and "energy confinement time". Energy confinement time is defined with equation characterising the energy losses of the system. W – energy density of the system, P_{loss} – rate of energy losses, both quantities are scaled per unit volume. For steady-state fusion operation, the plasma has to be maintained at constant temperature, so the losses from the system have to be replenished – either directly from reaction products or by external heat sources. Based on particular reaction, the triple product yields absolute lower limit for ignition, i.e., for fusion heating to overcome losses. From a broad range of existing fusion reactions, the reactions of hydrogen isotopes were identified as the most promising based on the lowest value of the Coulombic barrier. Among these, D-T reaction was identified as the most promising because of the lowest minimum value of the triple product. The minimum occurs at T=14 keV, i.e., approx. 160 million Kelvin, and reaches $3 * 10^{21}\mathrm{keV} * \mathrm{s/m}^3$.

2.2 Fusion facilities

Originally, the research was conducted on linear facilities, but briefly, tokamaks and stellarators became the most common fusion facilities, because of higher potential to fulfil the Lawson criterion. The Eastern Bloc – mainly the Soviet Union, built tokamaks, while Western Europe and mainly the USA focused on stellarators. In 1965, major breakthrough was announced on T-3 tokamak: reaching of the temperature of 10 million Kelvin. After confirmation of the results by British experts' measurements, a majority of current and future fusion facilities was built as tokamaks. Both of these concepts use magnetic confinement of the plasma, but feature significant differences. Tokamak is basically characterized by strong toroidal magnetic field and electrical current induced in the plasma. Schematical view of tokamak is displayed in Figure 1.

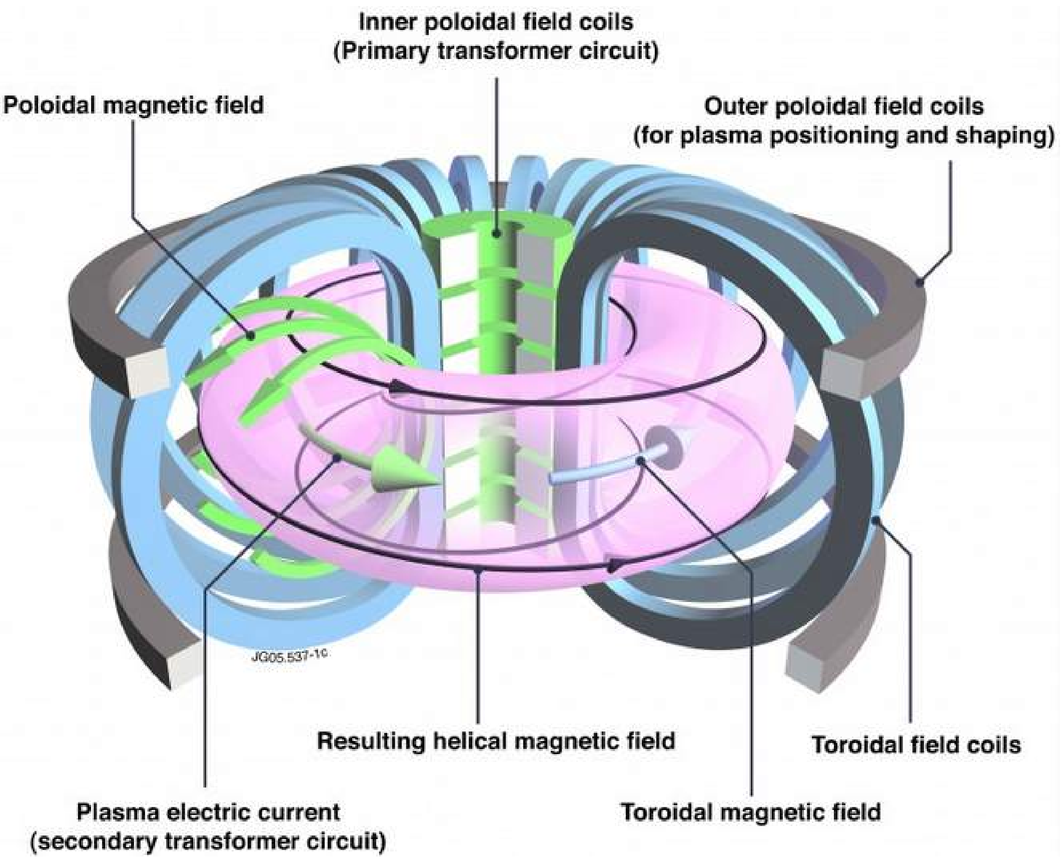

Figure 1: Schematical view of a tokamak [3]

The current generates another magnetic field, perpendicular to the toroidal field and superposition of these fields constitutes the resulting helical field. Initial heating of the plasma is also provided by this current, but with increasing plasma temperature, the efficiency of the heating decreases. Other means of heating, such as injection of neutral particles or microwaves need to be used. For additional stability and plasma shaping or positioning, other poloidal coils are installed. Stellarators, on the other hand, do not have electrical current induced in the plasma. The confining magnetic field is generated by a set of complex-shaped toroidal coils, surrounding the plasma. This feature increases difficulty of stellarator manufacturing, but as a result, stellarators do not suffer from current-1induced instabilities. Schematical view of a stellarator is displayed in Figure 2.

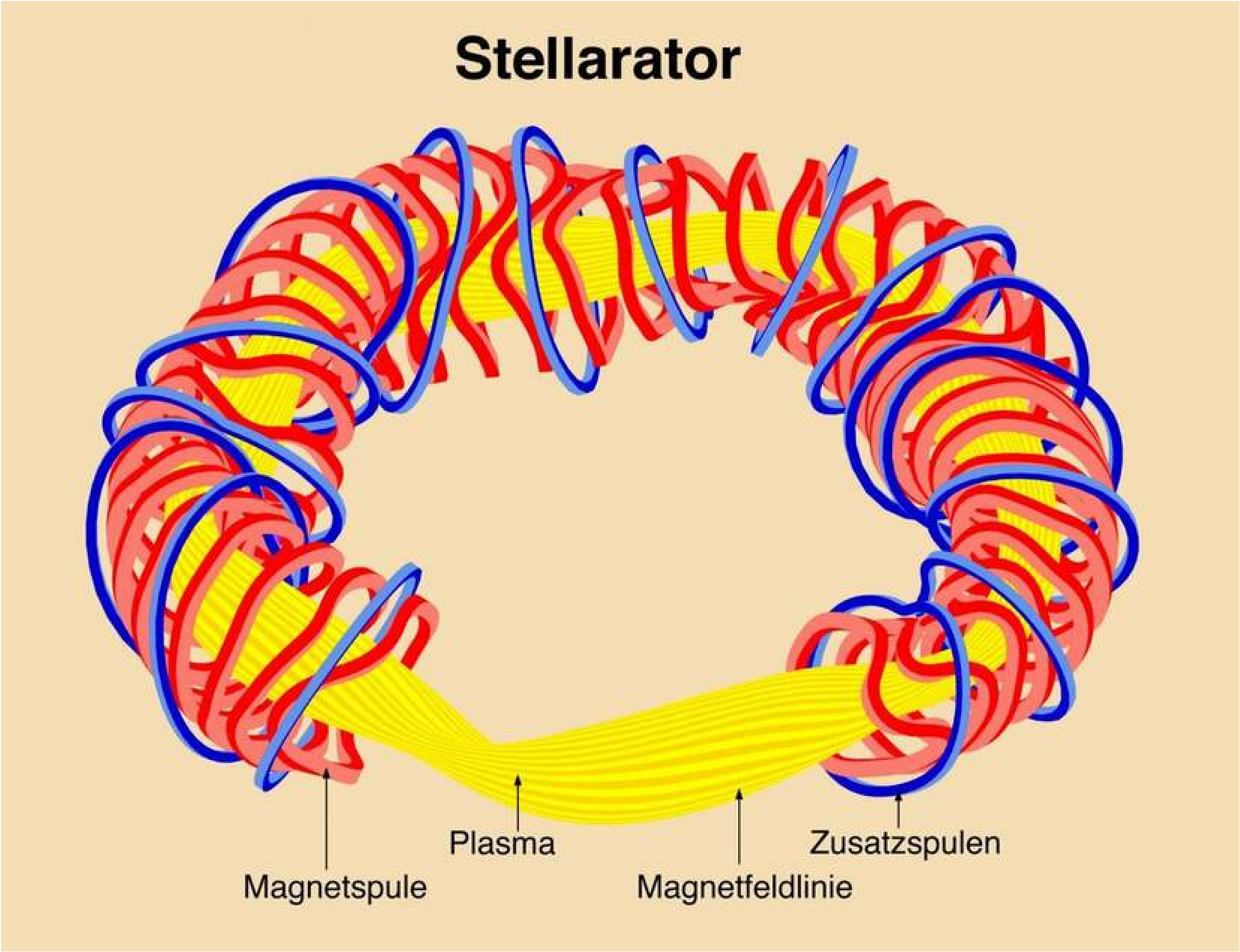

Figure 2: Schematical view of stellarator, Magnetspule - magnet coils, Magnetfeldlinie - magnetic field lines, zusatzspulen - auxilliary coils [2]

The minimum required value of Lawson criterion has not been reached yet by any fusion facility, but the latest generation machines have come close – JT-60, Japanese tokamak with comparable parameters with JET (Joint European Torus, world´s largest tokamak in Culham, Great Britain) and TFTR, tokamak of Princeton plasma physics laboratory, dismantled in 1997. Major breakthrough is expected from ITER, international experimental thermonuclear reactor, which is now under construction in Cadarache, France, and possibly Wendelstein 7-X, world´s largest stellarator recently put into operation in Greifswald, Germany. After proving the ability of energy gain from fusion, next step is construction of the demonstrational power plant - DEMO - facility focused not mainly on the science understanding of the fusion, but on delivering the fusion power into grid. This is foreseen for year 2060 and it is predicted that multiple DEMO facilities will be constructed around the world.

3 ITER

ITER (International Thermonuclear Experimental Reactor, or from Latin “the Way”) is a research facility currently under construction in southern France, in Cadarache. ITER is a tokamak-type machine with nominal inductive operation of 400 s, repetition period of 1800 s and production of 500 MW of power, with injection of 50 MW of auxiliary power. Main machine and plasma parametres are shown in Figure 3.

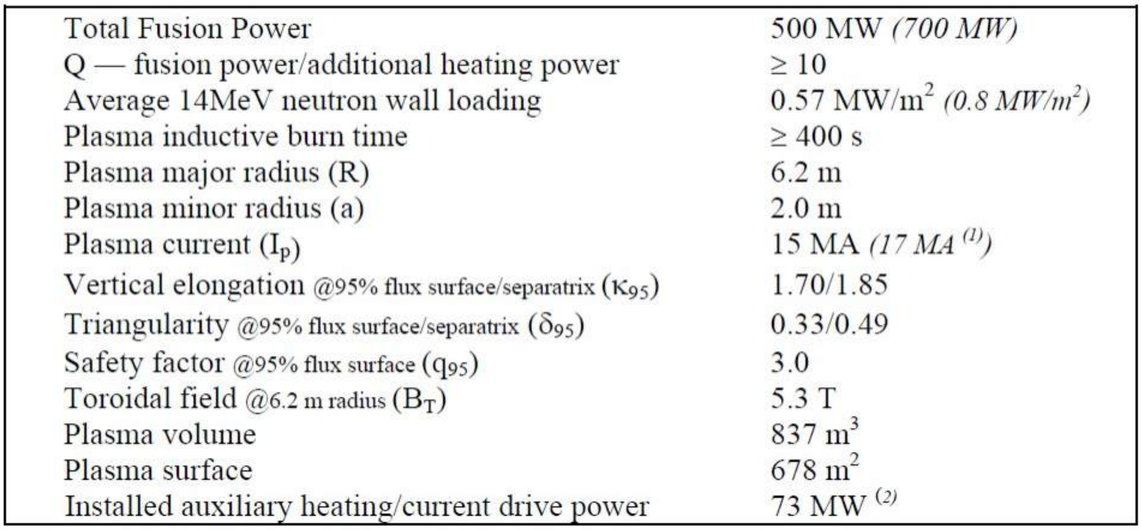

Total Fusion Power	500 MW *(700 MW)*
Q — fusion power/additional heating power	≥ 10
Average 14MeV neutron wall loading	0.57 MW/m^2 *(0.8 MW/m^2)*
Plasma inductive burn time	≥ 400 s
Plasma major radius (R)	6.2 m
Plasma minor radius (a)	2.0 m
Plasma current (I_p)	15 MA *(17 MA* $^{(1)}$*)*
Vertical elongation @95% flux surface/separatrix (κ_{95})	1.70/1.85
Triangularity @95% flux surface/separatrix (δ_{95})	0.33/0.49
Safety factor @95% flux surface (q_{95})	3.0
Toroidal field @6.2 m radius (B_T)	5.3 T
Plasma volume	837 m^3
Plasma surface	678 m^2
Installed auxiliary heating/current drive power	73 MW $^{(2)}$

Figure 3: Parameters and dimensions of ITER facility, (1) - limit values of plasma current (then, the values in parenthesis apply) achievable within some limitations of other parameters, e.g., pulse length etc., (2) - in subsequent operational phases, plasma heating may be upgraded to 110 MW [87]

The programmatic objective of ITER is ”to demonstrate the scientific and technological feasibility of fusion energy for peaceful purposes” [86]. Main technical objectives of ITER have been interpreted as follows:

- demonstration of reliability of nuclear components - superconducting magnets, remote maintenance, exhaust system
- demonstration of tritium breeding - test breeding modules, leading to future tritium self-sufficiency, high grade heat extraction and electricity production
- achieving 14 MeV-neutron power load on first wall $\geq 0,5\mathrm{MW/m^2}$ and neutron fluence $\geq 0,3\mathrm{MWa/m^2}$
- achieving well controlled divertor plasma configuration

- achieving extended burn in inductively driven plasmas with Q $\geq$ 10 (ratio of fusion power to auxiliary heating) for a range of operating scenarios and with a duration sufficient to achieve stationary conditions
- aim at demonstration of steady-state operation using non-inductive current drive reaching Q $\geq$ 5
- providing fusion material testing data relevant for a future fusion reactor

The possibility of controlled ignition is not precluded. The major components of the tokamak are superconducting toroidal and poloidal field coils, central solenoid, correction coils and the vacuum vessel. Double-wall vacuum vessel is divided into 9 sectors. Inside the vacuum vessel, internal replaceable components, such as blanket modules, divertor cassettes and port plugs, are installed. Vacuum vessel has multiple functions, namely:

- provides a boundary consistent with generation and maintenance of a high quality vacuum
- support the in-vessel components
- participates in neutron shielding
- provides a continuous conductive shell for plasma MHD stabilisation with toroidal one turn resistance of $\sim 8\,\mu\Omega$
- provides the first confinement barrier for tritium and activated dust with a very high reliability

All these functions are crucial for successful ITER operation and therefore require very robust mechanical design, analysed namely for stresses in all normal and off-normal conditions. The vessel is built with two shells linked by ribs, fitted with neutron shielding and ferromagnetic inserts to mitigate toroidal field ripple. Two independent coolant loops are used to a) remove heat loads from plasma and decay heat from in-vessel components and b) to bake out the vessel (removing impurities). Blanket modules serve as primary heat and radiation protection for vacuum vessel and magnet coils. The design does not preclude later replacement of blanket modules by test blanket modules (TBM). Blanket modules and later TBM are cooled by tokamak cooling water system. Schematical structure of blanket module, including first wall panels, is displayed in Figure 4.

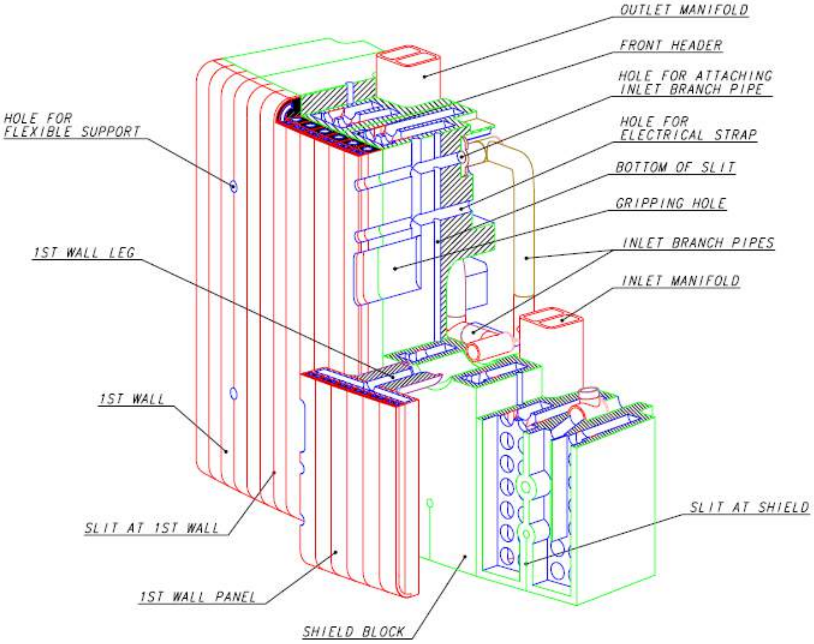

Figure 4: ITER blanket module and first wall [87]

Test blanket modules are mock-ups of future breeding blanket (BB) components. The breeding blanket modules are supposed to sustain the fusion reaction with tritium, produced by fission of lithium. They are equipped with internal structure for placement of the breeding material, cooling channels and permeation/radiation protection, if needed. Different designs of the breeding blanket modules are investigated by the ITER domestic agencies. Basic aspect is the lithium-containing-compound, its state and cooling medium - eutectic solution of Pb containing ca. 17% Li (Pb-Li) or ceramic materials (Li_4SiO_4 or Li_2TiO_3) in form of pebbles are considered. As a cooling medium, helium and water under high pressure are considered. Pb-Li can act as a secondary cooling medium, but its cooling properties are not sufficient. Extensive overview of TBM/BB modules can be found in [96]. Essential questions which are expected to be solved after tritium campaign on ITER are: "Can tritium be produced in the blanket and extracted from the blanket at a rate equal to tritium consumption in the plasma plus losses by radioactive decay from tritium inventories in reactor components?" and "Can heat be extracted from the blanket, simultaneously with tritium breeding, at temperatures high enough for efficient electricity generation?". Overall testing objectives are following:

- validation of the theoretical predictions of the breeding blankets structural integrity under relevant combined thermal, mechanical and electromagnetic loads

- validation of tritium breeding predictions
- validation of tritium recovery process efficiency and tritium inventories in the different blanket materials
- validation of thermal predictions for strongly heterogeneous breeding blanket concepts with volumetric heat sources and magnetic fields
- demonstration of the integral performance of the BB systems

Regarding vital information about long-term radiation effects and failure modes, these are obtained in parallel in other facilities. [96] Materials selected for vacuum vessel are various stainless steels: SS 316LN for main structure, SS 304 with 2% boron addition for internal shield plates and SS 430 for ferromagnetic inserts to reduce toroidal field ripple. Blanket modules are divided into two parts: front part - first wall - consisting of diverse materials - beryllium armor, copper heat sink and steel structure, and back part, made solely from steel and water, serving as shielding. The modules are firmly attached to the vessel in radial way, but toroidal and poloidal movement is allowed. This flexibility is required due to periodic thermal expansion and compression of the modules during the plasma pulses (steady state operation including instabilities) and break periods. Groups of two or three blanket modules are cooled with separate water pipes. In the lower part of vacuum vessel, the divertor is installed. Divertor consists of 54 cassettes and its main function is to exhaust helium ash and impurities from vacuum vessel. Main parts of divertor cassette are showed in Figure 5. The most exposed part of the divertor will be the baffles, where the magnetic induction lines will penetrate into the material, thus providing the most intense particle flow.

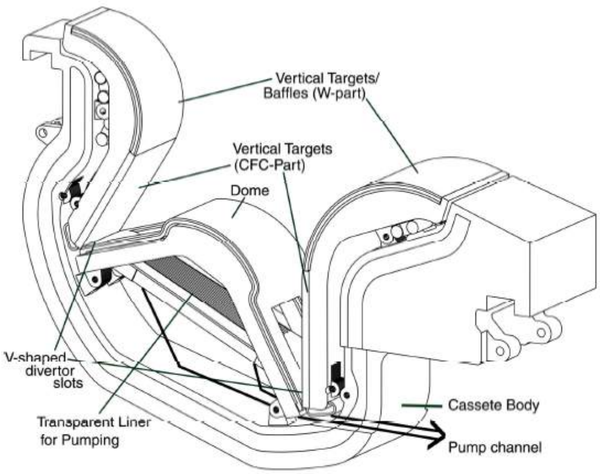

Figure 5: ITER divertor cassette [87]

Each cassette is provided with separate water cooling pipe, because of high heat loads from plasma particles, especially associated with ELMs and disruptions. Input temperature of cooling water is maintained below 100 °C, whereas output temperature would be around 150 °C at nominal fusion power. During standby, the coolant flow is reduced, and during the maintenance, water coolant is used to heat and bake the in-vessel components at 240 °C. Magnetic field responsible for plasma confinement is generated from three main sources: toroidal and poloidal field coils and plasma current. Toroidal field value on the axis is designed to be 5,3 T, leading to maximum field of 12 T on the conductor. Because of such high magnetic fields and future steady-state operation, all ITER coils are superconducting. Selected material is Nb_3Sn for toroidal field coils and central solenoid, whereas NbTi is used for poloidal field coils - maximum field value is lower than 6 T. All magnets are cooled by a flow of supercritical helium at 4,5 K and ca. 0,6 MPa. Total magnetic energy stored in toroidal field is about 40 GJ, which leads to significant forces on each coil. The coils are therefore connected together with bolted structures, to mitigate these forces. Toroidal field coils windings are enclosed in strong cases used also to support the poloidal field coils, the vacuum vessel and all core machine components. Plasma current is generated by 6 segments of central solenoid, capable of magnetic flux change of 277 Vs (magnetic field change from +13,5 T to -12 T). In total, 6 poloidal field coils are located outside the toroidal field coils and are responsible for plasma shaping and position control. The entire tokamak is enclosed in a cryostat and a biological shield of borated concrete. The concrete walls should limit the radiaton levels to values insignificant for the activation of components and provide appropriate shielding against emission from activated components during their transports to the hot cell.

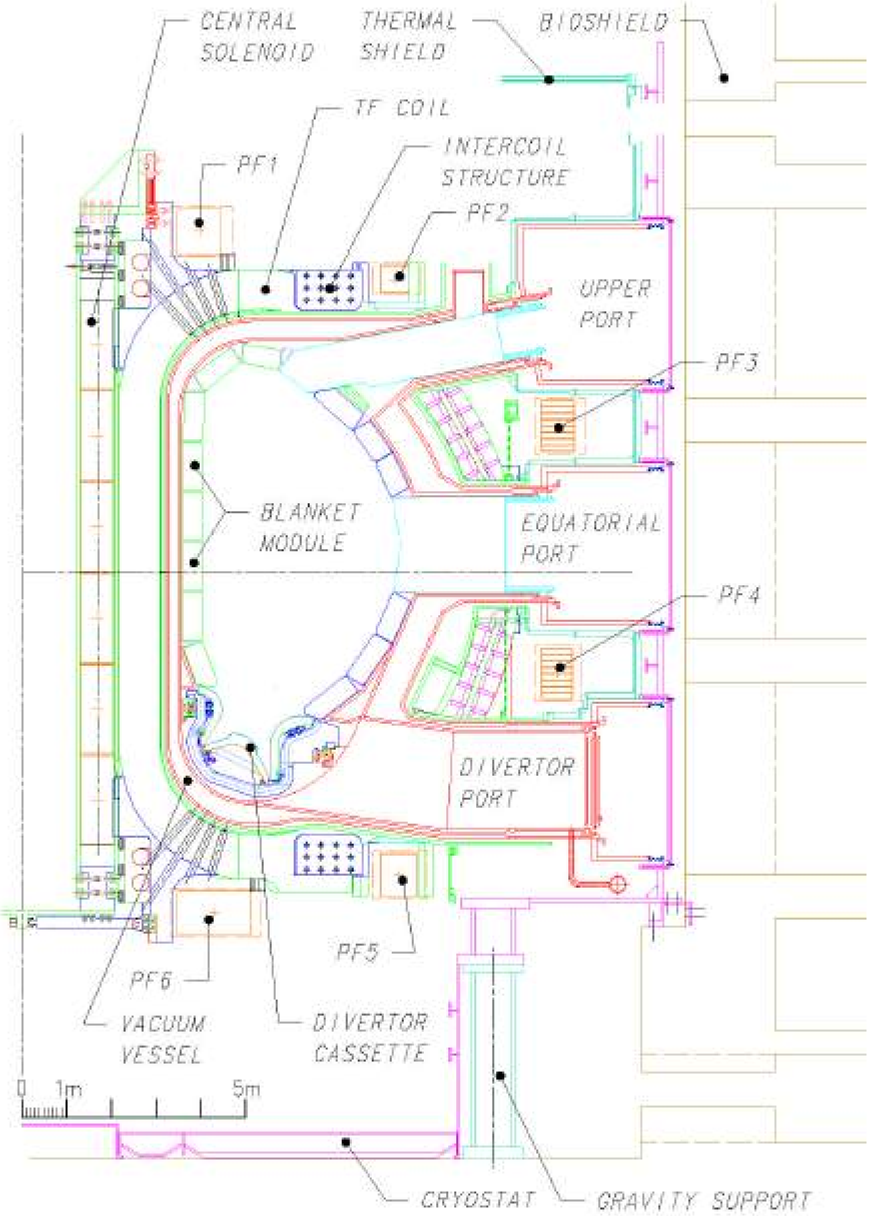

Figure 6: ITER tokamak cross section [87]

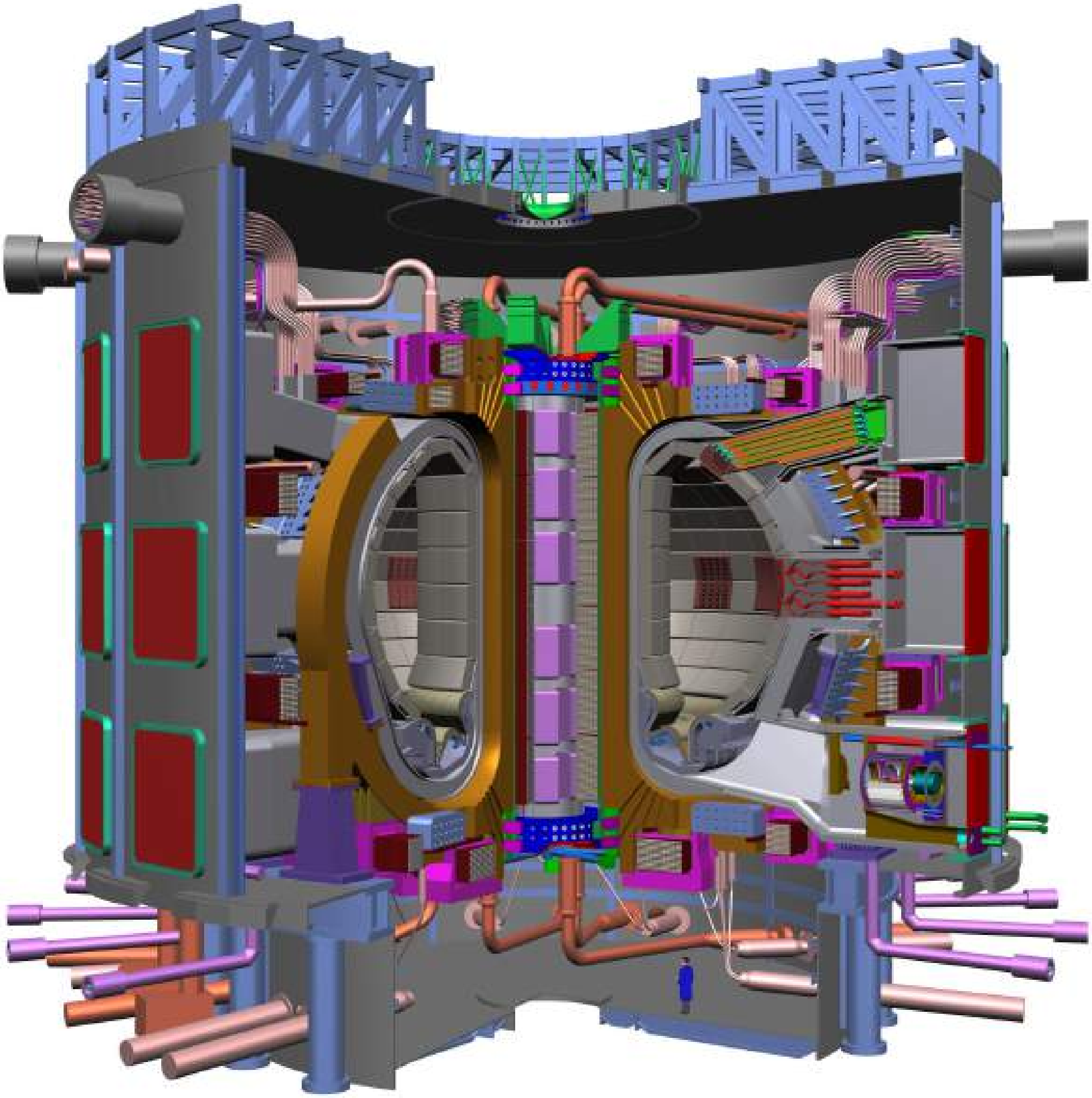

Figure 7: ITER tokamak cutaway [87]

The development and construction is carried out by ITER Organisation, which involves: The European Union, the United States of America, the Russian Federation, the Republic of India, People´s Republic of China, Japan and the Republic of Korea. Such broad international collaboration and large budget (EUR 5 billion estimated in 2001, updated to approximately 13 bilion in 2008) make ITER the largest and most expensive scientific project on the Earth (2nd in the history of mankind, after the International Space Station). The assembly phase of the ITER has already started, after manufacturing all the components, assembling and commissioning of the device, first plasma is so far scheduled for the end of the year 2025.

4 PERMEATION BARRIERS

Permeation barriers are considered to be one of the most important parts of future thermonuclear facilities. The importance of permeation barriers stems out of the selected reaction. D-T reaction, targeted because of the lowest temperature of cross section maximum, uses heavy and super heavy hydrogen isotopes. Both of them are highly permeating and in addition, tritium is radioactive. Therefore, fusion devices operating with tritium need to provide its good confinement.

4.1 Tritium transport in materials

Important parameters, which determine the applicability of a particular barrier are the material composition and the quality of manufacturing. Materials suitable for permeation barriers would be discussed in section 4.3. Quality of manufacturing is essential aspect of permeation barrier preparation which can dramatically scale down the performance of material, with otherwise excellent potential for permeation reduction. Requirements on the location and quality of permeation barriers arise from the mechanism of hydrogen permeation through the material, described in [17, 19, 89]. In the first stage, hydrogen is adsorbed on the material surface. Diatomic molecules dissociate and atomic hydrogen is dissolved in the lattice. Secondly, hydrogen diffuses through the material, favourably using cracks, pores, other structural defects, grain boundaries in the material or, as common edge length of materials is several times size of the hydrogen, simply through the crystal lattice. In the final stage, hydrogen desorbs on the other side of the material [19]. The process is schematically described in Figure 8. After absorbing in the grain (1), tritium diffuses internally to the grain boundary. Then the transport along the boundaries occurs (2), in the direction of cracks or pores (3,4), which further accelerate the transport.

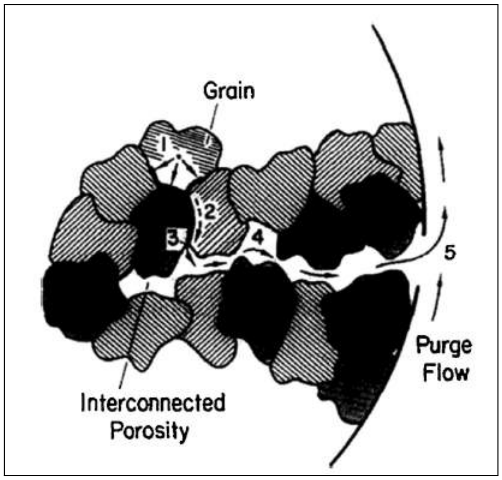

Figure 8: Tritium transport in material after absorption of tritium [19]

This particular example is based on hydrogen transport through a single ceramic pebble which is foreseen to be used in pebble-bed-based TBMs. However, the mechanism can be also applied to the issue of thin permeation barrier. Following this pattern of hydrogen transport, several requirements can be identified:

- permeation barriers must have capability to prevent or reduce the hydrogen adsorption
- permeation barriers must have low diffusion rate of hydrogen
- the occurrence of cracks, pores and other structural defects in the permeation barriers has to be maintained as low as reasonably achievable.

The rate of steady-state tritium permeation depends on the material properties, mainly solubility, diffusivity and trapping. Diffusion is a process of matter moving or hopping through the structure of the material. Tritium diffuses through most materials rather rapidly, even at relatively low temperature. Diffusivity is a thermodynamical parameter, which follows temperature dependence

$$D = D_0 exp(-\frac{E_D}{RT}) \tag{1}$$

where D_0 is a constant, E_D is activation energy for diffusion, R is universal gas constant equal to 8.31 $Jmol^{-1}K^{-1}$ and T is temperature in Kelvin. The solubility represents equilibrium between diatomic tritium molecule and tritium atoms in the metal. Solubility follows the same temperature dependence as diffusivity

$$K = K_0 exp(-\frac{\Delta H_S}{RT}) \tag{2}$$

where ΔH_S is the standard enthalpy of dissolution of tritium. Permeability is a material property; that characterizes diffusional transport through bulk material, i.e. it is a relative measure of tritium transport, when diffusion-limited transport dominates. It is defined as a product of diffusivity and solubility and using this definition, one can obtain steady state diffusional flux using Fick´s first law of diffusion through semi-infinite plate as

$$J_\infty = -D\frac{c_{x_2} - c_{x_1}}{x_2 - x_1} = \frac{DK}{t} p_{TT}^{1/2} = \frac{\Phi}{t} p_{TT}^{1/2} \tag{3}$$

by substituting from Sievert´s law

$$c_0 = K(p_{TT}^{1/2}) \tag{4}$$

where c_x is concentration at position x, t is the thickness of the plate and p_{TT} is tritium partial pressure. Substituting from equations 2 and 1, temperature dependence of permeability can be expressed as follows

$$\Phi = D_0 K_0 exp(-\frac{\Delta H_S + E_D}{RT}) \tag{5}$$

Permeability is by definition independent of surface conditions (as well as diffusivity and solubility), it is related only to diffusion of hydrogen isotopes through the material and to the thermodynamic equilibrium between the gas and the material. However, experimental measurements are strongly afffected by surface conditions. As a result, under some conditions, the measured transport properties might not correspond to diffusion-limited transport. At low pressures and specific conditions, permeability can be limited by dissociation at the surface and recombination. Trapping of hydrogen can also significantly change transport properties of the material. Generally, trapping is characterised as bonding to microstructural features, such as vacancies, interfaces, grain boundaries, dislocations etc. It is a thermally governed process with a characteristic trap binding energy - $\mathrm{E_T}$. This energy represents the decrease of the trapped particle energy with respect to the lattice and can be reffered to as the strength of the bond. Fraction of the trapping sites filled with tritium depends sensitively on the trap binding energy and on the concentration of tritium in the lattice. The amount of trapped hydrogen can affect further transport and distribution in the material. Depending on the concentrations of trapped and lattice hydrogen ($\mathrm{c_T}, \mathrm{c_L}$, respectively) and the fraction of trapping sites filled with hydrogen (θ_T), the effective diffusivity of tritium in material can be expressed as follows

$$D_{eff} = \frac{D}{1 + \frac{c_T}{c_L}(1 - \theta_T)} \tag{6}$$

where D is the lattice diffusivity. The diffusivity of the lattice can be lowered by several orders of magnitude due to trapped hydrogen.

4.2 Application aspects

The issue of permeation barriers has been discussed since the first designs of ITER-like facility. The basic confinement is provided by the vacuum vessel and the bio shield. Unfortunately, bulk structural materials have low permeation resistance to hydrogen, so the permeation fluxes through unprotected vacuum vessel would be significant. Leaving the confinement function for the concrete bioshield would on the other hand imply serious difficulties during decommissioning of the machine. Moreover, losses of tritium are not only environmental threads, they are also losses of fuel, which threatens steady-state operation of the machine. In addition, permeated hydrogen can negatively affect properties of structural materials, which could be fatal for safe operation or even structural integrity of the machine. Functional and reliable permeation barriers are therefore crucial for successful fusion device operation.

Review by Füterer et al. stated, that permeation barriers were to be applied to all surfaces in contact with Pb-17Li to minimize presumably costly coolant detritiation. The paper however envisaged to optimize detritiation processes to minimize or even eliminate the use of permeation barriers[38]. Recent overview [35] was not decisive regarding the breeding blanket coolant: the issue is still open and tritium permeation and coolant purification are among technical issues influencing the choice. Interesting calculation demonstrating the urgent need for permeation barriers was done by Causey et al. [17]. The authors used design parameters from a similar study for a larger fusion reactor [34] and values identified by Maeda et al. in his study focused on hydrogen solubility [53]. Basic assumptions yielded, that for 800 MW fusion reactor, based on liquid Pb-Li blanket concept, 150g of tritium are needed to be bred each day. According to [34] this value corresponds to molar fraction of tritium in Pb-Li equal to $6.7 * 10^{-7}$. This amount will circulate through the piping at elevated temperature exceeding 600 K. Another assumption was made about the surface of the tubes for the heat extraction, passing through the liquid Pb-Li. This surface will cover approximately 10,000m^2. Final calculation of a permeation rate through 1 mm of MANET steel with aluminized coating (permeation reduction factor (PRF) of 1,000 - tritium flux through the coated material is 1,000 times lower than throught the bare material), at temperature of 700 K, showed the daily permeation rate of 1.4 grams. Further permeation can occur through the steam generator tubes, which need to permit effective heat transfer and therefore have to be thin. In present, annual tritium losses limit is commonly set between 0.6 - 1 gram per year, to fulfill environmental and economic constraints. This clearly confirmed urgent need for intense R&D activities in this field. However, the calculations were made in 2009 on a different substrate; than the one currently proposed as structural material for ITER and following fusion facilities - a reduced activation feritic martensitic steel EUROFER. Literature survey showed, that permeation flux through MANET steel in temperature range 573-773 K at 100 kPa of deuterium pressure reached values $\sim 10^{-5} - 10^{-6}$ molm^{-2}s^{-1} [60, 59, 67]. Concerning EUROFER, numerous studies mentioned its properties regarding hydrogen exposure, including permeability [33, 54, 57]. Under similar experimental conditions, permeation flux of $10^{-7} - 10^{-10}$ molm^{-2}s^{-1} were reached [36, 52, 21]. These values are lower by more than two orders of magnitude, which puts the calculated tritium losses from [17] into proposed safety margins. This results in lower PRF values envisaged for sufficient permeation protection [80, 105]. Despite the lower coating demands, difficulties with reaching the sufficient PRF values persist, mainly in reactor conditions - i.e., in radiation environment and in contact with the tritium breeder, mainly with liquid Pb-17Li due to its corrossion behaviour. This implies further need for extensive and intensive R&D in the field of permeation barriers.

However, during the operation of ITER, leak rates from areas with tritium handling would be so low that extensive use of permeation barriers is not expected. The design of the facility involves tritium plant and detritiation systems, which should handle the whole range of foreseen situations, normal as well as emergency. The main component, responsible for recovery of unspent D-T fuel and basic detritiation of exhaust gases, is the Tokamak Exhaust Processing System. The overall detritiation factor verified by R&D is $\geq 10^8$ [79].

The system is composed of three subsystems:

- front end permeator
- impurity processing
- final clean-up

The waste gas is then sent to the normal vent detritiation system, although the level of tritium activity is extremely low, below 1 mCi[1]/d. Tritium leakage will also occur into the cooling water. To lower this permeation stream, air detritiation dryers would be installed in the tokamak confinement volume as a part of HVAC - heating, ventilation and air condition system. Permeation rates are however estimated to be relatively low, so the dryers will be installed later, when required by the operational programme. Nevertheless, one of the assignments for tritium campaign in ITER is to verify components for achieving tritium self-sufficiency and heat extraction, so significant amount of research and experiments has been carried out. Gastaldi et al. performed study on tritium transfer, which describes mechanisms of tritium release from primary circuit of fusion facilities [80]. The study was focused on Helium cooled lithium lead breeding blanket (HCLL, see [89] or [96] for more breeding blanket designs and abbreviations) and the limit for tritium release into cooling water and inventory. The target values are 1 g/year and 200g respectively. The calculations of these values were done by establishing loops according to the blanket structure, computing mass balance equations for each hydrogen isotopes and some FEM calculations. Internal structure of HCLL TBM is shown in Figure 9.

---

[1] $1\ \mathrm{mCi} = 3,7 \cdot 10^{7}\mathrm{Bq} = 3,7 \cdot 10^{-5}\ \mathrm{g\ T}$

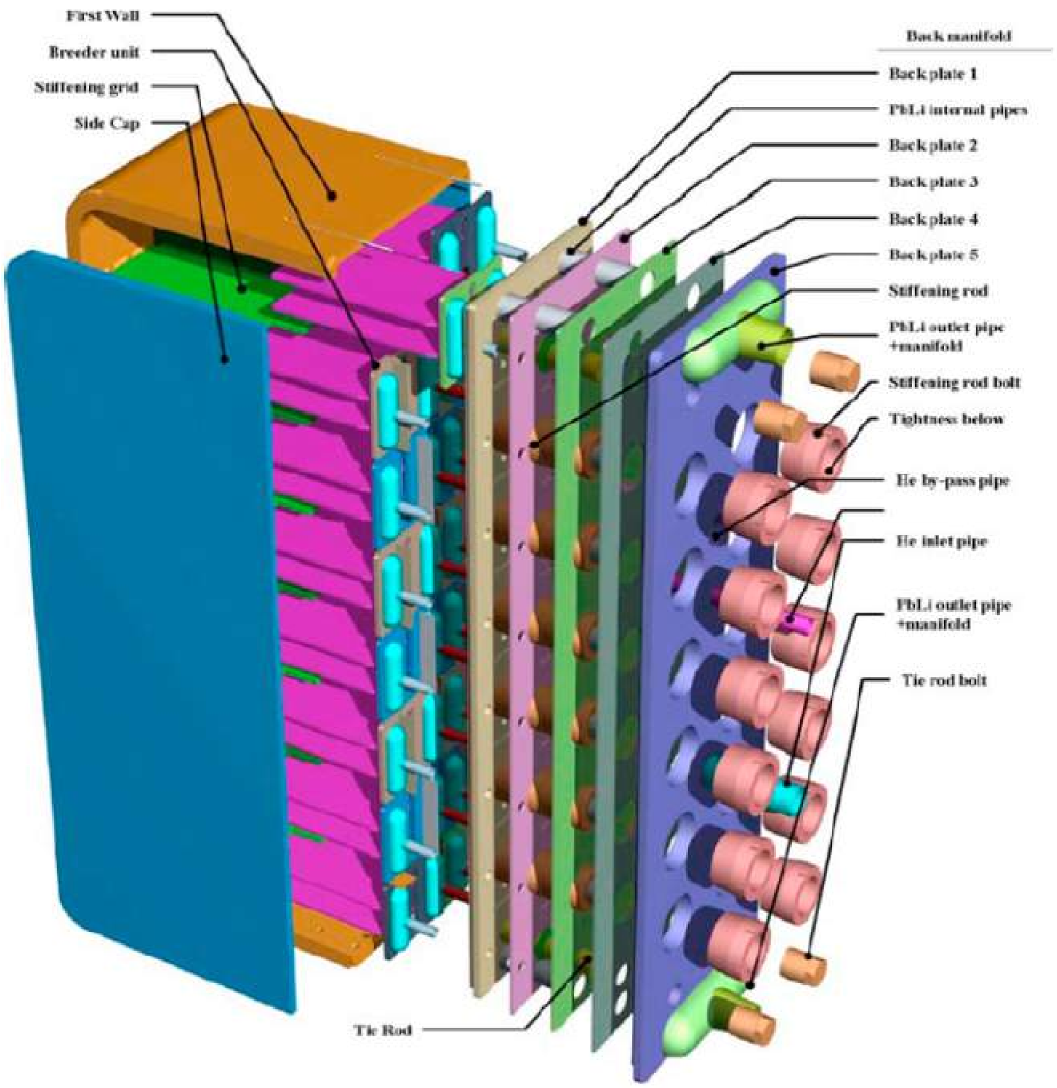

Figure 9: Helium cooled lithium lead TBM concept [96]

Results showed that parameters with greatest effect on tritium permeation are permeation reduction factor of steam generator and blanket. The above mentioned values for maximum tritium losses and inventory were not reached throughout the calculations, however, the authors suggested that in conjunction with other parameters, such as fraction of purified He and efficiency of tritium extraction system and coolant purification system, minimal PRF values were determined as 40 for the blanket and 200 for the steam generator. Similar results were obtained by Santucci et al. [105]. The authors completed literature survey on the values of Sievert´s constant for tritium in lithium lead. Based on the values identified in works of Reiter [81] and Aiello [83], values of PRF for first wall and steam generator for satisfying the tritium losses were determined. Calculations with K_S

from [81] showed, that the condition of tritium losses ≤ 1g/y, corresponding to 27Ci/d is hardly fulfilled with PRF of 400 for both first wall as well as steam generator. The calculated losses reached 25,65 Ci/d. Results of calculations with the value from [83] showed more promising results, the losses were successfully mitigated by PRF 100/100 or 5/400 at first wall/steam generator. Average losses reached 15,8 Ci/d and 10,5 Ci/d respectively. Permeation barriers were also included in the improvements of WCLL breeding blanket, designed as one of the four alternatives for EU DEMO facility [38, 35]. Other developed designs were helium cooled pebble bed, helium cooled lithium lead and dual cooled lithium lead blankets [35].

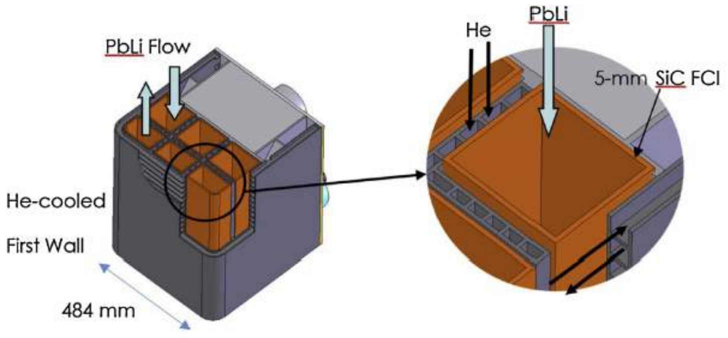

Figure 10: Dual cooled lithium lead TBM [19]

Regarding the application of permeation barriers, basic criterion is if the area is affected by presence or generation of tritium. In lithium lead blanket concepts, the whole piping system containing the Pb-Li should be equipped with the barrier. Due to severe corrosion, caused by Pb-Li circulating at elevated temperature [22, 48], the barrier should combine anti-permeation and anti-corrosion protection, if possible. Tritium, generated in the breeding area, would be either transported to central tritium plant through the piping system or the permeation would be directed to the vacuum vessel, without further circulation. In the first case, without the permeation barriers, significant losses of tritium will occur obviously, and the leakage hazard with following activation will be non-negligible. In the latter case, complete extraction of tritium from Pb-Li in the TBM volume will not be probable, therefore some residual activity will remain after escaping the TBM, which has identical consequences as in the first case. Wong et al. [109] summarized the TBM concepts being developed across the ITER organization. The extensive overview studied various physical and engineering aspects, including the use of permeation barriers. Regarding the blanket design developed in the EU - helium cooled lithium lead TBM, the problem is assessed in two ways: the barrier, currently made of Al_2O_3, is deposited either on the side adjacent to PbLi reservoir or to flowing He, used as a coolant. The latter option seems to be favourable, because the experiments at ENEA Brasimone proved the potential of the barrier self healing. PRF values measured during these experiments reached 10-30. The use of permeation barriers in HCLL TBM is envisaged by Giancarli et al. [96] too. The extensive overview covers all concepts developed through the ITER organisation, including the internal structure of the modules, arrangement of the ITER first wall, definition of auxiliary systems required for the TBM etc. Apart from the HCLL TBM, use of permeation barriers is envisaged for the WCCB TBM - water cooled ceramic breeder, proposed by Japan. In this concept, permeation barriers are applied to reduce the permeation from breeder zone towards water coolant.

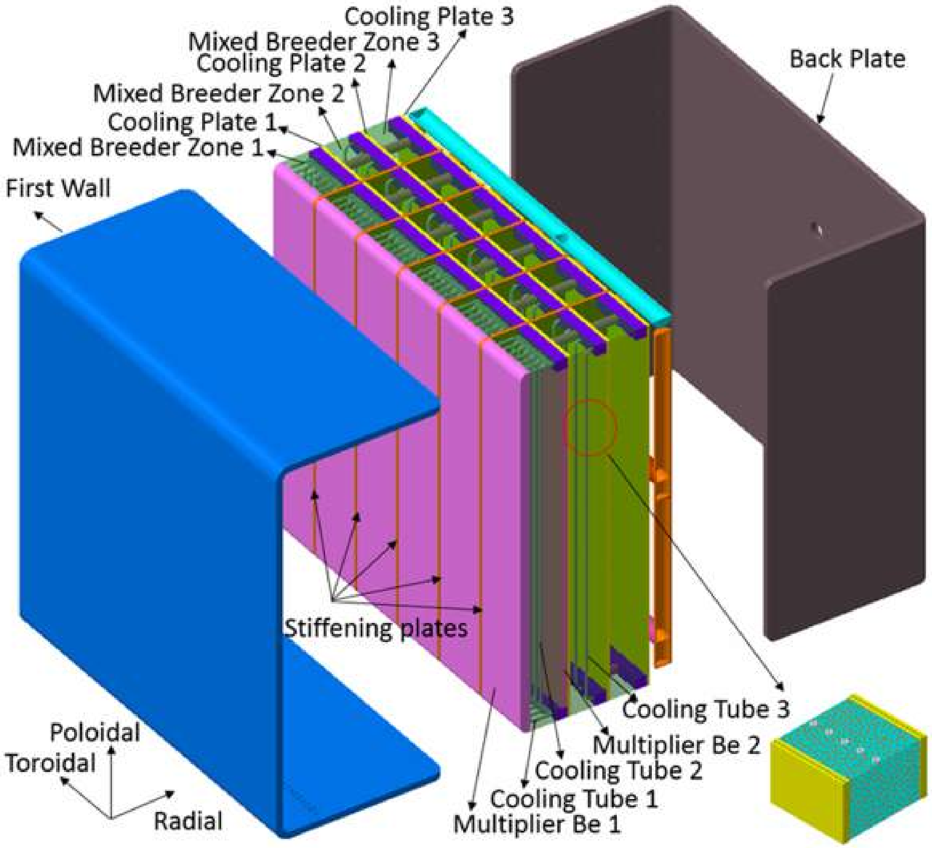

Figure 11: Water cooled ceramic breeder TBM concept [103]

In concepts using pebble beds instead of liquid Pb-Li, the piping would be required not for the breeding material, but for the coolant. It means that undesirable tritium transport can occur only through permeation. The barriers are therefore advised to be placed on the back side of the TBM, facing the plasma, and in the coolant pipes within the breeding module area. These positions should prevent the activation of further parts of the reactor. While for ITER, permeation barriers as essential part of the reactor are not considered, due to low exposure to tritium and they are rarely mentioned in design reviews of TBM, for example in [64], for some blanket designs for advanced fusion reactor concepts, the use of permeation barriers is strongly advised. Ihli et al. proposed several concepts in their review [44], focusing on the issues and demands on R&D connected with each concept. Dual coolant concept, using helium for first wall cooling and PbLi as self-cooled breeder, is expected to be equipped with reliable permeation barriers on areas outside the tritium extraction system. For self-cooled Flibe concepts blanket module using molten salts consisting of F, Li and Be, e.g., $(LiF)_2(BeF)_2$ permeation barriers are considered too. Evaluation of double-walled tube concepts have identified He gas or pure Flibe with low flow rates as sufficient and feasible permeation barrier, leaving tritium leakage as a severe problem only to the area of heat exchanger.

Not only permeation of deuterium and tritium, but also their retention in the reactor is an issue to be solved. Tetsuo Tanabe stated that in today tokamaks, up to 10% of fueled hydrogen is piled in the vacuum vessel, which in unacceptable in the reactor [107]. Due to the low natural abundancy of tritium and low tritium breeding ratio designed for the blanket system (1.1 or less), reduction of tritium retention is one of the major economic factors for future DEMO. Since the public exposure to tritium is regulated at level of several Bq/cm^2, the handling systems have to provide strict and reliable confinement of tritium. Tritium leakage can be easily identified by measurement of β electrons from tritium decay. However, due to their low energy, the electrons can cover the distance only up to 10 mm, which makes majority of tritium leaks unmeasurable and tritium mobility through bulk materials remains problematic issue. For example, tritium easily permeates into coolant, where hazardous tritiated water, HTO, is formed when water coolant is used. While tritium exposure of skin is not so harmful due to thin penetration of β electrons, in the form of HTO, tritium can be usually taken into the organism and possess greater risk for people. In addition, detritiation of such diluted water is very cost consuming, resulting in increase of fusion energy cost. Because of these reasons, Tanabe assigned the need for permeation barrier with significant PRF of 5-6 orders of magnitude for ferrite as structural material. Moreover, the issue of permeation through the reactor walls would be significant, because of the high operation temperatures. This should be solved by dual tubing or facilitating of permeation barriers [107]. D. Demange et al. review breeding blanket designs developed for European DEMO - helium cooled pebble bed, helium cooled lithium lead and water cooled lithium lead, emphasizing tritium management and anti-permeation strategies[31]. They conclude that high efficiency of processes in the breeding and cooling loops in addition to available and efficient anti-permeation barriers are required to achieve acceptable tritium losses through breeding blanket (BB) and steam generator (SG). Confinement requirements commonly discussed allow tritium losses between 0.6 and 1 g/y, while the annual amount of tritium needed for 1 GWe would be around 100 kg. There are only few possibilities how to mitigate tritium losses - implementation of tritium extraction and coolant purification systems (TES and CPS, respectively) and the use of anti-permeation barriers. Numerical study using FUS-TPC tritium permeation code was performed using characteristic of particular breeding blanket - dimensions of breeding and cooling zones, PbLi and coolant flow rates, tritium production etc. In addition, input parameters such as TES and CPS efficiency, Sievert constant values and permeation reduction factors for BB and SG. Keeping these parameters constant for all three BB, large differences among tritium permeation, losses and inventory were computed. These values were adopted as "starting scenario outcomes" and can be found in Figure 12.

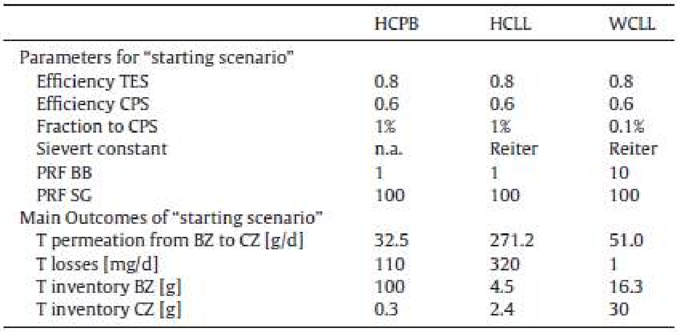

	HCPB	HCLL	WCLL
Parameters for "starting scenario"			
Efficiency TES	0.8	0.8	0.8
Efficiency CPS	0.6	0.6	0.6
Fraction to CPS	1%	1%	0.1%
Sievert constant	n.a.	Reiter	Reiter
PRF BB	1	1	10
PRF SG	100	100	100
Main Outcomes of "starting scenario"			
T permeation from BZ to CZ [g/d]	32.5	271.2	51.0
T losses [mg/d]	110	320	1
T inventory BZ [g]	100	4.5	16.3
T inventory CZ [g]	0.3	2.4	30

Figure 12: Main input parameters and outcome values of the "starting scenario", TES - tritium extraction system; CPS - coolant purification system; PRF - permeation reduction factor; BB - breeding blanket; SG - steam generator; BZ - breeding zone; CZ - coolant zone; [31]

Considering 2-3 mg/d of tritium losses as the acceptable limit, only WCLL blanket design fulfilled this condition, with PRF BB 10, as double-wall tubes were considered. Beyond these "starting scenarios", Demange et al. performed broader range of experiments, in which several set of minimum technological requirements for all three BB concepts were identified. WCLL blanket seemed to be relaxed mainly because of rather low operational temperatures and double-wall design, which provide PRF BB of 10. However, tritium accumulation in the coolant, 10 times higher than in HCLL, constitutes potential radiological hazard. The feasibility also depends on the efficiency of TES and CPS system, which was not yet proved in 2014. Results for HCPB blanket vary with transport model used for tritium. Using diffusion limited model, TES and CPS of efficiency greater than 95%, PRF BB of 10 and PRF SG of 100 are required. Switching to surface limited regime, permeation decreases and tritium processes can be significantly relaxed. Regarding tritium migration, HCLL is the most critical blanket design with PRF BB and SG of ≥ 100 required. Main reasons for such high values are limited PbLi recirculation rate and low tritium solubility. The authors put together the following general guidelines for mitigating tritium migration and implementation of anti-permeation strategy.

- Removing as much as possible tritium in breeding zone remains the best strategy
- Increasing tritium process efficiencies is very beneficial but cannot solve migration issues by itself
- Increasing tritium process throughput in BZ seems affordable for HCPB (within pressure drop limit)
- Increasing tritium process throughput in the coolant side is not really practicable (already at limit)
- For HCLL, efficient anti-permeation barriers at BB will be required (in good synergy with anti-corrosion function, but high issue for reliability under high neutron loads and thermal cycles)
- He gas chemistry in purge and coolant sustaining oxide layers is a promising approach to reduce permeation significantly [31].

Mohamed Abdou et al. [19] described exhaustively the issue of permeation barriers and membranes concerning R&D on the pathway to European DEMO facility. The issue is rather challenging because, depending on the location and function, two branches of materials are required: materials with high permeability to permit efficient tritium extraction from breeder and coolant; and reliable barriers to mitigate undesired tritium permeation. Abdou et al. surprisingly stated, that DCLL breeding blanket could be put out of this discussion, as due to relatively high PbLi circulation, supported by highly efficient tritium extraction system, this concept has potential to avoid any tritium permeation into coolant or the environment. Development of permeation barriers reached so far mixed success with alumina/FeAl coatings and sandwich coatings of Er_2O_3 and Al_2O_3 together with W. The first coatings were prepared with various methods, the most successful samples were produced by Hot-Dip Aluminizing and reached PRF of about 100. However, all samples degraded after thermal cycling and neutron exposure. The latter, sandwich coatings, were successful only in rather idealized conditions. Major concerns remain about achieving applicable and reliable permeation barriers on large complex surfaces in the environment featuring:

- strong thermal gradients
- contact with high temperature PbLi
- presence of significant neutron and secondary charged particle irradiation

Otherwise, as candidate materials for DCLL and HCLL breeding blanket concepts, SiC, respectively alumina/aluminides or erbium oxide layers with over-layers of tungsten are proposed. In case of DCLL BB, SiC is already desired as flow channel insert material (FCI) to provide electrical and thermal insulation. Erbium oxide layers in HCLL BB on the other hand, can be utilized as anti-corrossion barriers as well [19].

4.3 Materials

As mentioned above, materials suitable for permeation barrier fabrication should have positive impact on hydrogen repellence and throughput. The decisive criterion regarding hydrogen transport is the permeation reduction factor. It is a ratio of hydrogen flux through the bare and coated substrate material. This is however not the only criterion that should be applied during material selection. The following aspects also influence the functionality and applicability of a material as a permeation barrier:

- stability and reliability of the coating
  - at elevated temperatures
  - under irradiation
  - in possibly highly corrosive environment
- compatibility with the substrate material
- capability to form dense and defect-free layers on complex surfaces

There are also some benificial effects, which can be considered during material selection, e.g., self-healing ability. Some requirements can be met or balanced with properly chosen deposition techniques, desribed in more details in section 4.4.

4.3.1 Oxides

One big group of materials with desired properties are oxides. These materials have been studied since the beginning, because of very low intristic hydrogen permeability. Oxide barriers might suffer from different coefficient of thermal expansion compared to the substrate. Therefore, spallation and crackings might occur. On the other hand, in the environment with oxygen presence, the oxide layer might replenish or even grow [17]. Particulary Al_2O_3 or Er_2O_3 were extensively investigated recently [26, 27, 50, 60, 65, 75, 101]. This group of materials was broadly surveyed in our previous work as well [89] and thus, considering the aim of this thesis, only few major results will be pointed out. Measurements of Cr_2O_3 film deposited on 316L stainless steel by MOCVD (Metal Organic

Chemical Vapour Deposition, see section 4.4) showed permeation reduction factor (PRF) of 24 - 117 for temperatures of 823 - 973 K [93]. Experiments conducted by Nakamichi et al. [56] provided PRF of 300 and analysis of permeation by Tritium Migration Analysis Programme (TMAP code) indicated possible decrease by four orders of magnitude (in case of 2 µm perfectly deposited layer in tubular specimen). Al_2O_3 layer deposited on MANET steel by hot-dipping technique was capable to reach PRF of more than three orders of magnitude [18]. Coatings prepared by pack cementation exhibited PRF of 10^3 – 10^4 on planar substrate, however on tubular specimen, the performance was lowered. PRF 30 – 70 was reported in temperature range of 623 – 823 K [75]. The efficiency of the coating was also often decreased due to cracks or imperfections. Regarding Er_2O_3, 1 µm PVD (physical vapor deposition, see section 4.4) coating was deposited by Koch et al. [46]. Measured PRF value reached 200. Large number of experiments was performed by T. Chikada. Hot dipped planar Er_2O_3 samples reached PRF of 500 - 700, after measuring for 1 day for finishing of the crystallization even exceeded 1000 [28]. Tubular specimens were prepared too; the permeation was reduced by two orders of magnitude above 870 K, below this temperature, the signal was undetectable [28]. In further experiments of T. Chikada, electro chemical deposition was used and ca. 1 µm coating was deposited on 0.5 mm thick substrate of several steels. Reported PRF reached 2 - 3 orders of magnitude, depending on the substrate [26].

4.3.2 Nitrides

Besides oxides, native nitrides of the base substrates or other nitride depositions can be also applied as permeation barriers. In comparison with oxide barriers, nitrides are researched to a lesser extent, but several promising and applicable compounds have been identified. One of the most common native nitrides is Fe_2N, which is formed during steel nitriding. Permeation reduction of one to three orders of magnitude can be reached. The most researched nitride coating is TiN, because of its good adhesion and easy deposition. The effectivity of the coating depends on its placement with respect to the hydrogen stream, the permeation reduction vary from less than one to six orders of magnitude, better results are achievable at upstream side [17]. TiN can be deposited also as a multilayer coating, e.g., with TiC as a bilayer or TiC and Al_2O_3 as a trilayer. 1 mm thick samples of 316L were coated with 3 µm of bilayer and 4 µm of Al_2O_3 on 2 µm of bilayer. The bilayer reached 1 order permeation reduction, which was not improved by additional Al_2O_3, probably due to defects in deposited layers [37]. Permeation measurements of TiN ion-plasma deposited coatings on various substrates were performed by Tazhibaeva et al. [71]. Designation and chemical compositions of used substrates is shown in Figure 13.

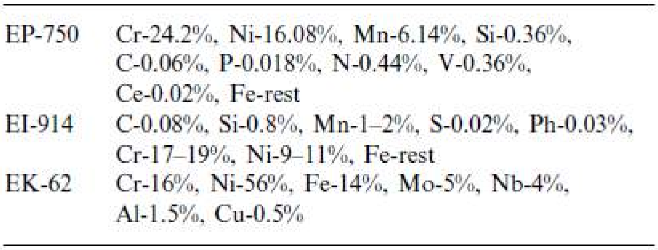

EP-750	Cr-24.2%, Ni-16.08%, Mn-6.14%, Si-0.36%, C-0.06%, P-0.018%, N-0.44%, V-0.36%, Ce-0.02%, Fe-rest
EI-914	C-0.08%, Si-0.8%, Mn-1–2%, S-0.02%, Ph-0.03%, Cr-17–19%, Ni-9–11%, Fe-rest
EK-62	Cr-16%, Ni-56%, Fe-14%, Mo-5%, Nb-4%, Al-1.5%, Cu-0.5%

Figure 13: Chemical compositions of substrates used for permeation measurements, wt. % [71]

Samples dimensions were as follows: thickness 1.5 mm diameter 35 mm. Before the deposition, the samples were not thermally treated. During the deposition process, samples were sputtered by titanium ions for 10 min, following 10-40 min deposition at 773-873 K. Resulting coating thickness was 10-30 µm, with best adhesion for 10 µm thickness, which were selected for permeation measurements. Results showed 2-4 times permeation reduction, depending on the substrate. After annealing for 72 h at 1123 K in hydrogen atmosphere, coating exhibited certain degradation. Rather broad investigation of ceramic coatings on SiC/SiC composites was performed by Racault et al. [63]. The samples were 32 mm in diameter and 3.5 mm in thickness. Coating materials were TiN, TiC, SiC, Al_2O_3 and SiO_2 in various thickness. Several coatings were deposited as bilayers, depositions methods were CVD or PVD. Three kinds of TiN samples were prepared - 15 µm CVD, 25 µm CVD and 15 µm CVD + 8 µm PVD bilayer. Observations showed that all coatings were well bonded to the substrate and did not exhibit defects. The authors do not provide any comparison of permeation through bare and coated sample, however, the permeation rates are compared among the coatings. As a result, 15 µm CVD TiN coating was determined as the least effective (along with SiO_2 coating), whereas the bilayer of CVD and PVD TiN layer obtained the best results. Measurements of tritium permeation through 316L stainless steel with multiple coatings were performed by Yao et al. [76]. Films of TiN+TiC+TiN and TiN+TiC+SiO_2 were produced by means of hollow cathode deposition, annealed at 350°C in a mixture of hydrogen and argon and subsequently cooled rapidly to room temperature. Thickness of the films were 2-3 µm and observations showed very good diffusion bonding to the substrate, no cracks or spallation off for temperatures below 500 °C. Tritium permeability measurements showed 4-5 orders of magnitude reduction for TiN+TiC+TiN films and 4-6 orders reduction for TiN+TiC+SiO_2 in comparison to 316L steel coated with Pd film for oxidation protection. At 600 °C, permeation reduction was decreased due to oxidation of TiC, but still reached 3-4 orders of magnitude. This decrease was smaller for films containing SiO_2, because of its better oxidation resistance, compared to TiN.

Other nitrides taken into consideration were for example boron nitride or (Al,Ti)N coating.

Boron nitride was confirmed to reduce the permeability of hydrogen by one or two orders of magnitude, however, coatings from this material do not seem to be favourable due to high neutron cross section of boron, which may result in difficulties in maintaining proper tritium breeding ratio[17]. Other experiments with cubic boron nitride coating of 316L stainless steel were performed by Tamura et al. [70]. Thickness of the substrate was 0.1 mm, TiN, SiC and BN coatings were deposited by means of magnetically enhanced plasma ion plating. Before the deposition of BN, additional 0.5 µm SiC layer was deposited for adhesion improvement. Total thickness of the coating was 1.5 µm and this value was obtained by other coatings as well. Observation of coating surfaces showed slight oxidation of TiN to TiO_2, while no boron oxides were found. Permeation measurements confirmed, that both TiN and BN coatings are able to decrease the permeation flux through the material to less than 1/10. At higher temperatures (773K), BN showed slightly better permeation reduction than TiN, but both of the coatings reached PRF $\sim 10^2$, see Figure 14.

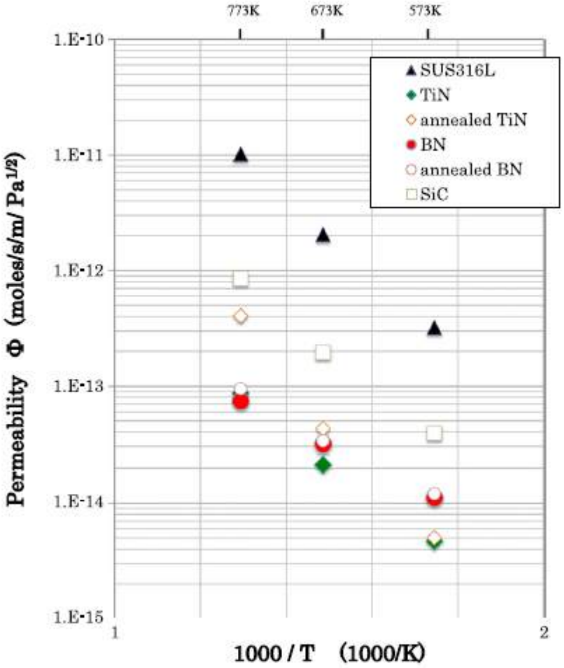

Figure 14: Arrhenius plot of hydrogen permeability as a function of temperature [70]

In addition to boron nitride deposition, boronization of tokamak vacuum vessel walls was considered. Early experiments on Tore Supra, TEXTOR, JT-60U and other tokamaks proved suppression of oxygen contamination to core plasmas, reduction in hydrogen recycling compared with carbon walls and suppression of contamination by wall materials [58, 74, 39, 43, 45, 41]. Positive effect on hydrogen retention/permeation was demonstrated on 200 nm thick boron film deposited by glow discharge in helium/diborane mixture in SUT (Surface modification Teststand) on National Institute of Fusion Science. After the deposition, several cycles of hydrogen glow discharge followed by thermal desorption were performed. Measurements of desorbed hydrogen showed roughly the same amount as which was absorbed during the glow discharge. This occurred for temperatures below 400°C. No permeation into the substrate steel was recorded during the experiments. However, the maintainability of boron film and boron migration remained serious issues. By experiments in SUT it was showed, that boron hydrides are very fragile, but they tend to be re-deposited inside the vessel, not to be removed from the vessel through the pump duct. Results from retention and permeation measurements supported the use of boronization in future fusion facilities, but detailed studies were needed to confirm the migration and redeposition issues. Low diffusivity of hydrogen in (Al,Ti)N was confirmed by measuring of 1.7 µm coating on 0.1 mm thick 316L substrate. The permeability was reduced by two to three orders of magnitude [17]. Performance of AlN as possible permeation barrier was investigated by Wang et al. [72]. AlN coating were prepared on 316L stainless steel by RF magnetron sputtering. Substrate was cut into wafers with 25 mm in diameter and 0.5 mm thickness, which were ground and ultra-sonic cleaned before the deposition. AlN layer was uniform with thickness of approximately 0.4 µm, closely adherent to the substrate, dense, with no structural defects. Results of permeation measurements can be seen in Figure 15, best result of PRF 144 was achieved at 250°C. After permeation measurements, several cracks occurred on the surface, nano-hardness and the elasticity modulus of the coating increased from 5.96 GPa to 7.41 GPa and from 156.6 GPa to 210.6 GPa, respectively.

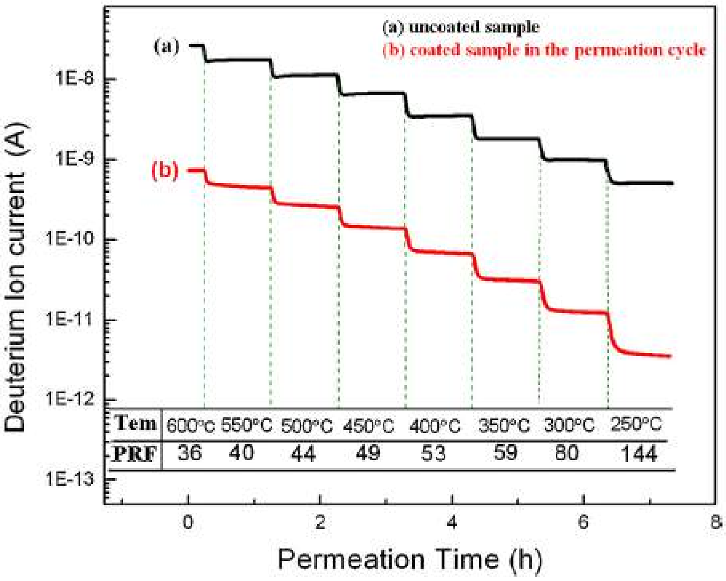

Figure 15: Comparison of permeation current through uncoated and AlN coated sample [72]

4.3.3 Carbides

Experiments on hydrogen solubility, diffusivity and permeation were performed using various carbonized materials as well. In the work of Causey et al. [17], results of boron, silicon and titanium carbides investigations are given. No direct measurements of permeation reduction of boron carbide coatings were presented, only diffusivity and solubility values of solid B_4C. Solubility was expressed by Shirasu et al. [69] as $K = 3.8\exp(\frac{3{,}590}{T})$ mol $H_2m^{-3}MPa^{-1/2}$. The diffusivity values were determined by Elleman et al. for unaffected B_4C [32] and by Schnarr and Munzel for both unirradiated and irradiated B_4C [84, 85]. From [32], diffusivity was given as $D = 1.1x10^{-10}\exp(\frac{-8{,}450}{T})m^2s^{-1}$. Schnarr and Munzel measured the diffusivity as $D = 1.23x10^{-11}\exp(\frac{-9{,}720}{T})m^2s^{-1}$ for unirradiated and $D = 4.3x10^{-8}\exp(\frac{-26{,}000}{T})m^2s^{-1}$ for irradiated sample, respectively. The apparent diffusivity decreased with increasing radiation damage, until the percentage of ^{10}B exceeded 10%.

In case of silicon carbide, permeation and permeation reduction has been measured, in addition to diffusivity and solubility. Two sets of experiments by Causey et al. yielded diffusivity and solubility values of silicon carbides after implantation of energetic tritium particles [23] and without implantation [24]. Resulting equations for diffusivity were $D = 1.58x10^{-4}\exp(\frac{-37{,}000}{T})m^2s^{-1}$ and $D = 9.8x10^{-8}\exp(\frac{-21{,}870}{T})m^2s^{-1}$, respectively, while for solubility $K = 1.1x10^{-3}\exp(\frac{18{,}500}{T})$ mol $H_2m^{-2}MPa^{-1/2}$ and $K = 2.2x10^{-2}\exp(\frac{7{,}060}{T})$ mol $H_2m^{-3}MPa^{-1/2}$ respectively. Solubility for unimplanted sample is one to two orders of magnitude lower, compared to the samples after implantation, while diffusivity is one to two orders of magnitude higher. Permeation measurements of RF sputter-coated steel samples done were by Yao et al. [78]. 1.3 µm coating with several percent of oxygen and traces of iron decreased the permeation rate through steel by two orders of magnitude, although the observations of the coating showed its significant porosity.

Titanium carbide has been also tested as a permeation barrier, either as a part of multilayer, as mentioned above [37] or alone. Non-metalic materials (nitrides, carbides, etc.) are favourable because of their high melting points, good corrosion and thermal shock resistance. However the mismatch of Young modulus of TiC in comparison with steels may give rise to adhesion failure probability. Checchetto et al. prepared TiN-TiC films on MANET II disc samples by ion-beam assisted deposition [25]. The samples had 18 mm in diameter and 0.5 mm in thickness. The deposition process consisted of following steps

- sputter cleaning of the substrate
- deposition of Ti film and N_2^+ ions - transition layer between steel and TiN
- deposition of Ti film in N_2 atmosphere - TiN layer
- deposition of Ti film in acetylene atmosphere - TiC layer

Thickness of the final coating was 1250 nm, 250 nm of TiC over 1000 nm TiN. Permeation measurements were performed in temperature range 470-570 K and showed significant difference depending on the barrier placement. Coating of the low pressure side showed only little permeation reduction, while the high pressure side exhibited PRF of approximately 50. Shan et al. deposited 2.5 µm film using CVD and reported PRF of $10^5 - 10^6$ [68]. Calculations of permeation reduction by silicon carbide coatings were made by Causey and Wampler [102]. The calculations were based on data from previous experiments with vapor deposited silicon carbide on graphite substrate. The samples were prepared by decomposition of methyltrichlorsilane, further followed by removal of graphite and thin SiO_2 layer. Calculations of tritium retention and permeation were performed with the use of DIFFUSE computer code [99]. Assuming 1 cm graphite substrate coated with 100 µm SiC layer and exposed to hydrogen pressure of 0.1 Pa, tritium inventory in graphite is expected to be reduced by 4 orders of magnitude during the effective lifetime of fusion reactor(10^7s assumed), see Figure 16.

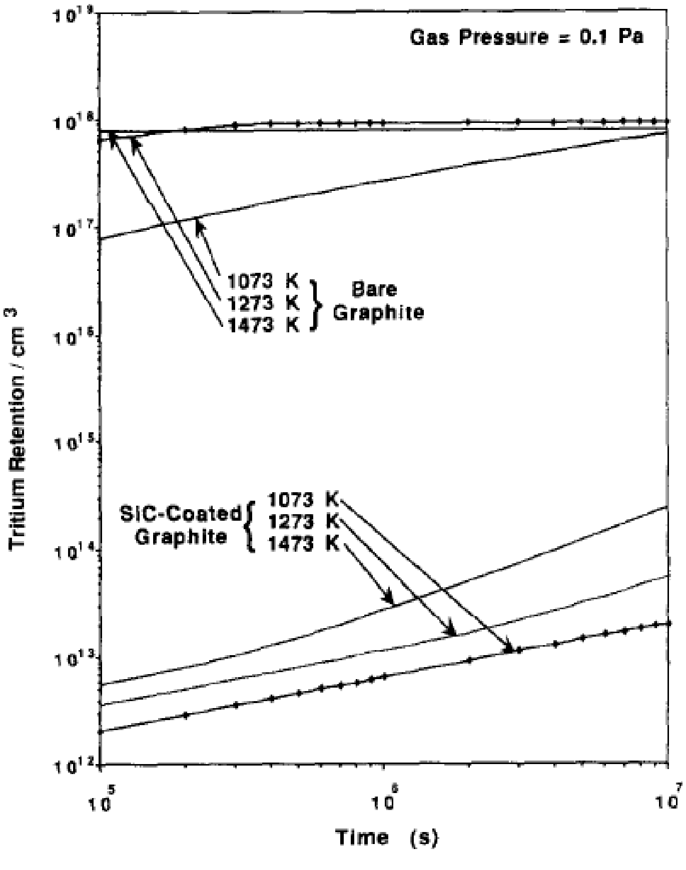

Figure 16: Comparison of tritium retention in bare graphite to 100 µm SiC coated graphite [102]

Comparison of tritium permeation through first wall material - 5 mm Be/5 mm Cu duplex structure - is complicated. Measurements at temperatures suitable for bare Be/Cu would show no permeation through coated material. Results are plotted in Figure 17 and it can be assumed, that permeation is reduced by 5-8 orders of magnitude, although the temperatures do not overlay very much. Although the results present SiC coatings as very effective permeation barriers, authors present certain difficulties in fabrication of such coatings, which have to be solved. The CVD process is too slow for producing whole slabs of SiC, while hot pressing or sintering produces usually porous materials. These are open for rapid gas permeation. Therefore SiC has to be deposited by CVD on another material, that can withstand the deposition temperature ($> 1400K$) and will not flake off or crack during thermal cycling, for example graphite etc.

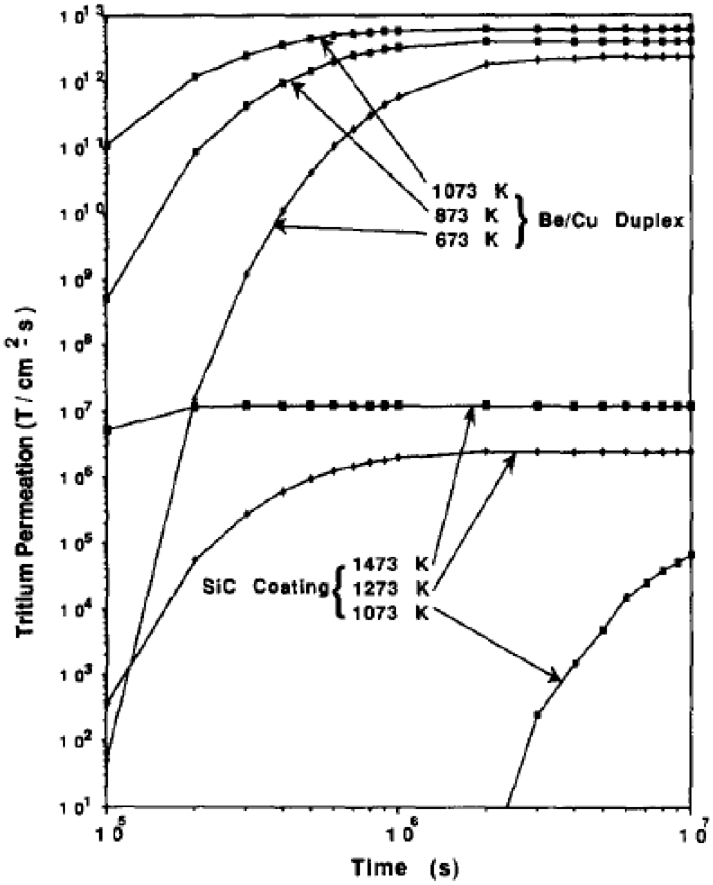

Figure 17: Comparison of tritium permeation through bare and SiC coated Be/Cu duplex structure [102]

4.3.4 Liquid breeder and coolant effects on the materials

In all the above mentioned studies investigating permeation barriers efficiency, the performed measurements were based on exposure of gaseous hydrogen/deuterium to the coated sample. This covers the solid breeding blanket designs, where the lithium is present in the form of pebble beds. Regarding lithium lead breeding blanket, one has to take into the consideration the effect of the Pb-Li exposure on the barriers, namely its corrosion properties. The urge for permeation barriers to possess sufficient corrosion resistance was confirmed by extensive study of J. Konys and W. Krauss [48, 47, 49]. By investigating the Pb-Li effect on bare EUROFER-97, alarming results were received. The measurements were performed at reactor relevant temperatures and flow rates of Pb-Li, at 480°C to 550°C, and 0.22 to 0.3 m/s, respectively. In order to acquire detailed information in this issue, the measurements lasted up to 12,000 h, with evaluation of selected samples after shorter exposure. Resulting values of corrosion rates are shown in Figures 18 and 19.

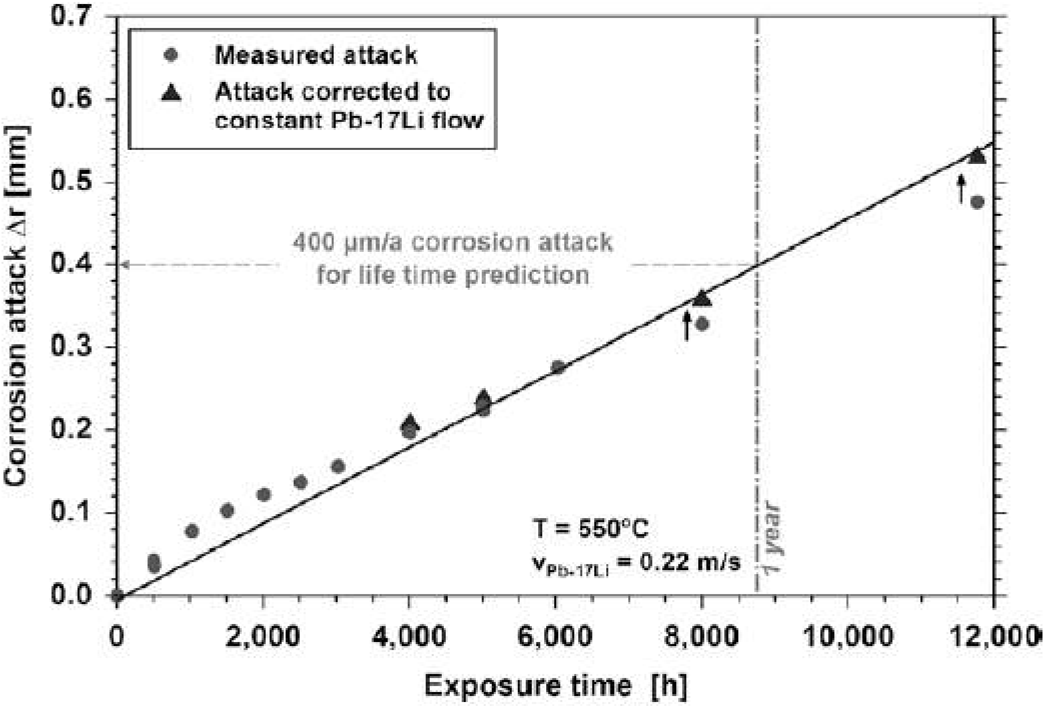

Figure 18: Corrosion attack of EUROFER 97 at 550 °C [49]

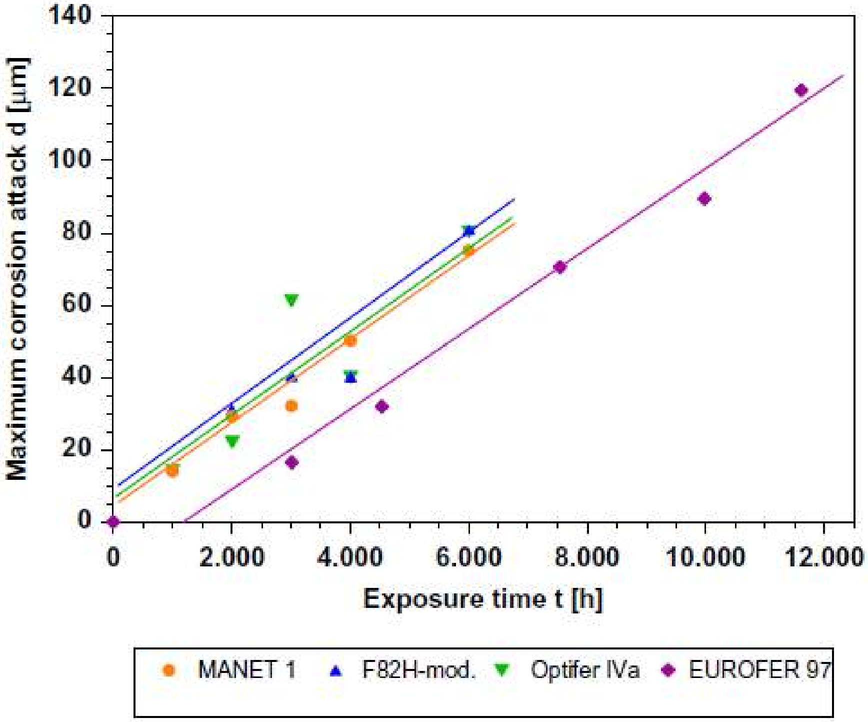

Figure 19: Comparison of corrosion rates of various ferritic martensitic steels [47]

Corrosion attack was uniform in all cases and calculations yielded values of 90 µm/year for 480°C and 400 - 700 µm/year for 550°C. Adjustment of the device parameters, such as flow velocity or impurity levels in Pb-Li, may cause corrections up to several percent. Such corrosion rates are equal to 4 kg of dissolved material per year and square meter [50]. Eventhough EUROFER reached best results among ferritic-martensitic steels, the values are still significantly off the safety range. Furthermore, the dissolved mass will probably form precipitates in cooler sections of the Pb-Li loops, which may result in line plugging. This phenomenon was drastically enhanced by the presence of magnetic fields [49] and was not avoided after installment of filtering components - magnetic traps. Metallographic analysis of test loop sections detected significant number of such precipitates and the Pb-Li flow was reported to be heavily suppressed by their presence after approximately 3,000 h of corrosion testing. These results clearly show the need for anti-corrosion coating on structural materials. Corrosion rates measured by Benamati et al. [22] at 480°C and flow velocity of about 10^{-2} m/s were about 40 µm per year. Surprisingly, tensile properties of the samples after 1,500; 3,000 and 4,500 hours measurements seemed to be unaffected or only slightly affected.

Several combinations of material and deposition technique were already tested, aiming to protect the base material from corrosion. For example aluminium was deposited by means of electro chemical deposition [50]. Ability of this method to deposit thin as well as thick (8 - 20 µm) homogenous layers was confirmed and during the testing of cylindrical specimens in 0.22 m/s Pb15.7Li flow at 550 °C, no corrosion attack was measured. Aluminium-hot-dipped and subsequently annealed EUROFER and MANET samples were investigated in previous study by Konys [48]. Hot dipping and heat treatment of MANET samples resulted in 150 µm of FeAl and α-Fe(Al) equilibrium phases. Such coating withstood the corrosion testing at 480 °C without visible attack. Similarly coated EUROFER obtained 20 µm layer of $FeAl_2$ phase, followed by FeAl layer and region with continuous Al percentage decrease. Total thickness of Al-affected zone was roughly 120 µm While exposed to PbLi, $FeAl_2$ phase was strongly attacked and partially removed, but the corrosion effect was slowed down or stopped after reaching the FeAl phase. Effect of not flowing, but static PbLi exposure was investigated by Pint et al. [61], PbLi was introduced into CVD β-SiC capsules, the measurements lasted for 1,000 - 5,000 hours at 800°C to 1200°C and the capsules were weighted after the measurements. In addition, measurements of CVD SiC layers on 316 stainless steel and Al+Ni containing alloys were performed. Significant mass gain was recorded after 5,000 h measurement at 800 °C only. All other experiments showed greatly enhanced corrosion resistance in comparison with bare 316 stainless steel (see Figure 20). Corrosion rates of Al and Ni based alloys were greater than those of SiC, but still reached better results than bare substrate material.

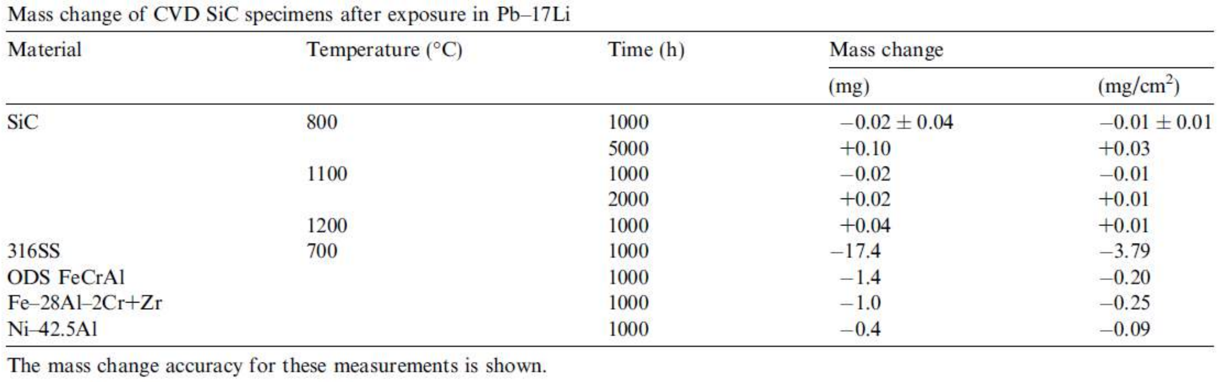

Mass change of CVD SiC specimens after exposure in Pb–17Li

Material	Temperature (°C)	Time (h)	Mass change	
			(mg)	(mg/cm^2)
SiC	800	1000	−0.02 ± 0.04	−0.01 ± 0.01
		5000	+0.10	+0.03
	1100	1000	−0.02	−0.01
		2000	+0.02	+0.01
	1200	1000	+0.04	+0.01
316SS	700	1000	−17.4	−3.79
ODS FeCrAl		1000	−1.4	−0.20
Fe–28Al–2Cr+Zr		1000	−1.0	−0.25
Ni–42.5Al		1000	−0.4	−0.09

The mass change accuracy for these measurements is shown.

Figure 20: Mass change of specimens after static Pb-17Li exposure [61]

PbLi compatibility of $SiO_2 - Cr_2O_3$ and Y_2O_3 was examined by Terai et al. [108]. $SiO_2 - Cr_2O_3$ samples were prepared by chemical densification coating (CDC, see section 4.4), while Y_2O_3 was prepared by plasma spraying. Compatibility of $SiO_2 - Cr_2O_3$ was tested by 49 hour exposure to PbLi at 873 K. Afterwards, the coating layer was severely damaged, presumably due to the reduction of Cr_2O_3. The substrate was further invaded by the internal corrosion. Tritium permeability of the coating was examined too, however, it was stated, that $SiO_2 - Cr_2O_3$ can be effective permeation barrier only in absence of molten PbLi. Plasma sprayed Y_2O_3 reached simillar results, the coating was severely attacked and most of the coating was destroyed. On the other hand, in compatibility testing of sintered Y_2O_3 with liquid lithium, no significant change, such as fragmentation or crack formation was observed after 1419 hours at 773 K.

The permeability increase after exposure to PbLi was already reported by several studies. Yao et al. measured PRF of hot-dip aluminized coatings and reported PRF of 45, compared with 140 for gas measurements [77], while theoretically achievable values are 260 - 1000 [66]. Aiello et al. investigated tubular EUROFER 97 specimen coated by hot dipping and exposed to PbLi, PRF reached values 17 - 45, compared to 30 - 100 for gas measurements [82]. Permeation reduction of tubular MANET samples was examined by T. Sample et al. [65]. The MANET tube was coated by vacuum plasma sprayed aluminium externally and the measurements were performed under hydrogen gas and under exposure of PbLi. The obtained PRF values in temperature range 723 - 523 K were 44 - 117 during the gas measurements, but only 15 - 20 during measurements with liquid PbLi. Perujo and Forcey [92] investigated CVD and pack cementation deposited Al_2O_3 layer on capsules used for PbLi measurements. 3 µm CVD layer was deposited on 1 µm TiC and the permeation reduction was unaffected by the PbLi, having reached approximately 1 order of magnitude. On the other hand, the effectiveness of aluminium layer deposited by pack cementation was completely eliminated by exposure to PbLi.

4.3.5 Radiation effects on the materials

In addition to corrossion effects on the materials, radiation effects constitute second major issue in the barrier applications. Even though the above presented experiments managed to achieve PRF up to 10^6 in the most successful cases, several studies investigated PRF under more relevant reactor conditions, i.e., after neutron irradiation. Results were surprising, even alarming in some cases: significant drop in PRF occurred in almost every study. Experiments performed in Netherlands measured permeation reduction of 146 µm Al_2O_3 coating on 316L steel. Tritium was produced from liquid Pb-17Li by fission of the lithium, in nuclear reactor at HFR Petten, and over the temperature range 540 - 760 K, PRF reached 80 [62, 29]. Further experiments tested three different coatings: a) 6-8 µm CVD layer of TiC, b) 0.5-1.5 µm TiC layer followed by 2-3 µm Al_2O_3 layer and c) 5 µm Al_2O_3 layer on 120 µm Al rich layer prepared by pack cementation. PRF reached 3.2, 3.4 and 14.7 for coatings a),b) and c), respectively [30]. Surprisingly, the values are significantly lower than those reached in laboratory experiments. Causey et al. even stated, that achieving PRF larger than 1,000 in reactor conditions is impossible [17]. Experiments with unirradiated and irradiated Al_2O_3 and Macor samples were performed by A. Morono et al. [55]. After cleaning of the samples at 800 °C, deuterium gas was introduced and kept at constant pressure of 1.2 bar at room temperature. One set of samples was irradiated with 1.8 MeV electrons at a rate corresponding to 500 Gy/s, i.e. 10^{-10} dpa. Measurements of the two sample sets yielded enhanced deuterium absorption for Al_2O_3 as well as Macor. Furthermore, temperature increase for deuterium desorption from irradiated samples was observed during thermo stimulated desorption measurements. For temperatures below 450 °C, deuterium in Macor was trapped so deeply, that no deuterium release was recorded. Higher temperatures were needed to release the deuterium (see Figure 21).

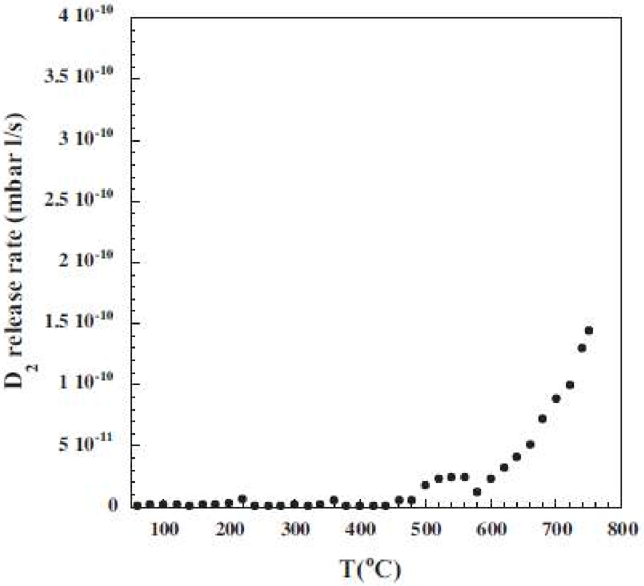

Figure 21: Deuterium release rates for irradiated Macor ceramics [55]

This indicates that radiation environment of breeding blankets has to be taken into account when classifying permeation barriers performance.

4.4 Methods of fabrication

Through the history of permeation barriers development, several deposition techniques have been tried. The most explored range of deposition techniques include

- physical vapor deposition - PVD
- chemical vapor deposition - CVD
- hot-dip aluminization - HDA
- electro chemical deposition - ECD(ECA/ECX)
- plasma spraying - PS

All these techniques fabricate separate protective layer over the substrate material, favourably uniform and homogenous over the whole surface. Detailed description of particular processes was given elsewhere numerous times (including [101]), therefore these techniques will be described only briefly. In addition, other methods have been used, based on changing the properties of the substrate to fulfil the desired requirements, e.g. plasma nitriding, ion implantation, carburizing/nitrocarburizing etc. Samples, presented in the experimental part of this thesis, were prepared by the means of PVD and nitriding, therefore they will be described with emphasis on the performed deposition and measurements.

4.4.1 PVD

PVD is a physical process of evaporation, sputtering or ionization through which the source material is converted to gaseous atoms, molecules or ions under the vacuum condition, and then deposited on the substrate. PVD has been confirmed as possible deposition technique for laboratory scales experiments, but certain disadvantages remain, which are responsible for limited employment of PVD for permeation barriers. These disadvantages may include nonuniform coating, difficult deposition on complex-geometry structures, poor bonding to the substrate etc. [75] Schematic arrangement of some PVD techniques is in Figures 22 and 23.

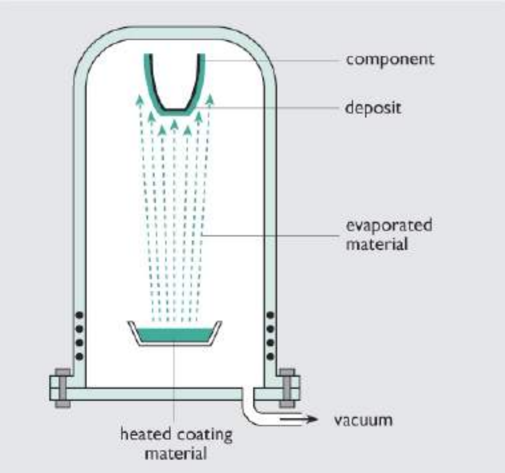

Figure 22: Evaporative PVD deposition [106]

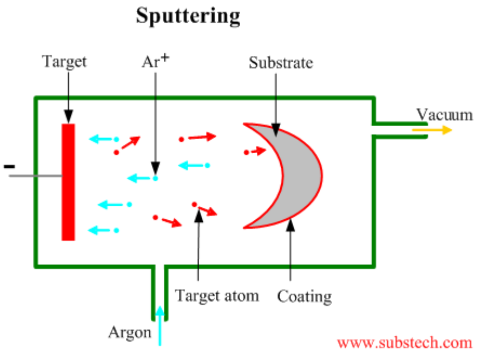

Figure 23: Sputtering PVD deposition [106]

4.4.2 CVD

CVD is a deposition process when the substance containing film composing element is firstly provided to the substrate, and then the solid film is formed via chemical reactions. The process is schematically shown in Figure 24.

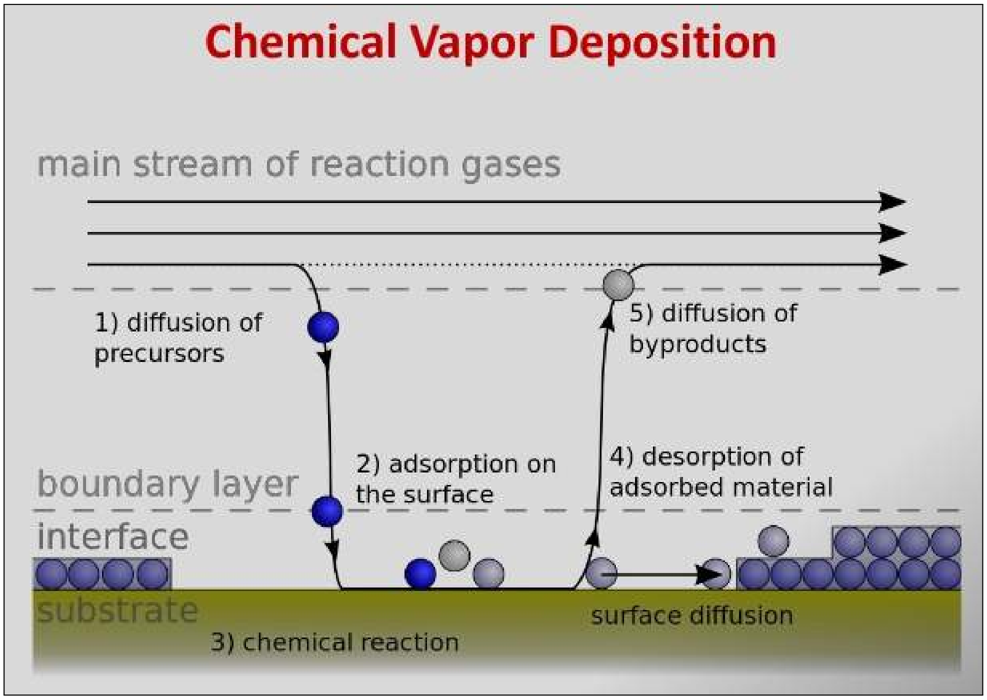

Figure 24: Chemical vapour deposition - scheme [94]

The deposition requires simple facility, it is possible to reach continuous and controllable film deposition and dense and uniform surface. Coating of structures with complex geometry is available using CVD. However, some materials are not suitable for standar CVD due to high temperatures involved, which negatively affect their mechanical properties. Therefore, advanced CVD techniques that enable coating at lower temperatures have been developed, for example metal organic chemical vapor deposition (MOCVD) or chemical vapor deposition in fluidized bed reactors (CVD-FBR). [75]

4.4.3 HDA

HDA is a preparation technique consisting of dipping the iron-based substrate into molten Al. After this, a layer of intermetallic Fe-Al phase is formed, which can be transformed into single- or multi-layered structure of FeAl and alumina oxides via thermal oxidation. HDA coatings can suffer from Kirkendall effects - formation of voids - which can lead to degradation of the coatings. Formation of voids can be suppressed by doping or hot isostatic pressing [75]. Hot isostatic pressing (HIP) is an established post-processing technique of porosity reduction and enhancement of mechanical properties by applying high pressures and temperatures. Several studies showed reduction of pore size and overall porosity, improvement in fatigue strenght and ductility, reduction of tensile strength etc. [97, 20, 51]

4.4.4 Electro chemical deposition

Electro chemical deposition is widely used in the industrial surface protection. The required facility is very simple and easy to operate, thickness and composition of the coating is easily controllable and coating of complex-geometry surfaces is available. This makes ECD a promising technique for tritium barriers preparation. However, for increasing of the ECD layers performance, the involment of thermal oxidation, annealing or HIP treatment is advised or neccessary [75]. A scheme for electro chemical deposition is in Figure 25. Deposition of fusion relevant materials (Al, W etc.) requires the use of specific electrolytes - so called aprotic (water free) electrolytes for Al, due to high electronegativity of Al, and ionic liquids (salts in liquid state) for W - for thermal and chemical stability, low vapour pressure and high electrical conductivity [75].

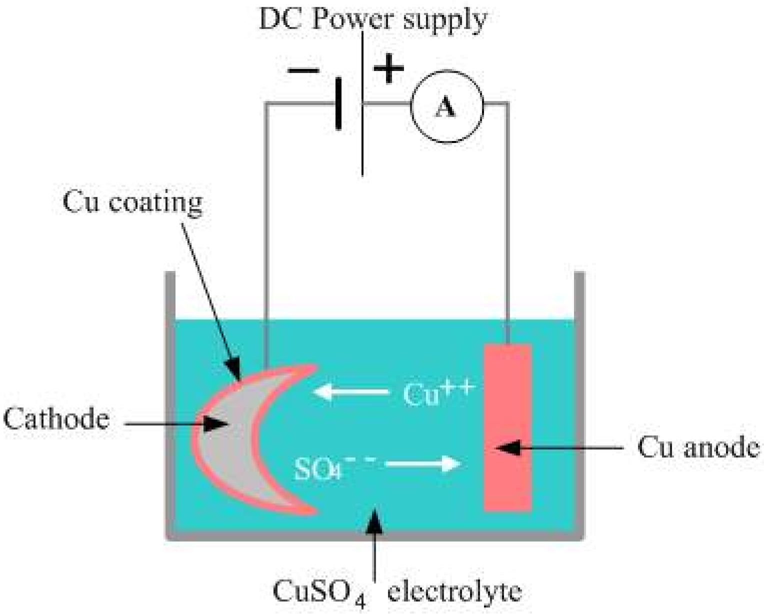

Figure 25: Electro chemical deposition [91]

4.4.5 Plasma spraying

Plasma spraying technique was used for example for fabrication of aluminide layers as permeation barriers. Al powder is introduced into plasma jet and molten or semi-molten particles (depending on their size) are sprayed on the surface. Subsequently, the impinged particles solidify and the resulting surface is composed (see Figure 26). [75]. Plasma spraying is capable of fast deposition, so the fabrication of thick layers is possible. However, the resulting coatings suffer from the presence of porosity, residual stresses and the need for "line-of-sight" deposition. Furthermore, during atmospheric plasma spraying, oxidation of fused particles might occur. This usually influence the coating negatively, but during the deposition of particular compounds (for example Al_2O_3), the coating is deliberately left to oxidize.

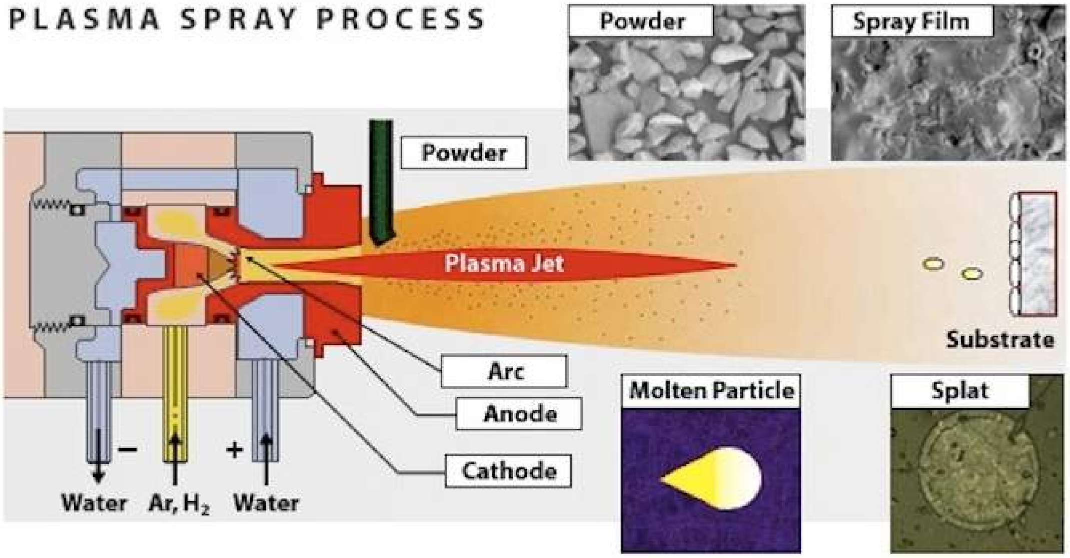

Figure 26: Plasma spraying [4]

4.4.6 Nitriding and carburizing

Nitriding is a thermochemical treatment that consists of the introduction of nitrogen into metallic material. According to the method of nitrogen introduction, several nitriding techniques are being distinguished:

- gas nitriding
- plasma/ion nitriding
- solid/liquid nitriding

Plasma nitriding is schematically shown in Figure 27.

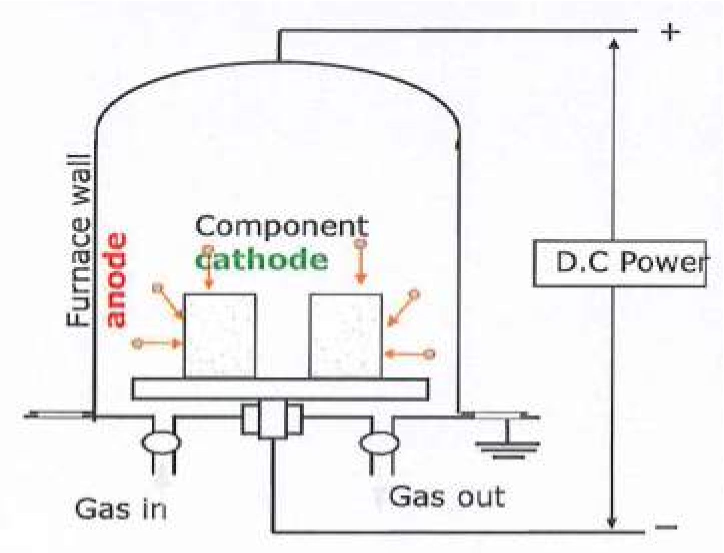

Figure 27: Plasma nitriding [13]

Gas nitriding is conducted at fixed temperature, submitting the samples to nitrogen containing atmosphere, commonly ammonia or various nitrogen mixtures e.g. H_2 and N_2; N_2, NH_3 and CO_2 etc. Ion/plasma nitriding uses a glow discharge to introduce nitrogen into the material, nitrogen ions are accelerated and impinge the surface. During solid nitriding, granulate containing nitrogen compound is used e.g. Fe_4KCN. The samples are surrounded by granulate and placed into heating oven for enabling the diffusion.

Gas and plasma nitriding are well established and widely used and researched techniques, however the required facility is complicated. During gas nitriding, temperature may affect the hardness of the nitrided material. Plasma nitriding is faster than conventional gas nitriding and promotes better control of the treatment parameters. This allows the control of the nitrided layer microstructure and also enables higher reproducibility of the results. Solid nitriding is a low-cost process in comparison to gas and plasma nitriding, when the only requirement is the furnace providing the heating. The heating generates atomic nitrogen, that is able to diffuse into the material.

Nitriding promotes higher hardness of the specimen, increases wear resistance, fatigue resistance, corrossion resistance and, as it was observed, some nitrided materials have favourable permeation properties. Regardless the used technique, surface cleaning of the samples is vital, because the contaminants can form a barrier preventing nitrogen from diffusing into the material. During the deposition, different layers are produced - diffusion and compound layer. Diffusion zone is a region characterized by solid solution in the original core microstructure with hardening precipitations. Compound layer consists of mixture of iron nitrides, in case of steel nitriding. In case of plasma nitriding, by controlling the process parameters, it is possible to determine the composition or even avoid the formation of the compound layer. [90]

Carburizing is analogous process of increasing the carbon content in the material. Carburizing is always carried out at elevated temperatures, as the carbon solubility in high temperature iron modification - austenite - is higher than in ferrite. Typical treatment temperatures are 850 - 950 °C. Similarly to nitriding, one can distinguish several techniques according to the carbon containing medium - gas, liquid and solid carburizing. For gas carburizing, atmosphere containing methane or propane is used, with neutral carrier gas added, usually a mixture of N_2, H_2, CO, CO_2 and CH_4. Liquid carburizing is usually carried out in cyanide salts baths - cyanide-chloride-carbonate mixtures. The solution is highly toxic and during the deposition, small amount of nitrogen is introduced to the material too. During solid (pack) carburizing, samples are usually surrounded by coke or charcoal mixed with barium carbonate, see Figure 28.

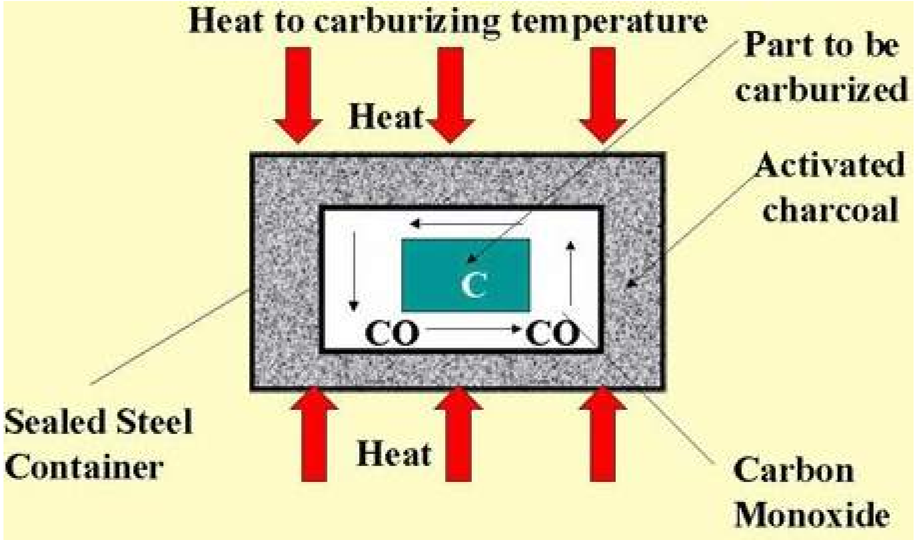

Figure 28: Pack carburizing [14]

Pack carburization is the least sophisticated technique and therefore remains widely used, although the liquid carburization is the fastest. The deposition times reach from 4 to 36 hours for several millimetres of carburized layer. However, it is applicable only for small components and the toxicity remains an issue [9]. Carburizing increases the wear resistance of the sample, fatigue strength and toughness is improved as well. The increase is dependent on the substrate composition. The depth of hardening due to carburizing is usually from 0.1 to 3 millimetres. Before the deposition, the samples should be cleaned and free from stress. Carburizing also causes small changes of sample dimensions, which has to be taken into account. The adherence of the layer is very good [10].

In addition to these two techniques, modification of each of them has been developed and used: carbonitriding and nitrocarburizing. Carbonitriding is a form of carburizing: ammonia is introduced into carburizing atmosphere in order to add nitrogen into the diffusion layer. This results in shallower affected depths than by carburization, as nitrogen inhibits the diffusion of carbon. Carbonitriding is performed at lower temperatures than carburizing, due to thermal decomposition of ammonia. The addition of nitrogen enhances hardenability, increases the resistance to softening and further enhances wear resistance (in comparison to carburizing).

Nitrocarburizing, on the other hand, is a modification of nitriding: carbon is introduced into the steel simultaneously with nitrogen below the temperature of austenite growth. Nitrocarburizing is typically carried out at temperatures slightly higher than nitriding, ca. 550°C - 600°C, in atmosphere containing CO_2, endothermic gas or air. Diffusion layer formed during the deposition increases hardness and improves fatigue properties, corrossion and wear rate etc. [11, 12].

5 EXPERIMENTAL PART

Experimental part of my thesis consists of 2 major topics:

- preparation, remelting and characterization of plasma sprayed ceramics coatings
- preparation and permeation measurements of thin nitride layers

The part dedicated to plasma sprayed coatings is an extension of a previous study [89]. Further experiments with plasma sprayed alumina were performed, in order to improve critical properties of the coatings, mainly cracks, eventually surface roughness, homogeneity or remelting depth. A rather broad matrix of experimental conditions was explored, and the effects of selected experimental parameters were evaluated. The characterization focused on the surface morphology and structural observations on cross section by SEM.

The latter part includes fabrication of very thin surface layers by physical vapour deposition (PVD), diffusion-based nitriding and carbonitriding. After literature survey, a series of less frequent but promising nitrides was chosen, e.g. CrN, ZrN, WN... Several µm thin layers were deposited on EUROFER97 substrate. The characterization included surface and cross section SEM evaluation, adhesion measurements by a scratch test, phase analysis and stress measurement by x-ray diffraction (XRD). The key characteristic included in the study was the permeation reduction factor (PRF) for hydrogen.

5.1 Plasma spraying & remelting

Motivation of the study is growing interest in oxidic ceramic layers towards their application in nuclear facilities. Facilities utilizing thermonuclear fusion could suffer from hydrogen-isotopes leaks (permeation) even without structural defects. The permeation should be mitigated because of economical and environmental reasons. Oxidic ceramics have favourable properties regarding application as a permeation barrier and plasma spraying is fast and simple deposition method. However, because of certain properties of plasma sprayed coatings (e.g. significant porosity and rough surface), a suitable post-treatment is neccessary. In this work, electron beam remelting was studied as a prospective technique for porosity elimination.

5.1.1 Previous study

Previous remelting study was performed in July 2015 [89]. Total number of 31 Al_2O_3 samples were prepared in three different thicknesses - 100, 200 and 300 µm. As it was the first attempt in electron beam remelting of ceramics coatings and one of the main aims of the study was to remelt the coating completely, majority of the samples had 100 µm thickness. The main parameters varied during the experiments were electric current of the beam, velocity of the sample movement and number of beam passes over the sample in one treatment. All these parameters influence the amount and time dependence of the energy delivered on the sample. Moderate success was achieved - the ability to reach beneficial changes in the surface roughness, microstructure, phase constitution and hardness by electron beam remelting was confirmed. However, the resulting surface smoothness and thickness of the remelted layer did not reach the expected values. Also the number of cracks was excessive and the level of homogenity was insufficient. A theory of thermal barrier was established - thicker coating was observed to act as a thermal barrier, preventing heat conduction into the substrate and improving the remelting conditions in the surface layer. Higher beam current resulted in thicker remelted layer and the level of surface remelting increased, also the homogeneity was increased, but the results were different for various thickness. Simillar results were reached for lower sample velocities while keeping the current constant. Double treatment of the samples was usually beneficial for lower combinations of current and velocity, but experiments with higher power degraded the coating. Nevertheless, the ultimate goal was not reached - smooth surface without defects and sufficiently thick remelted layer was not identified on any sample. Therefore, continuation of this study was planned and performed, with the objective to provide longer cooling time for the samples. Too high cooling rate for remelted ceramics was assumed to be the main reason for the surface cracks and defects.

5.1.2 Substrate and deposition parameters

Plasma spraying of ceramic coatings was performed at Laboratory of Plasma Technologies of Institute of Plasma Physics AS CR v.v.i. in Prague. General principle of plasma spraying was already mentioned in section 4.4.5. For our specimens, water stabilized plasma (WSP) torch was used. Its main parameters are listed in Table 1. The plasma torch and scheme of its internal configuration are displayed in Figure 29. Alumina samples were deposited on ordinary steel with dimensions 2.5x25x100 mm. The substrate was grit blasted and pre-heated to 100 °C before the deposition. Feed rate was 5 kg/h, spraying distance 360 mm. In total, 9 deposition cycles were performed with interpass temperature of 120 °C. Samples of two nominal thicknesses were prepared - 100 and 300 µm.

5.1.3 Electron beam remelting

After the deposition, samples were post-treated by electron beam remelting. This technique was also employed in previous research report [89]: by exposing the surface to the electron beam of sufficient power, the coating receives enough energy for melting. After the exposure, the sample cools down, causing the coating to solidify again and possibly recrystallize. During this process, there is a possibility of forming denser and more homogenous layers than during initial cooling after deposition, as well as reaching different phases of coating material (e.g. α/γ Al_2O_3). Remelting of the samples was performed at VUT in Brno, using electron beam facility of the NETME center - K26 15-150 ProBeam, with maximal input power of 15 kW at 150 kV and 100 mA [89, 6]. For post-analysis, primarily the scanning electron microscope (SEM) at IPP in Prague was used. All photos using secondary (SE) or backscattered electron (BSE) mode were taken there.

Table 1: Parameters of WSP-H torch at IPP in Prague [7]

Power	80 - 160 kW
Current	300 - 500 A
Voltage	270 - 320 V
Operation limits	up to 12 hours continuously
Deposition rate	$\geq$ to 30 kg/h
Plasma source	H_2O + Ar
Cooling water consumption	3 l/h
Plasma temperature	25,000 K

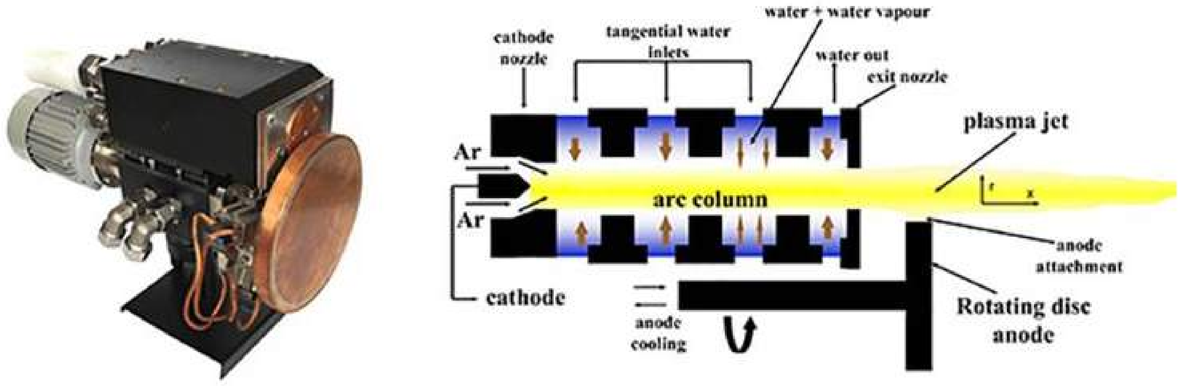

Figure 29: WSP-H torch (left) and its internal configuration [5]

Parameters of the remelting were chosen with respect to the experience obtained in the previous study [89], mentioned in section 5.1.1. The goal of the experiments remained indentical: identifying the parameters for smooth and defect-free surface and remelting of the whole plasma sprayed layer. The aim of the current study was to improve the results of experiments from [89].

The present study consisted of 41 samples, prepared in 4 sets. Designation of samples consists of order of the day in experimental campaign and order of the sample in particular day, e.g. 1.2 - second sample produced on first day. The remelting parametres are listed in Tables 2 and 3. Voltage of the beam was set to 20 kV for all specimens.

Table 2: Parameters of remelting, sets 1-3. d - coating thickness, I - remelting current, v - beam velocity, f - frequency of the beam, n - number of beam passes

Specimen	d [µm]	I [mA]	v [mm/s]	f [kHz]	n [-]
1.0	300	9	20	10	2 (5s delay)
1.1	300	9	20	10	2 (45s delay)
1.2	300	9	20	10	5 (5s delay)
1.3	300	9	20	10	5 (45s delay)
1.4	300	5	20	10	2 (45s delay)
1.5	300	9	20	10	2 (45s delay)
1.6	300	9	20	10	2 (180s delay)
1.7	300	9	20	10	5 (180s delay)
2.1	300	5	20	10	1
2.2	300	5	20	1	2 (45s delay)
2.3	300	5	20	1	1
2.4	300	5	100	10	1
3.0	300	10	100	0.1	1
3.1	300	10	100	10	1
3.2	300	15	100	10	1
3.3	300	10	100	1	1
3.4	300	15	20	10	1
3.5	100	5	20	10	1
3.6	100	7	20	10	1
3.7	100	9	20	10	1
3.8	100	5	20	10	2 (45s delay)
3.9	100	7	20	10	2 (45s delay)

Table 3: Parameters of remelting, set 4. d - coating thickness, I - remelting current, v - beam velocity, f - frequency of the beam, n - number of beam passes

Specimen	d [µm]	I [mA]	v [mm/s]	f [kHz]	n [-]
4.1	100	3	20	10	1
4.2	100	5	40	10	1
4.3	100	5	60	10	1
4.4	100	7	40	10	1
4.5	100	7	60	10	1
4.6	100	15	100	10	1
4.7	100	10	100	10	1
4.8	100	10	100	1	1
4.9	100	10	100	0.1	1
4.10	100	5	100	0.1	1
4.11	300	20	100	10	1
4.12	300	15	100	1	1
4.13	300	5	100	0.1	1
4.14	300	3,5,7	100	10	3 (45s delay)
4.15	300	7,5,3	100	10	3 (45s delay)
4.16	100	7,5,3	100	10	3 (45s delay)
4.17	100	3,5,7	100	10	3 (45s delay)
4.18	100	3	20	1	1
4.19	100	5	20	1	1

During sets 1 and 2, 300 µm samples were used and the parameters were derived from the most successful samples from [89]. The aim was to reach the complete remelting. After the examination of samples, the level of remelting was not as high as was expected, therefore the 300 µm samples were used only for comparison with previous results and for the rest of experiments, 100 µm samples were used. It was presumed, that it would be easier to reach complete remelting. Apart from the previous study, multiple treatments with the same setting were used only in the first set, where the depth was not significantly improved, and for several samples of set 4. Power of these samples was varying between the passes, but with the selected parameters, the results were not satisfactory. Also, a new parameter of the electron gun was changed - perpendicular frequency of the beam. The electron beam was moving perpendicularly to the sample movement, with the frequency usually in the range of several kHz. By changing the frequency, the time spent on a particular place of the sample and the repetition rate of heating is changed and therefore can influence the remelting.

5.1.4 Results

Overall result of the remelting experiments was 20 samples affected by the remelting to the extent that did not exclude possible use as a permeation barrier - showing desirable surface modification without severe defects. During sets 1 to 3, these were used as base samples for the following experiments. The rest of the samples was either unaffected/slightly affected by the remelting or over-remelted. The under-remelted samples showed coarse surface with various degree of partial remelting, not covering the majority of the area. The reasons were either low beam power, high beam frequency or high velocity of the samples. Characteristic feature of the over-remelted samples was revealed substrate - either the coating delaminated or the remelted layer re-solidified forming depressions on the surface. In the centre of such depressions, as-sprayed coating or substrate was revealed. Samples, which were considered as successful, showed smooth surface and predominantly continuous remelted layer. However, particular imperfections remained e.g. uneven remelted surface, varying remelted thickness, cracks etc.

Thickness of the remelted layer and the whole layer remaining after the remelting was measured on the successful samples. The results, including estimated thickness of as-sprayed layer, ratio of remelted and deposited/remaining layer, are summarized in Table 4. $\mathrm{d_{ini}}$ is a nominal thickness, expected to be reached after the deposition. Deposition parameters were set to achieve this goal, however the actual thickness was not measured routinely, so it may have varied slightly around these values. $\mathrm{d_{rem}}$ and $\mathrm{d_{tot}}$ are values measured on samples from Table 4. The mean and standard deviation were calculated based on six measurements from representative areas of the samples.

Table 4: Successfully remelted Al_2O_3 samples, d_{ini} - initially deposited layer thickness, d_{rem} - average remelted layer thickness, d_{tot} - average remaining layer thickness, r_{rem} - ratio of remelted and remaining layer thickness, r_{dep} - ratio of remelted and deposited layer thickness. Samples with superscript * reached the best surface conditions after remelting.

Sample	d_{ini} [µm]	d_{rem} [µm]	d_{tot} [µm]	r_{rem} [-]	r_{dep} [-]
3.4^*	300	226±46	252±48	0.9	0.75
3.7	100	65±24	83±24	0.78	0.65
3.6	100	59±8	80±12	0.74	0.59
3.9	100	68±18	102±21	0.67	0.68
4.19	100	49±12	74±14	0.66	0.49
1.3^*	300	102±57	156±57	0.65	0.34
3.5	100	32±17	51±21	0.63	0.32
3.8	100	63±36	103±43	0.61	0.63
2.2^*	300	178±33	297±40	0.6	0.59
2.3	300	172±26	295±30	0.58	0.57
4.4	100	53±14	95±21	0.56	0.53
1.0^*	300	144±24	296±27	0.49	0.48
1.1^*	300	118±14	270±22	0.44	0.39
2.1	300	92±12	252±22	0.37	0.31
4.11	300	71±16	204±26	0.35	0.24
1.5^*	300	96±14	287±26	0.33	0.32
4.12	300	63±26	200±32	0.32	0.21
3.2	300	58±12	194±25	0.3	0.19
1.6^*	300	89±18	324±23	0.28	0.3
1.4^*	300	76±15	330±30	0.23	0.25

The samples are ordered according to the ratio of remelted and total thickness remaining after the remelting.

Cross section SEM photos of the samples with the highest ratio demonstrate success of the remelting, but also display some imperfections (figures 30 to 33). In Figure 33, individual layers of the remelted sample are distinguished.

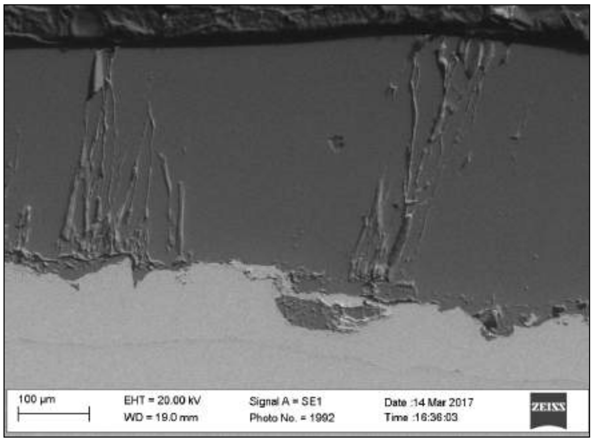

Figure 30: Sample 3.4 - cross section, ratio of remelting 0.9

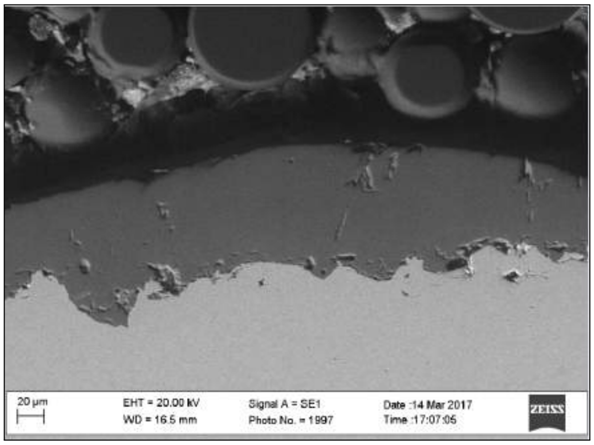

Figure 31: Sample 3.7 - cross section, ratio of remelting 0.78

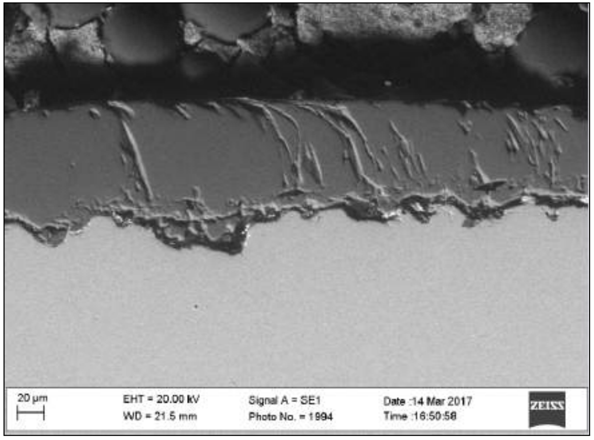

Figure 32: Sample 3.6 - cross section, ratio of remelting 0.74

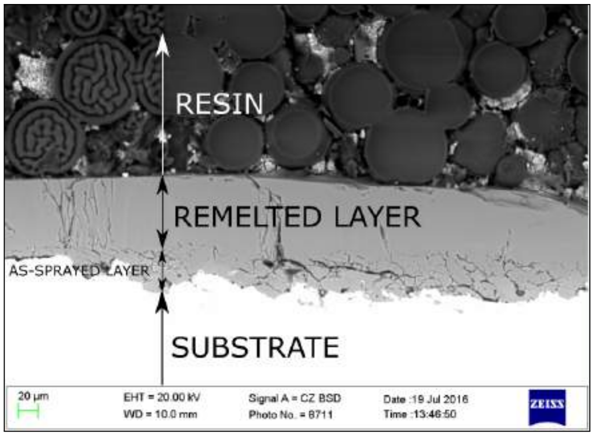

Figure 33: Sample 3.9 - cross section, ratio of remelting 0.67

Majority of the most remelted samples show cracks, reaching from the surface to the unmelted material. These cracks are visible in Figure 33. Such cracks would lower the permeation protection and therefore should be eliminated. In addition, the remelted layer was sometimes uneven and thickness of particular samples varied noticeably. This can be seen for example in Figure 32 but more clearly on less successful samples, for example Figures 34 or 35.

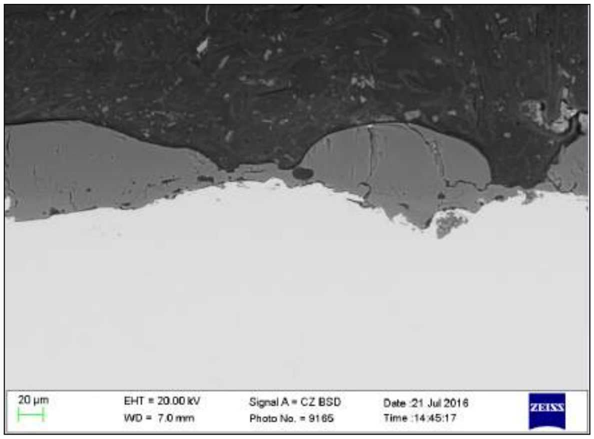

Figure 34: Sample 4.19 - cross section, uneven layer with severe cracks

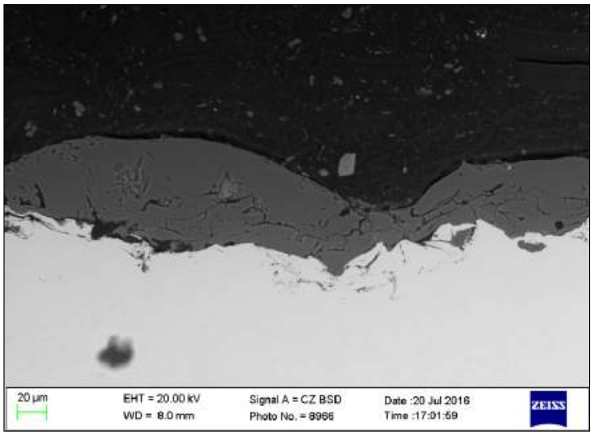

Figure 35: Sample 4.2 - cross section, uneven layer with large depression

In Figure 34, another phenomenon is visible - the as-sprayed layer is at some places almost completely removed by the remelting, forming blob-like structure. Similar results can be seen in Figures 36 and 37.

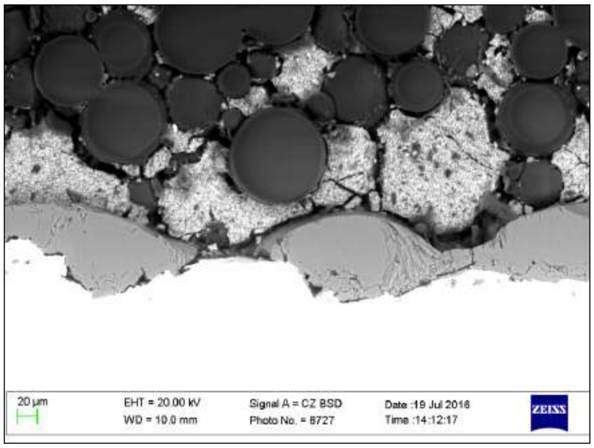

Figure 36: Sample 3.6 - cross section, blob-like structure

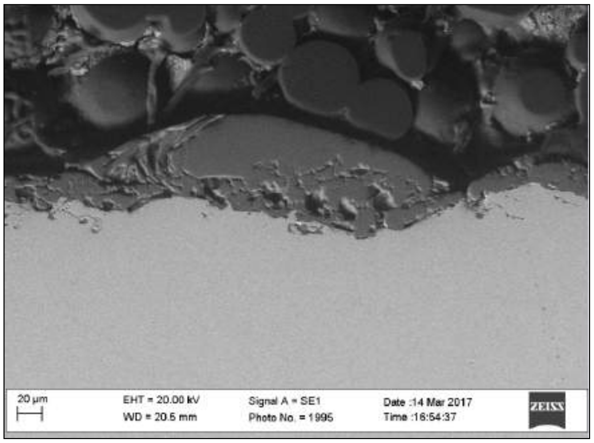

Figure 37: Sample 3.5 - cross section, blob-like structure

Delamination of the remelted layer and massive presence of cracks can be seen on numerous samples. Cross sections are displayed in Figures 38 and 39.

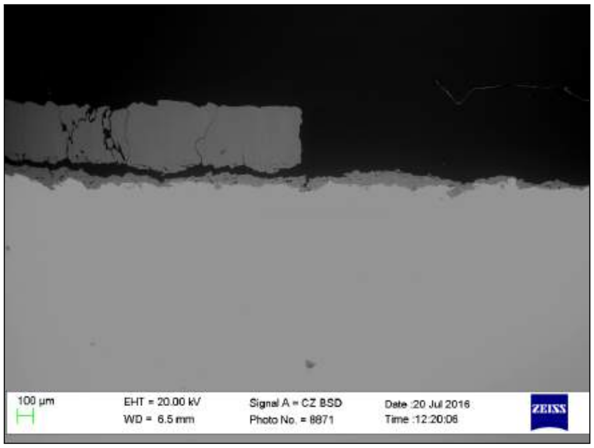

Figure 38: Sample 1.2 - cross section, delamination of the layer

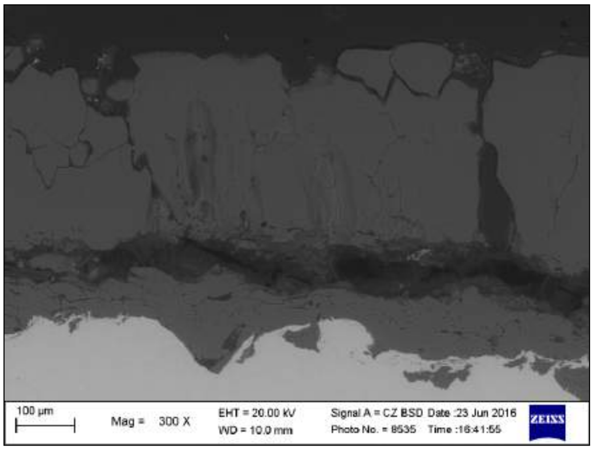

Figure 39: Sample 1.3 - cross section, cracks and spalling off

As mentioned above, majority of the samples remained below desired surface conditions. Half of the samples was fully or partially unremelted. Unremelted samples preserved structure typical for plasma sprayed layers, with significant degree of porosity and rough surface. This can be seen from Figures 40 and 41. Samples 4.13 and 4.16 were remelted using I = 5 mA and v = 100 mm/s, which proved to be insufficient.

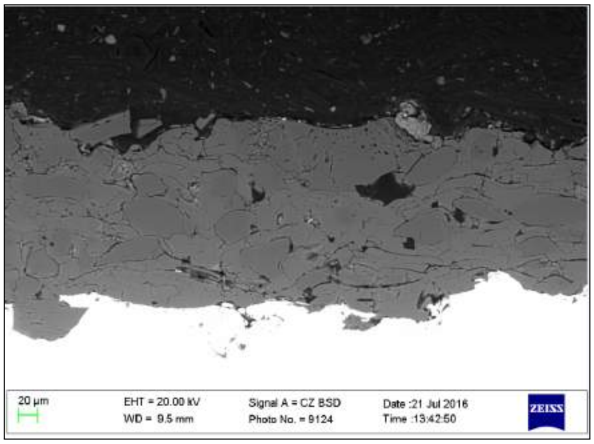

Figure 40: Sample 4.13 - cross section, unaffected sample, high velocity and low current

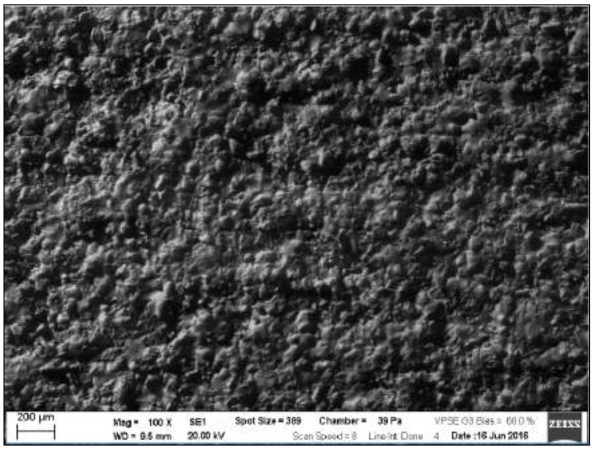

Figure 41: Sample 4.16 - surface, unaffected sample, repeated remelting with high velocity and decreasing current

Samples that reached only partial remelting but were obviously affected can be divided into four groups, depending on the extent of remelting. Representatives from these groups are displayed in Figures 42 to 45 in order of increasing degree of remelting.

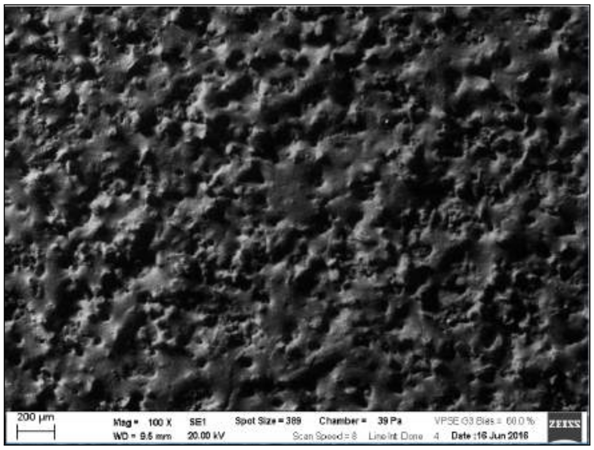

Figure 42: Sample 4.8 - surface, very low degree of remelting

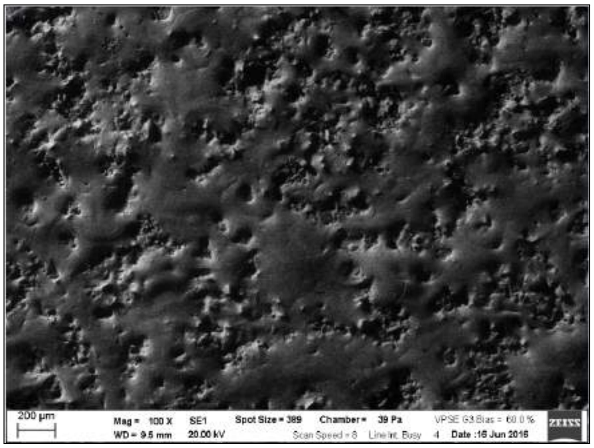

Figure 43: Sample 4.2 - surface, low degree of remelting

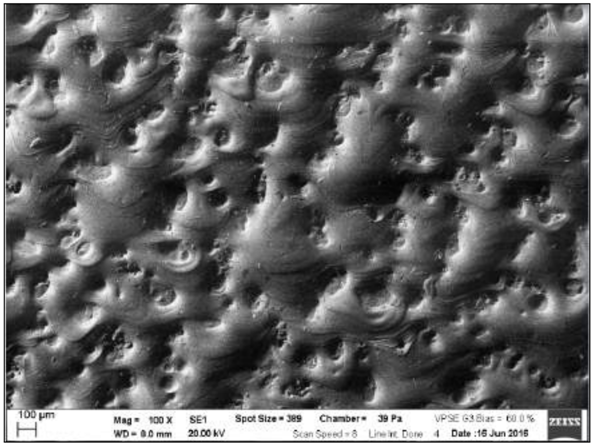

Figure 44: Sample 3.6 - surface, moderate degree of remelting

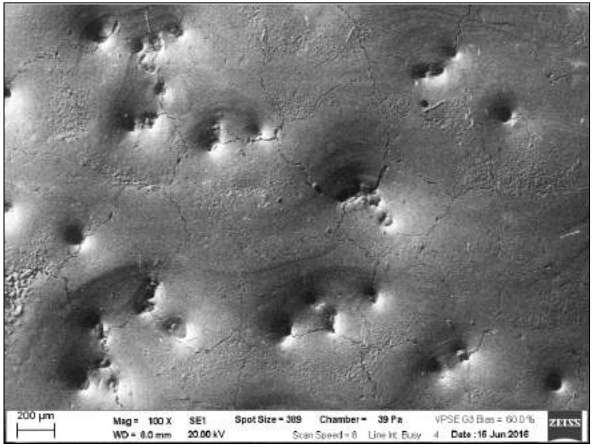

Figure 45: Sample 2.3 - surface, high degree of remelting

The sample are characterized by decreasing velocity - 100 mm/s for sample 4.8, 40 mm/s for sample 4.2 and 20 mm/s for samples 3.6 and 2.3. In addition, sample 2.3 had thickness 300 µm. Surface of sample 2.3 is considerably smoother than the previous samples, but some depressions are still remaining, therefore smoother samples were chosen as the successful ones. Sample 2.3, and to lesser extent sample 3.6 as well, show the unfortunate presence of cracks. For better recognition, images taken by backscattering detector (BSE) can be displayed - Figures 46 and 47. From these Figures it can be noted, that some depressions on sample 3.6 revealed the substrate, while on sample 2.3, the coating was still contiguous.

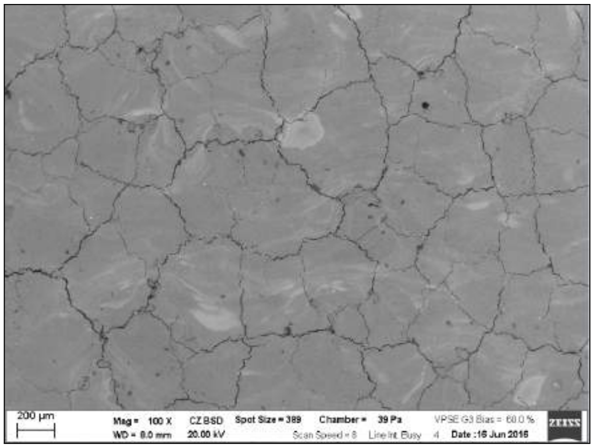

Figure 46: Sample 2.3 - surface BSE, cracked surface but substrate not revealed

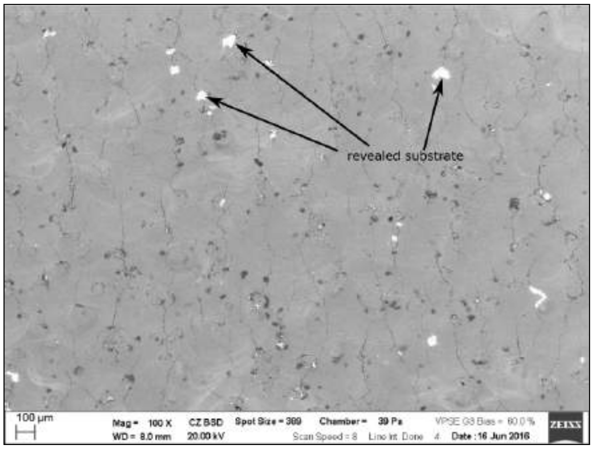

Figure 47: Sample 3.6 - surface BSE, partly revealed substrate

Cracks remained indeed a severe problem. All samples exhibited cracking, to lesser or greater extent. Some other defects emerged, degrading the surface quality. Namely serious delamination or over-melting, revealing part of the substrate (figure 48), or remelting with too low beam frequency, creating characteristic pattern of beam motion on the samples surface - Figure 49. Confirmation of revealed substrate can be seen from BSE photos - Figures 50 and 51.

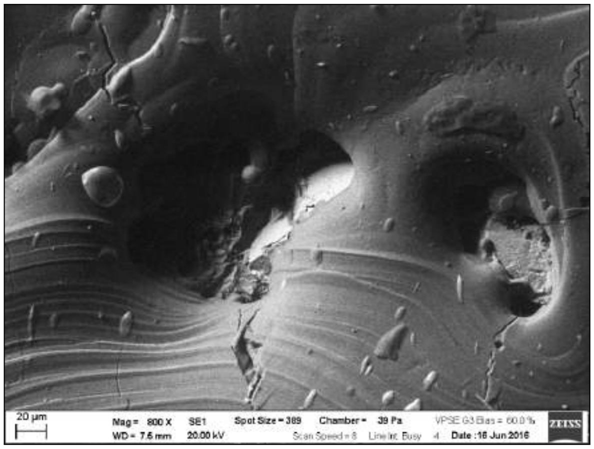

Figure 48: Sample 3.7 - surface

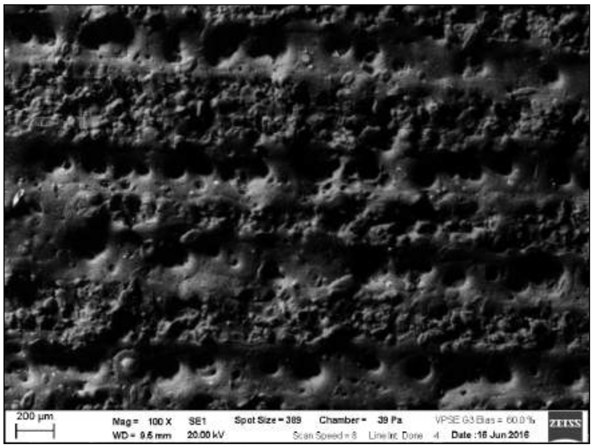

Figure 49: Sample 4.9 - surface, beam pattern, f = 100 Hz

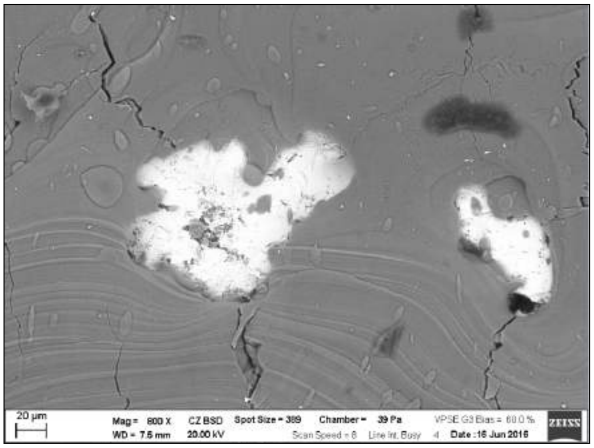

Figure 50: Sample 3.7 - surface, BSE

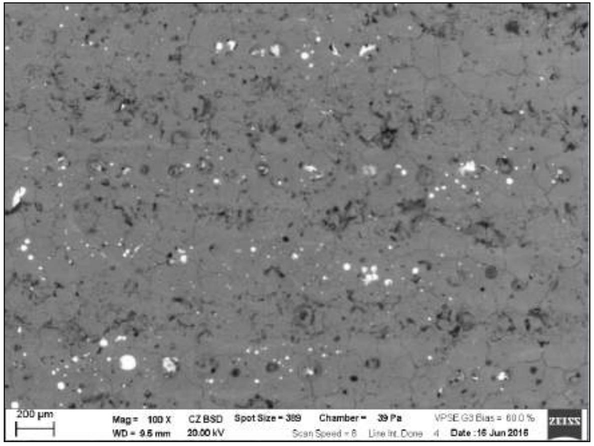

Figure 51: Sample 4.9 - surface, BSE

As can be seen from Table 4, the only samples that reached sufficient surface quality and remelting thickness are samples 3.4 (figure 52) and 2.2 (figure 53). Sample 2.2 exhibited slightly better surface conditions, but reached only 60% remelting, while sample 3.4 reached 75% remelting (90% if calculated from the thickness remaining after the remelting). Other representatives of reasonably well remelted surface are in Figures 56 and 57.

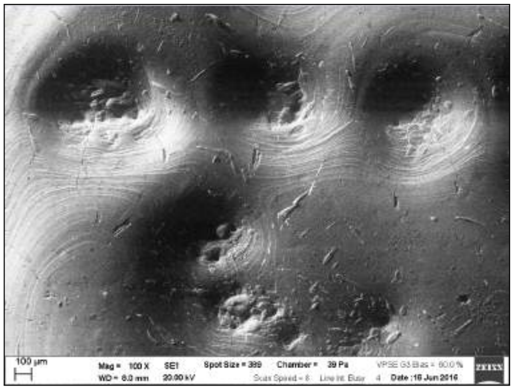

Figure 52: Sample 3.4 - surface

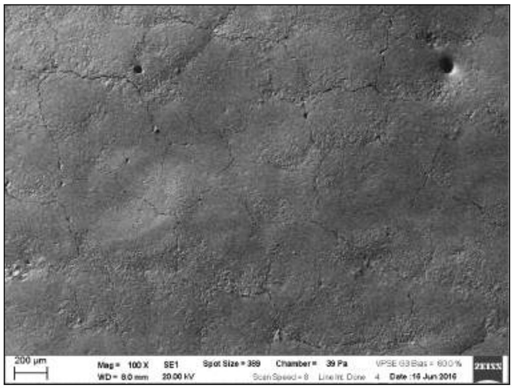

Figure 53: Sample 2.2 - surface

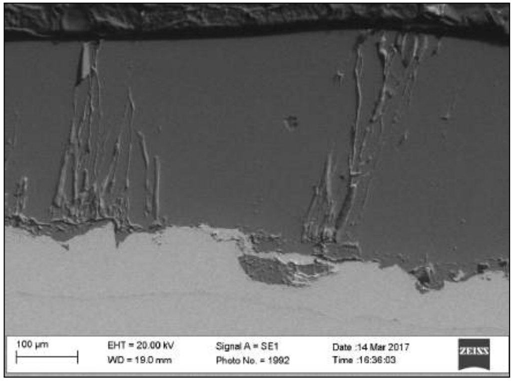

Figure 54: Sample 3.4 - cross section

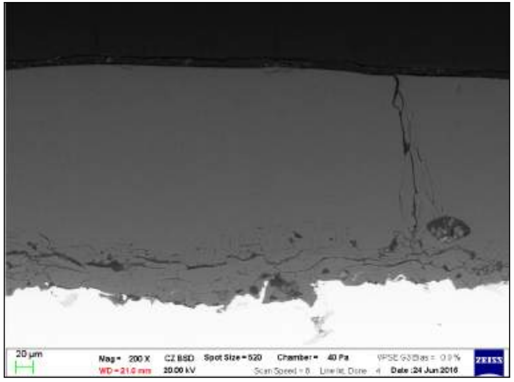

Figure 55: Sample 2.2 - cross section

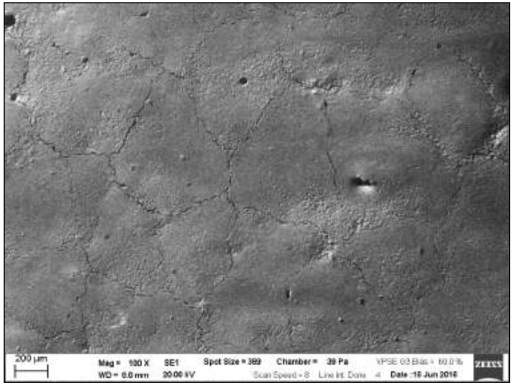

Figure 56: Sample 1.4 - surface

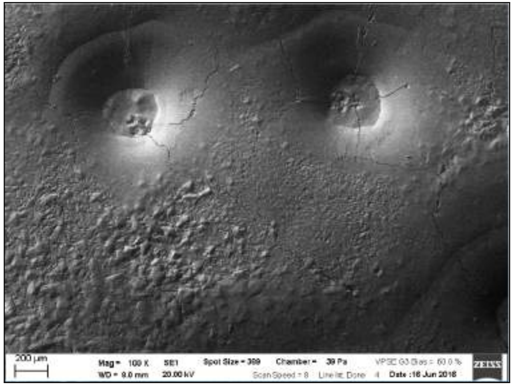

Figure 57: Sample 1.6 - surface

During the study, the parameter space was explored extensively and significant dependencies between the remelting parameters and characteristic of the resulting layer were observed. For example samples 3.6 and 3.9 or 3.5 and 3.8 differ only in number of beam passes - 3.6 and 3.5 were treated with one pass, 3.9 and 3.8 with two passes. Cross section photos of samples 3.6 and 3.9 were already displayed above - Figures 32 and 33. Surface photo was displayed only for sample 3.6, therefore for better comparison, surface photos are displayed in Figures 58 and 59.

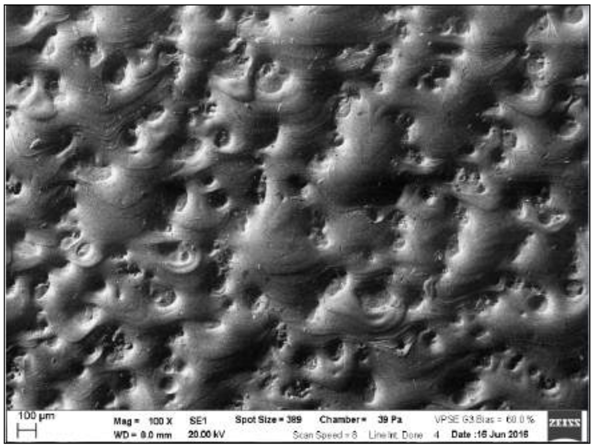

Figure 58: Sample 3.6 - surface, 1 beam pass

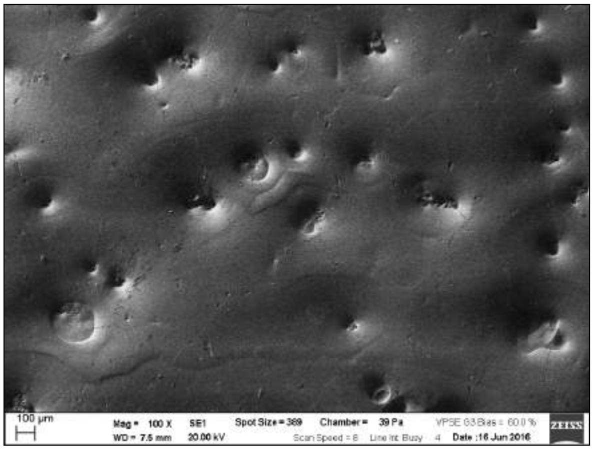

Figure 59: Sample 3.9 - surface, 2 beam passes

Cross section photos reveal more even and thicker layer of sample 3.9, not only remelted but also total thickness was higher after repeated remelting. Remelted depth increase is a beneficial effect of repeated remelting, as well as smoother surface with lower number of depressions, as can be seen in Figures 58 and 59. The same trend can be seen on samples 3.5 and 3.8, these samples are only remelted to lesser extent, as they were subjected to lower power - Figures 60 to 63.

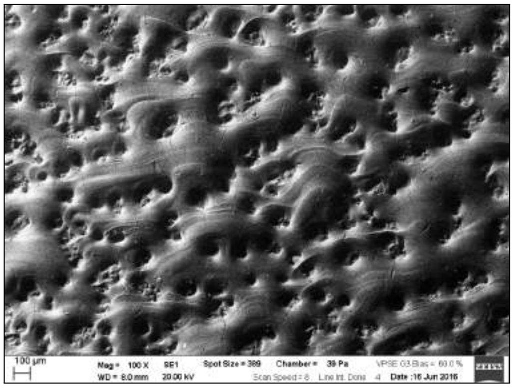

Figure 60: Sample 3.5 - surface, 1 beam pass

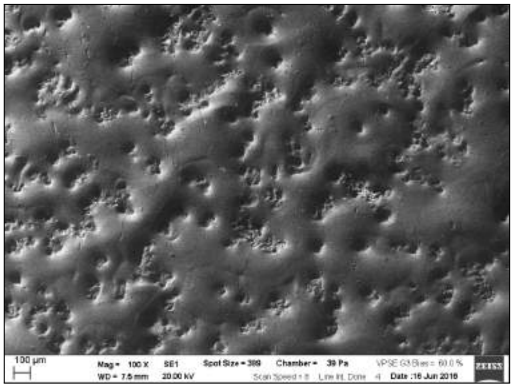

Figure 61: Sample 3.8 - surface, 2 beam passes

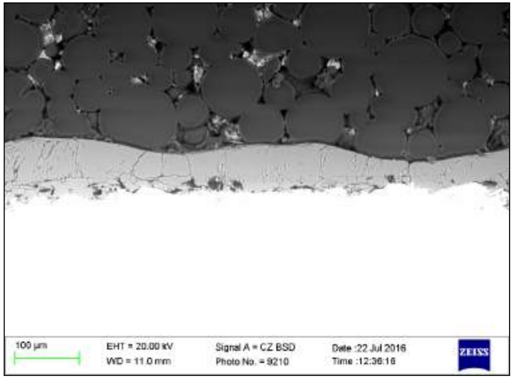

Figure 62: Sample 3.5 - cross section

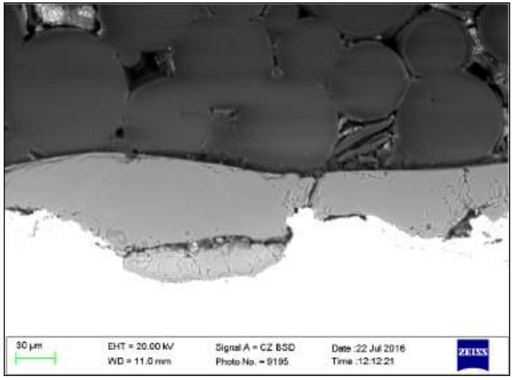

Figure 63: Sample 3.8 - cross section

However, in another set of samples with multiple treatment, namely 1.0+1.2, 1.1+1.3 and 1.6+1.7, such improvement was not observed. One sample of each pair was treated twice, the second one five times, with increasing delay between beam passes - 5, 45 and 180 seconds. All samples were treated with moderate power, I = 9 mA, and low velocity, v = 20 mm/s. Improvement in surface properties was observed rarely, all samples had quite coarse surface, overmelting, delamination and minor or major depressions were observed on the surface. Possible improvement can be identified comparing samples with same number of treatments - with increasing delay, the surface became smoother, however did not reach the desired level of smoothness. Regarding the cross section, the results can be summarized similarly - increasing the number of the treatments yielded worse results, lengthening the delay yielded better results. It may be connected with the power delivered to the samples; it was 33% to 100% higher than on samples 3.5 to 3.9, although the thickness was 300 µm, compared to 100 µm. Surface photo of sample 1.7 is in Figure 64, cross section in Figure 65.

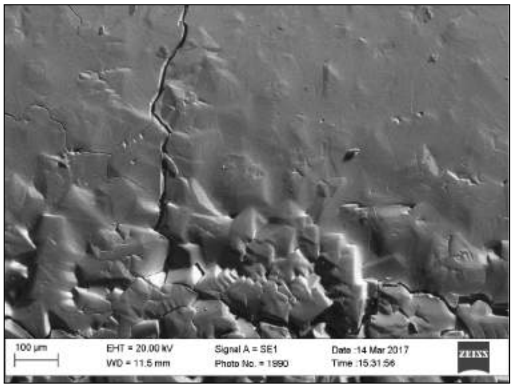

Figure 64: Sample 1.7 - surface, 5 beam passes, 180 s pause

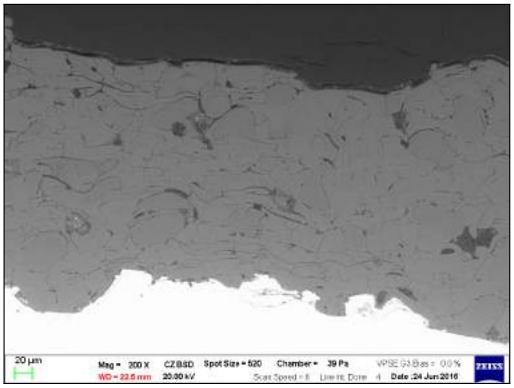

Figure 65: Sample 1.7 - cross section

During the experiments, particular interest was put on a new parameter - frequency of the beam. Sequences of samples 4.9+4.8+4.7 and 3.0+3.3+3.1 were prepared on 100 µm and 300 µm samples, respectively, under identical conditions with variable frequency - 0.1, 1 and 10 kHz. Surface photos of Figures 4.8 and 4.7 are displayed in Figures 66 and 67, surface photo of sample 4.9 was already displayed above at Figure 49.

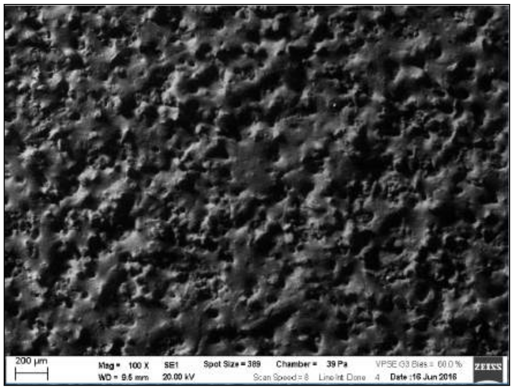

Figure 66: Sample 4.8 - surface, f = 1 kHz

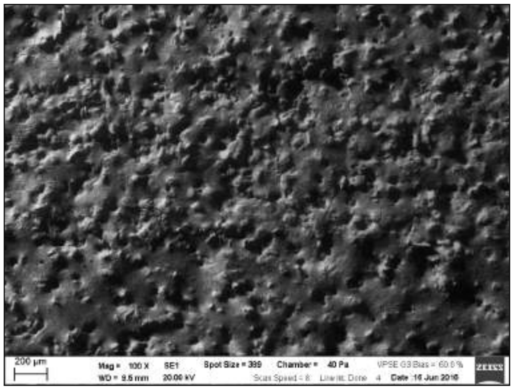

Figure 67: Sample 4.7 - surface, f = 10 kHz

Based on the surface photos, two conclusions can be made - 100 Hz frequency is too low for successful remelting (at least in connection with this particular current and velocity - 10 mA and 100 mm/s) and with increasing frequency, the smoothness and homogeneity of the surface is increasing. In Figure 49, periodical structure of overmelted and unaffected areas is displayed, caused by rather high velocity of the sample and rather low frequency of the beam. Surface photo of sample 3.0 is not preserved, however, sample 4.13 was prepared under similar conditions as sample 3.0, only with half the current, i.e. the power. Therefore, based on this sample, where the pattern is observed, one can assume that with higher power, same result would be gained.

Comparing 1 kHz and 10 kHz samples, 10 kHz samples seem to reach slightly smoother surface with higher ratio of remelted area. Among 100 µm and 300 µm samples, no significant differences were identified regarding both surface as well as the cross section. Samples were barely affected by remelting, only thin surface layer was remelted.

Figures 68 to 77 display comparison of surface and cross section photos for samples with the same power but different velocity. Samples 3.5 (20 mm/s), 4.2 (40 mm/s) and 4.3 (60 mm/s) had initial thickness 100 µm, 2.1 (20 mm/s) and 2.4 (100 mm/s) had 300 µm. All samples were remelted using I = 5 mA. From the Figures it is obvious that lower velocity has beneficial effect on the remelting - the surface is smoother and thickness of the remelted layer is increasing. Sample 4.3 showed almost no remelting effect, similarly to sample 2.4. However, the latter sample showed slight effect, even though the surface remained predominantly rough. This supports the hypothesis that thicker as-sprayed layer of Al_2O_3 may operate as a thermal barrier, concentrating the laser heat on the surface and promoting the remelting. Comparison of samples 3.5 and 2.1 supports this theory, as these samples differ only in the thickness - surface of sample 2.1 is smoother and contains less depressions. Thicker as-sprayed layer isolates the surface and promotes the remelting, therefore higher degree of remelting can be achieved. This seems to affect only surface conditions, thickness of the remelted layer seems to remain similar.

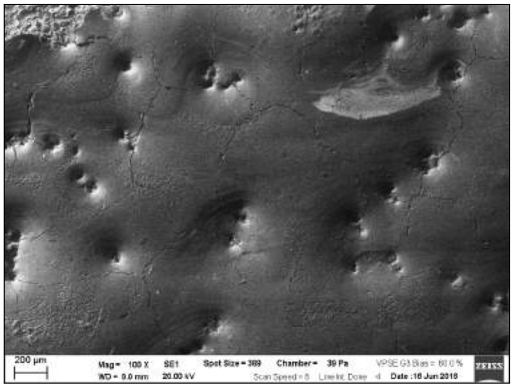

Figure 68: Sample 2.1 - surface, 300 µm as-sprayed, v = 20 mm/s

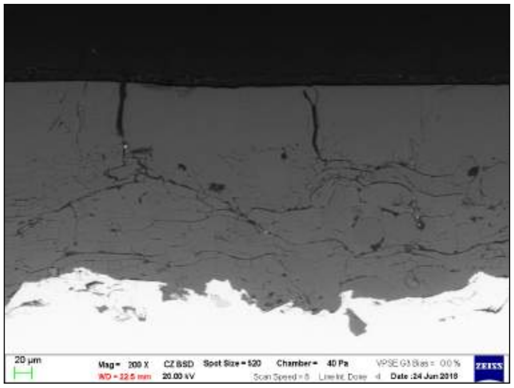

Figure 69: Sample 2.1 - cross section

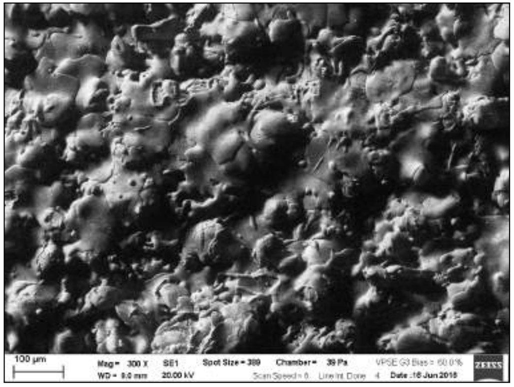

Figure 70: Sample 2.4 - surface, 300 µm as-sprayed, v = 100 mm/s

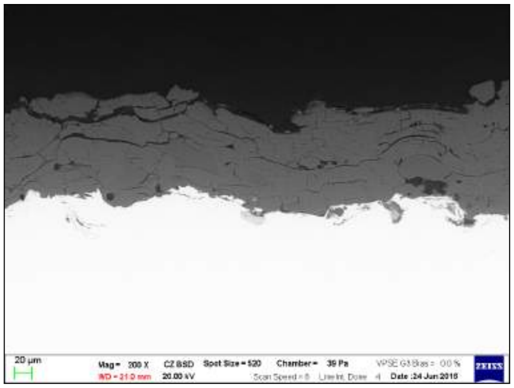

Figure 71: Sample 2.4 - cross section

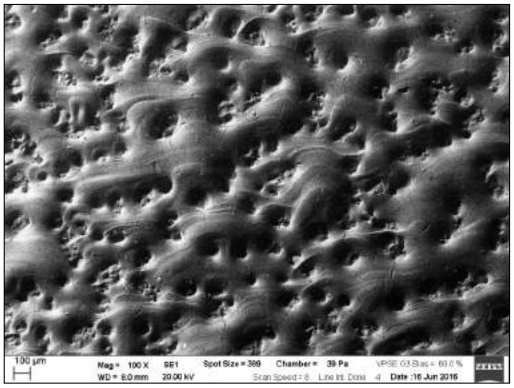

Figure 72: Sample 3.5 - surface, 100 µm as-sprayed, v = 20 mm/s

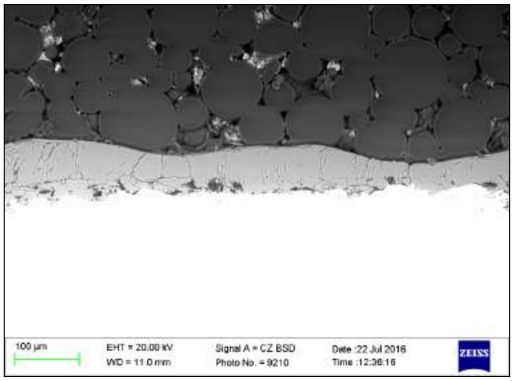

Figure 73: Sample 3.5 - cross section

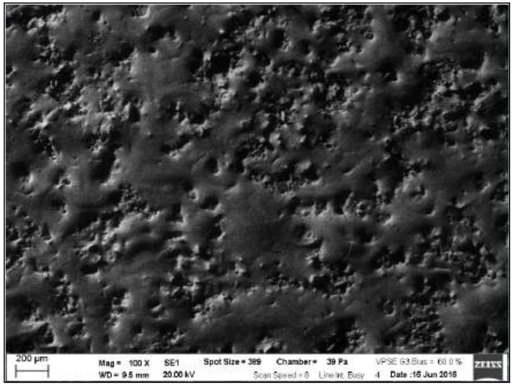

Figure 74: Sample 4.2 - surface, 100 µm as-sprayed, v = 40 mm/s

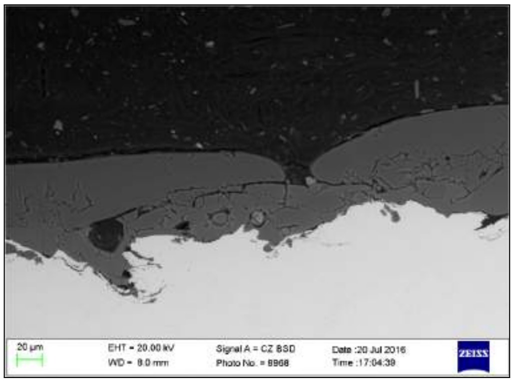

Figure 75: Sample 4.2 - cross section

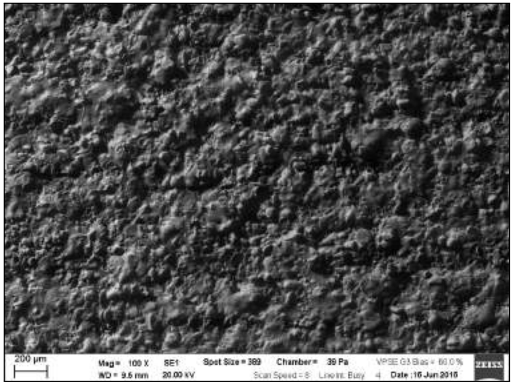

Figure 76: Sample 4.3 - surface, 100 µm as-sprayed, v = 60 mm/s

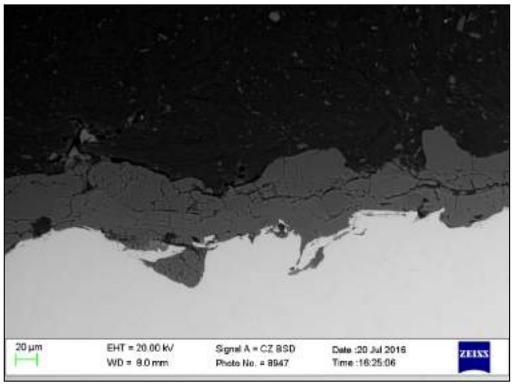

Figure 77: Sample 4.3 - cross section

Other samples can be compared with respect to the as-sprayed thickness of the coating, for example 2.3 and 4.19 or 4.10 and 4.13. First pair of the samples was remelted using moderate power (I = 5 mA, v = 20 mm/s) and frequency 1 kHz. Surface photos 78 and 79 support the thermal barrier theory, surface of sample 4.19 contains more depressions than sample 2.3 and some areas of probably unmelted coating remain. In addition, Figure 45 features slightly coarser surface between the depressions and considerably more cracks. These may be signs of overmelting, which further supports the theory, however it is not desirable. Analysis of the cross section yielded similar results. Sample 2.3 reached obviously higher remelted thickness, but the degree of remelting is similar - aproximately half of the initial coating was remelted. Surface of sample 2.3 is more even, without major depressions, but suffers from higher amount of cracks extending through the whole remelted layer. Sample 4.19 features areas with very thin remaining layer in areas where the cut intersects the surface depressions, on very few places, the substrate is almost revealed. The amount of cracks seem not to be as high as on sample 2.3.

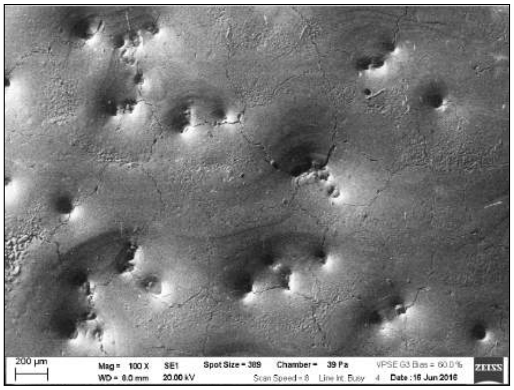

Figure 78: Sample 2.3 - surface, 300 µm as-sprayed

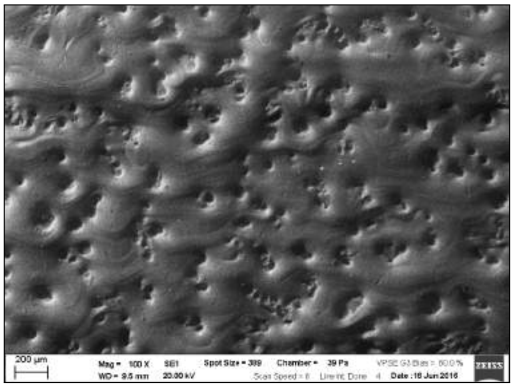

Figure 79: Sample 4.19 - surface, 100 µm as-sprayed

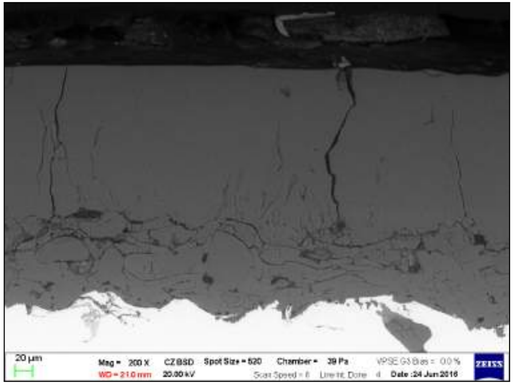

Figure 80: Sample 2.3 - cross section

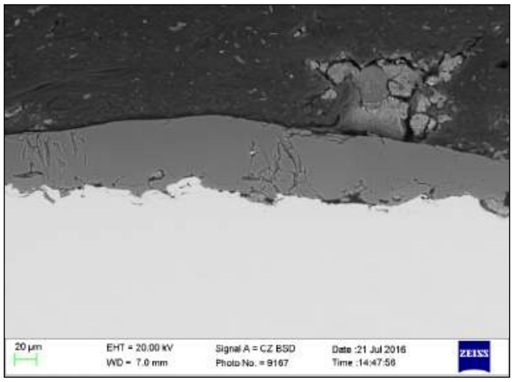

Figure 81: Sample 4.19 - cross section

Samples 4.1, 3.5, 3.6 and 3.7 allow comparison of increasing current (I = 3, 5, 7, 9 mA, respectively) for 100 µm samples, while samples 2.4, 3.1 and 3.2 (I = 5, 10, 15 mA, respectively) for 300 µm samples. Unfortunately the velocity of the samples differs - 20 mm/s for 100 µm samples and 100 mm/s for 300 µm samples, therefore cross comparison is possible only for selected samples.

Samples 4.1, 3.5 and 3.6 are displayed in Figures 82 to 87.

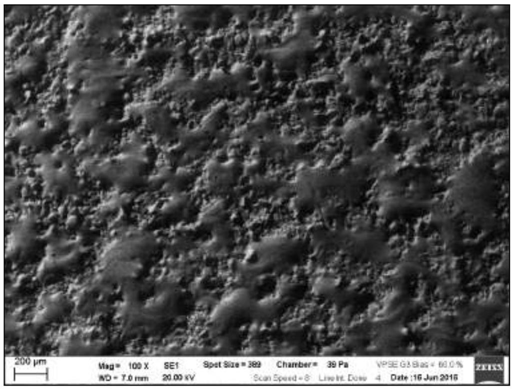

Figure 82: Sample 4.1 - surface, I=3 mA

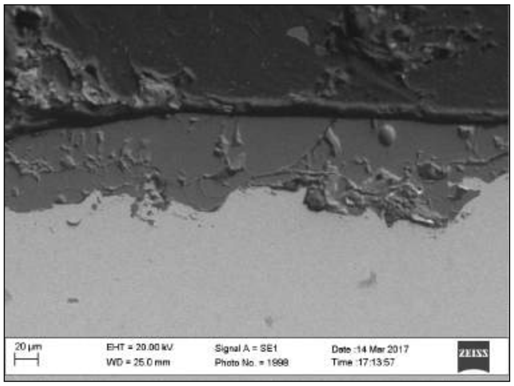

Figure 83: Sample 4.1 - cross section

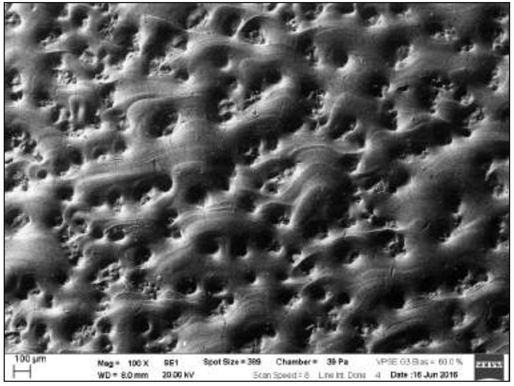

Figure 84: Sample 3.5 - surface, I=5 mA

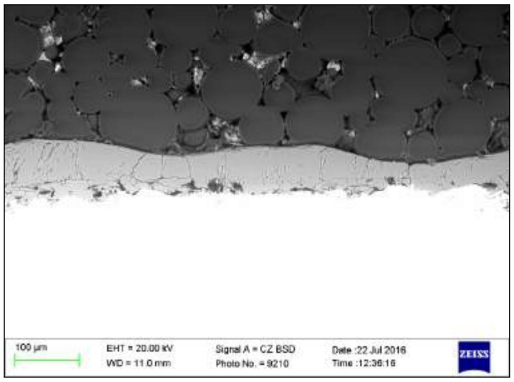

Figure 85: Sample 3.5 - cross section

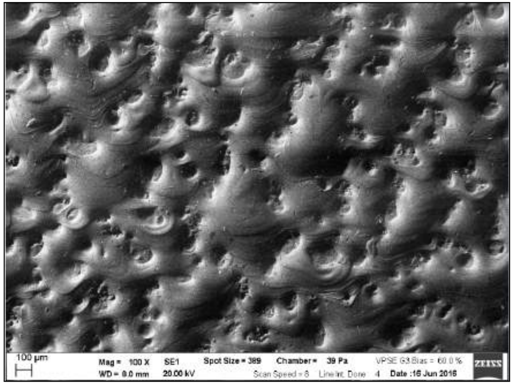

Figure 86: Sample 3.6 - surface, I=7 mA

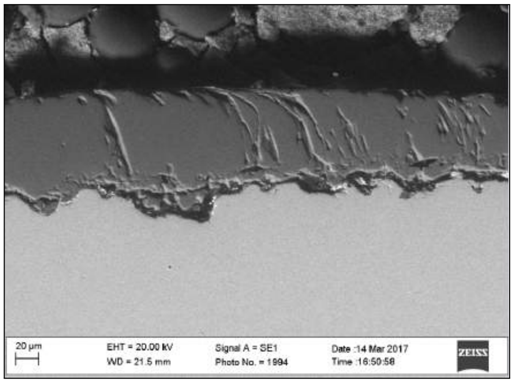

Figure 87: Sample 3.6 - cross section

It is obvious that with increasing current (i.e. the power), the degree of remelting is increasing too. The difference is negligible only while comparing sample 3.6 and 3.7 - the increase from 7 mA to 9 mA did not show major improvement. Similar result is observed in remelted thickness, the samples gradually improve, but the difference between 3.6 and 3.7 is again not as remarkable as between the previous samples. However some potential for improvement still remains, the surface of sample 3.7 still contains rather high amount of depressions, although almost whole layer is remelted. The latter samples - 2.4, 3.1 and 3.2 - are displayed in Figures 88 to 93.

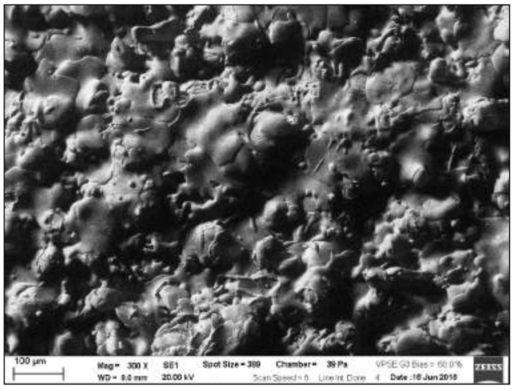

Figure 88: Sample 2.4 - surface, 300 µm as-sprayed, I = 5 mA

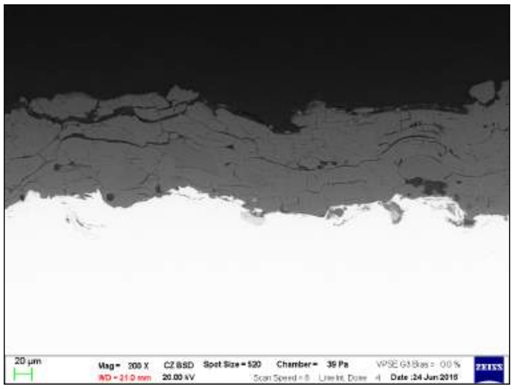

Figure 89: Sample 2.4 - cross section

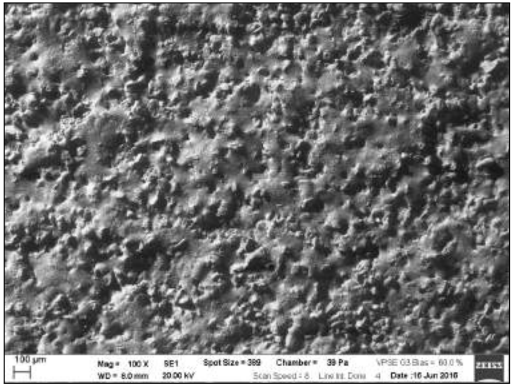

Figure 90: Sample 3.1 - surface, 300 µm as-sprayed, I = 10 mA

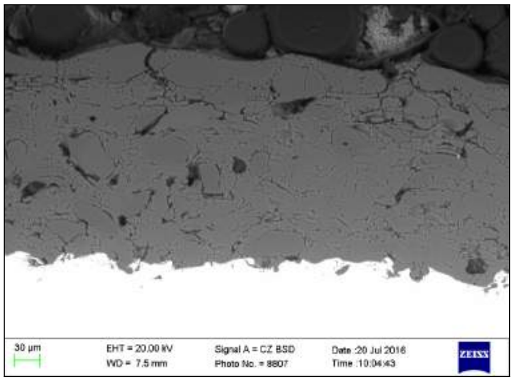

Figure 91: Sample 3.1 - cross section

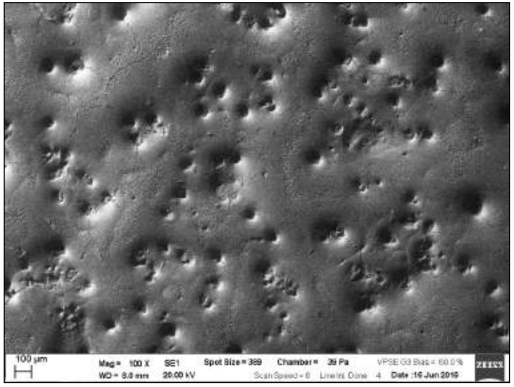

Figure 92: Sample 3.2 - surface, 300 µm as-sprayed, I = 15 mA

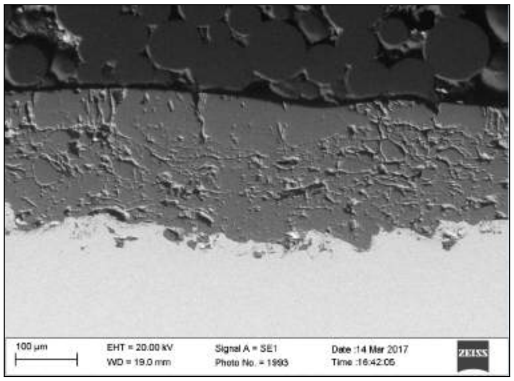

Figure 93: Sample 3.2 - cross section

These samples exhibit analogous behaviour as the 100 µm samples mentioned above. The increments of current were higher than for the previous samples, therefore the improvement is more obvious, but the trend is identical. Sample 2.4 exhibit lower remelting than sample 3.5, despite the same current used, but the samples differ greatly in velocity - 20 mm/s for 3.5 compared to 100 mm/s for 2.4. However, sample 3.2 exhibit better surface quality compared to samples 3.6 or 3.7, eventhough the current is only higher by 100% and 66%, respectively, while the velocity is 5 times higher. This may suggest that the amount of power may determine the results more than its distribution. Nevertheless it should be noted, that the effect of thermal barrier may contribute to this result as well, as sample 3.2 was of 300 µm thickness.

5.1.5 Remelting conclusion

Based on the presented results, brief conclusion can be made:

- 20 samples were remelted without critical defects
- best samples reached remelting of over 70% of thickness
- current of 5 mA (equal to 100W) was too low and velocity of 100 mm/s was too high for successful remelting
- increasing of the current promoted the remelting
- with decreasing velocity, surface smoothness and remelted thickness was increased, but risk of revealing the substrate emerged
- increasing the number of passes using lower current was identified as beneficial
- increasing the number of passes using higher current did not prove any effect, however increasing delay appeared beneficial
- low frequency of 100 Hz resulted in creating remelting pattern and revealing of the substrate
- increasing frequency showed beneficial effect
- thicker as-sprayed layer appeared to promote the remelting, acting as a thermal barrier

5.2 Nitride layers & permeation measurements

PVD and diffusion-based nitride layers broaden the range of promising permeation barriers. From literature review, particular nitrides with thermochemical stability, low hydrogen permeability and retention were identified. Available range of nitrides was deposited on structural materials desired for the construction of ITER and confirmation measurements of permeation reduction factor were carried out. Additionaly, the coatings were characterised in terms of surface quality, phase composition, adhesion and residual stress etc.

The experiments presented in this section were prepared in collaboration with several institutions – Jožef Stefan Institute in Ljublanja, Slovenia, providing substrate material and permeation measurement, Institute of Physics AS CR providing pre-treatment of the substrate and Institute for Nanomaterials, Advanced Technologies and Innovation (Technical University Liberec), Innovation Center for Diagnostics and Application of Materials (Faculty of Mechanical Engineering CTU Prague), Ionbond Czechia and Bodycote HT providing the coatings. Additional permeation measurements were arranged at Forschungszentrum Jülich. All activities were managed by me and my supervisor, Ing. Jiří Matějíček, Ph.D., and further examination of coating quality, e.g. composition, adhesion etc., was performed at the Institute of Plasma Physics and Institute of Physics AS CR v.v.i. in Prague.

5.2.1 Substrates

As substrate materials, EUROFER 97 and P92 steel were used. The reason of this choice was saving time during the permeation measurements, as the facilities of IJS and FZJ were calibrated on EUROFER97 and P92, respectively, so the measurement of reference permeation (for uncoated sample) was not necessary. EUROFER 97 was prepared as disks with diameter of 40 mm and thickness of 0.5 mm, P92 had diameter of 25 mm and thickness of 0.5 mm. EUROFER 97 is a Reduced Activation Ferritic-Martensitic (RAFM) steel, developed under Fusion for Energy (F4E) and dedicated as a structural and reference material for ITER Test Blanket Modules and DEMO. It is a 9% Cr 1.2% W 0.2% V 0.14% C steel with desired physical properties, tensile strength properties etc. P92 is a 9% Cr 1.8% W 0.5% Mo 0.12% C creep-resistant ferritic-martensitic steel. Detailed compositions are shown in Figures 94 and 95.

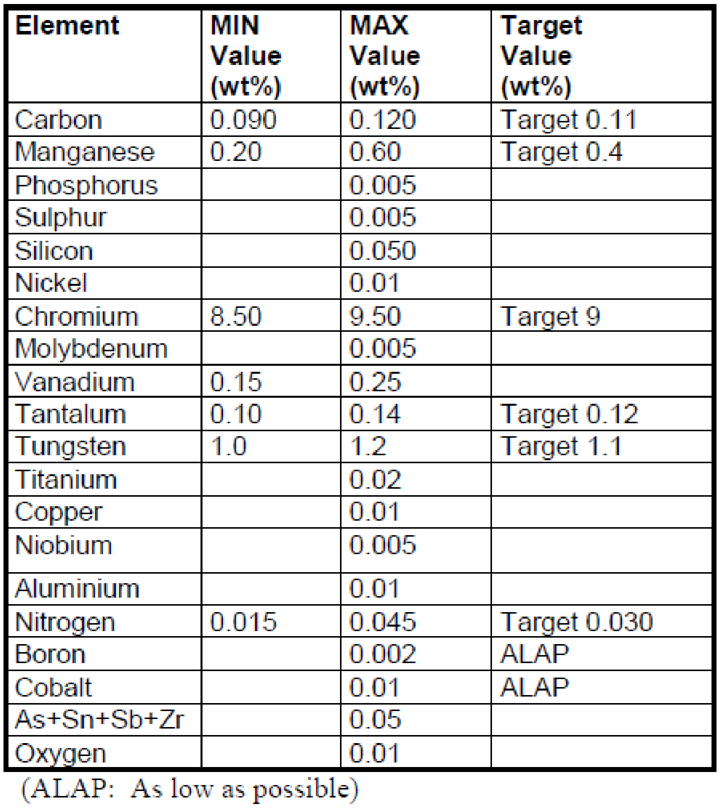

Element	MIN Value (wt%)	MAX Value (wt%)	Target Value (wt%)
Carbon	0.090	0.120	Target 0.11
Manganese	0.20	0.60	Target 0.4
Phosphorus		0.005	
Sulphur		0.005	
Silicon		0.050	
Nickel		0.01	
Chromium	8.50	9.50	Target 9
Molybdenum		0.005	
Vanadium	0.15	0.25	
Tantalum	0.10	0.14	Target 0.12
Tungsten	1.0	1.2	Target 1.1
Titanium		0.02	
Copper		0.01	
Niobium		0.005	
Aluminium		0.01	
Nitrogen	0.015	0.045	Target 0.030
Boron		0.002	ALAP
Cobalt		0.01	ALAP
As+Sn+Sb+Zr		0.05	
Oxygen		0.01	

(ALAP: As low as possible)

Figure 94: Reference chemical composition of EUROFER 97 steel [1]

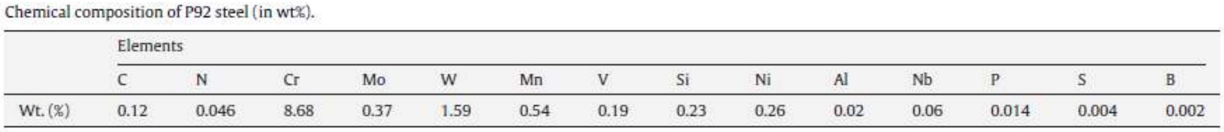

Chemical composition of P92 steel (in wt%).

	Elements													
	C	N	Cr	Mo	W	Mn	V	Si	Ni	Al	Nb	P	S	B
Wt. (%)	0.12	0.046	8.68	0.37	1.59	0.54	0.19	0.23	0.26	0.02	0.06	0.014	0.004	0.002

Figure 95: Reference chemical composition of P92 steel [40]

Rods of EUROFER97 and P92 for our experiments were kindly provided by Vincenc Nemanič and Anne Houben, respectively, cutting of the individual disks for samples was done at the Institute of Physics AS CR. Because of the required disk thickness, Wire Electrical Discharge Machining method (Wire EDM) was used [8]. In this process, thin wire is fed through the sample, which is usually submerged in a tank of dielectric fluid or deionized water. During the process, electric current flows through the wire and the cutting is performed due to erosion that occurs when a spark forms between the wire and the conductive material. The liquid is beneficial for cooling of the sample and removing the cut material.

Advantages of this process are

- high precision
- ability to produce very thin samples
- ability to produce relatively smooth surface with minimal polishing needed
- little change in material properties
- no additional residual stresses (no cutting force used)

After the cutting, substrate disks were ground with sand paperand metalographically polishedfor better results and transferred to the external deposition facilities. Eurofer substrates were used for the PVD coatings, P92 substrates were used for the diffusional surface treatments.

5.2.2 Coating material and deposition

The choice of the coating materials followed several criteria:

- **application in fusion research** - whether the other compounds of the element have already been tested or used in fusion research or if there were studies supporting the use of this element/compound; additionally, possible interaction with neutron radiation was considered, which excluded certain elements
- **abundance of studies and experiments** - in order to explore new possibilities, compounds with lower number of experiments or studies were chosen
- **coefficient of thermal expansion (compared to EUROFER97**) - for minimizing the risk of delamination during permeation measurements at elevated temperature (400-500 °C), compounds with CTE similar to that of EUROFER97 were preferred, temperature aspect was also important regarding the future operation in fusion reactor (ca. 550 °C)
- **possibility of deposition** - the choice of the compounds was influenced by the availability of particular coating at our partner facilities

Two groups of surface treatment were used - PVD coatings and diffusion-based nitriding. The first group included the following coatings: CrN, Cr_2N, WN, CrWN, CrAlN and ZrN. CrN, Cr_2N and WN were prepared at ICDAM by DC magnetron sputtering. Before the entire deposition, the samples were degreased in acetone, before the deposition of the nitride layer, additional layer of pure Cr or W, respectively, was deposited for better adhesion of the coating. This deposition lasted 10 minutes for CrN and Cr_2N, 15 minutes for WN. Nitride layers were then deposited at 250°C and in 0.2-0.3 Pa nitrogen-argon atmosphere, deposition time of CrN and Cr_2N was 3.5 hours, of WN 7 hours. CrWN, CrAlN and ZrN were prepared at Ionbond Czechia by means of cathodic arc plasma deposition. CrAlN was prepared at 450-500°C for 7.5 hours, ZrN at 300°C for 4 hours and CrWN at 350°C for 6.5 hours [15]. Assigned thickness of the coatings was 2-4 µm for CrAlN and ZrN samples, 4-6 µm for CrWN. The samples were initially coated on both sides, for ease of coating and to avoid bending of the thin substrates. However, the permeation through the first sample of this batch was found to be below the resolution limit of the facility (see section 5.2.5). Therefore, the coatings on one side were removed in this batch and subsequent batch was prepared with coatings only on one side. The second group consisted of diffussion-based nitriding processes. Samples using P92 as a substrate were prepared at TUL by plasma nitriding at 430 °C for 24 hours [13]. Thickness of the nitride layer was estimated at about 100 nm. Another pair of samples was produced at Bodycote using carbonitridation at 560 °C for 1.5 hours in a dissociated ammonia atmosphere with CO_2 addition. For each type of coating/treatment, two samples for permeation measurements were prepared.

5.2.3 Coating characterization

After the delivery, the coatings were analysed in various means. This analysis included:

- SEM observation
- Energy-dispersive X-ray spectroscopy - EDS
- X-ray diffraction - XRD
- thickness measurements
- adhesion measurements

SEM observations confirmed smooth surface for samples prepared at ICDAM, whereas samples from Ionbond featured small depressions and droplets. Results for both groups of samples were typical for the chosen method. Examples of SEM photos for CrN and CrAlN as representative samples are in Figures 96 anf 97.

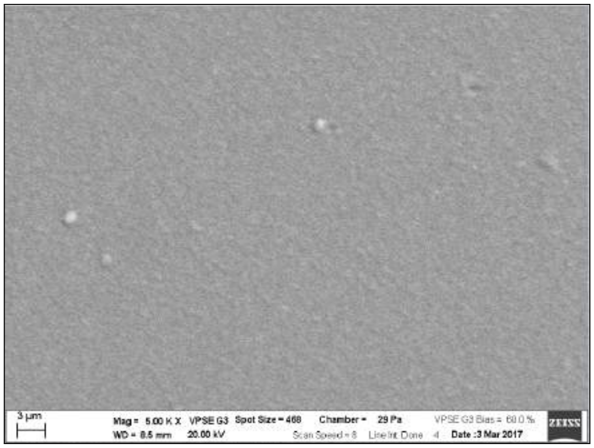

Figure 96: Surface SEM photo of CrN, prepared by magnetron sputtering

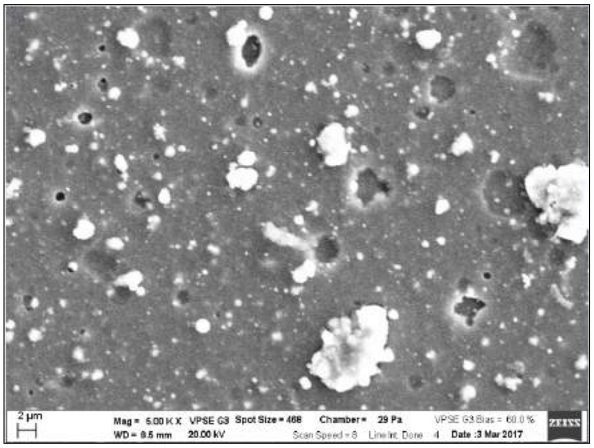

Figure 97: Surface SEM photo of CrAlN, prepared by arc sputtering

During the thickness measurements, the samples used for permeation measurements were examined in SEM as well and no surface change was identified.

Energy-dispersive X-ray spectroscopy is a chemical analysis method based on recording of the characteristic X-ray radiation, emitted from the material when exposed to a charged particles beam (electron or proton) or a beam of X-ray. The incident beam may excite an electron in an inner shell of the coating atom, ejecting it from the shell and producing an electron hole. This hole is filled with an electron from outer shell and the excessive energy is radiated in the form of X-rays. These are then measured by an energy-dispersive spectrometer [100]. The principle is demonstrated in Figure 98.

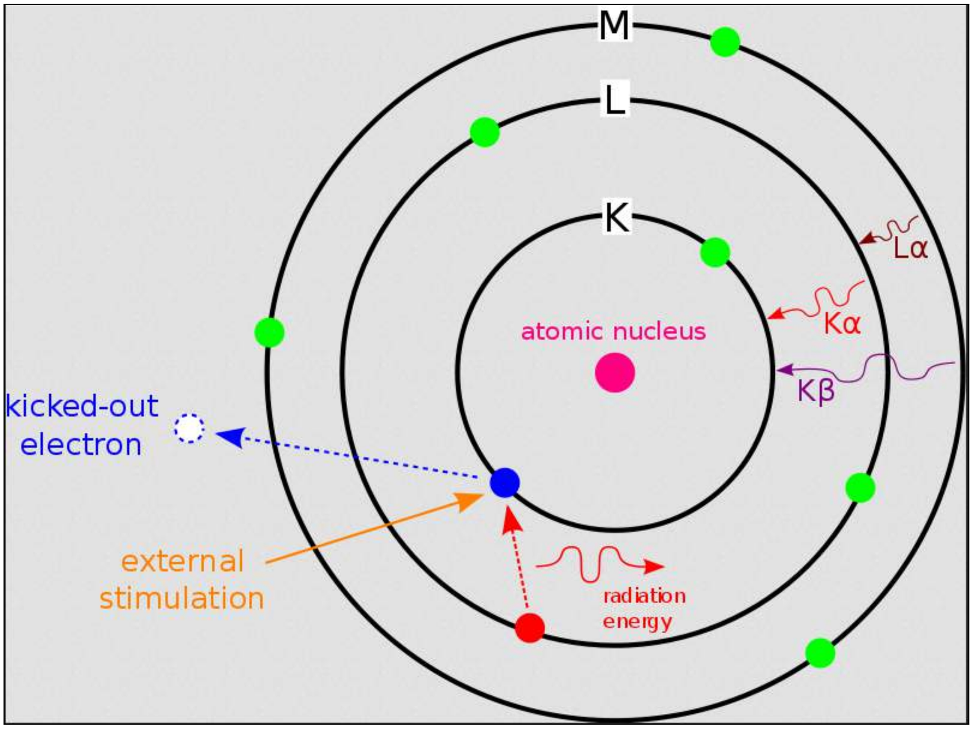

Figure 98: Principle of energy-dispersive X-ray spectroscopy [98]

During our measurements, due to very thin layers, signal from the substrate was recorded as well, however after the background deduction, no deviations from desired composition of the coatings were observed. The results are summarized in Table 5.

Table 5: Composition of the coatings measured by EDS, mass percent

Material	N	Al	Cr	W	Zr
WN	1.5			98.5	
CrWN	17.8		71.6	10.6	
Cr_2N	4.7		95.3		
CrN	8.9		91.1		
CrAlN	24.2	30.2	45.6		
ZrN	10.5				89.5

X-ray diffraction is an established method of determination of the sample crystallinity, phase composition and elastic strain. By measuring of the diffraction angle and application of the Bragg´s law, lattice spacing can be measured, crystallographic phases determined and elastic strain can be calculated (using so called $\sin^2\psi$ method [95, 73]). Phase composition of the coatings was uniform, with the exception of CrAlN and WN. Results of the diffraction and phase analysis by the Rietveld method are in Figures 99 and 100.

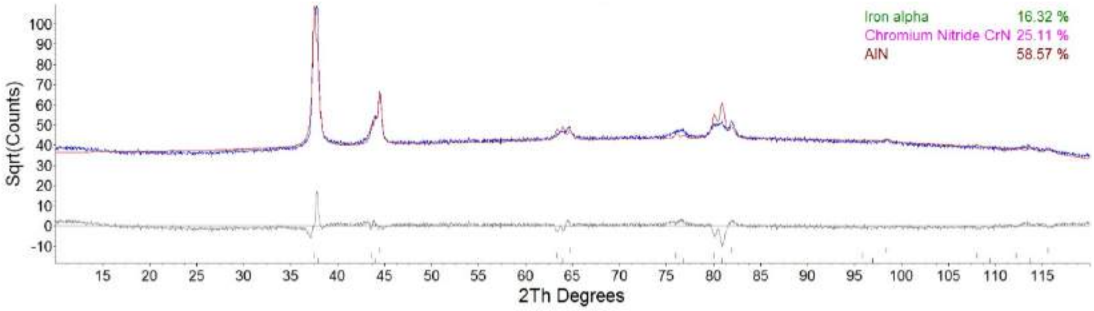

Figure 99: Diffraction pattern of CrAlN

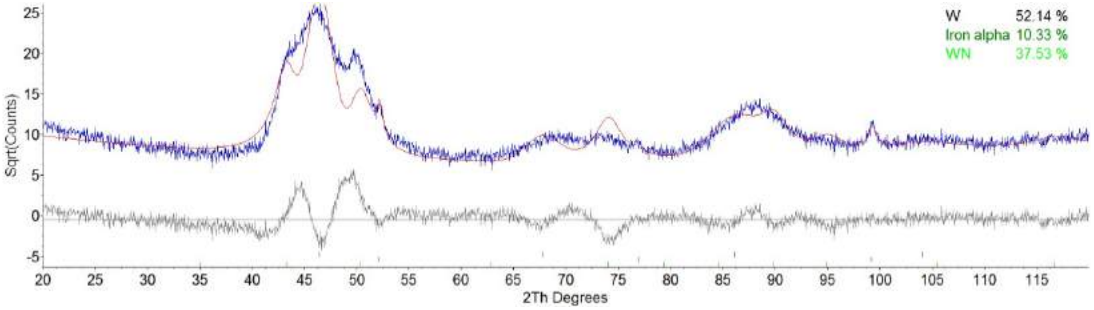

Figure 100: Diffraction pattern of WN

α-phase of iron is recorded because the penetration depth of X-ray is greater than the coating thickness. All the coatings featured noticeable texture (with the first diffraction peak being the strongest) and small crystallites (indicated by broad diffraction peaks; most prominent in the WN sample). Due to closely overlapping and broad peaks in the CrAlN sample, the AlN and CrN phases could not be unambiguously separated. Results of the strain calculations are displayed in Table 6.

Table 6: Approximate values of residual strain in nitride coating (ε)

Material	ε $[10^{-3}]$
CrWN	-11 ± 2
ZrN	-16 ± 1
CrAlN	-16 ± 1
CrN	-25 ± 2
WN	-9 ± 1

Residual strain of Cr_2N coating is not mentioned in the Table 6, as the determination was not successful. Structure of the deposited coating was not suitable for derivedproper determination of the lattice spacings, due to closely overlapping peaks whose intensity varied with the tilt angle. All remaining coating contain compressive residual strain, which is however beneficial regarding future application, than the tensile strain. Best results were reached by WN and CrWN coating, on the other hand, CrN suffered from the greatest strain.

Thickness of the coating was measured at ICDAM using a calotest method. It is an established method using rotating stainless steel ball and a diamond paste to wear through the coating and reach the substrate. During our measurements, calotest equipment of CSM Instruments, steel ball with the diameter of 30 mm and rotating at 600 rpm was used. When the coating is fully penetrated, the situation looks like in Figure 101 - circular crater is formed, exposing the substrate, as well as the coating. Photo from the actual measurement is in Figure 102.

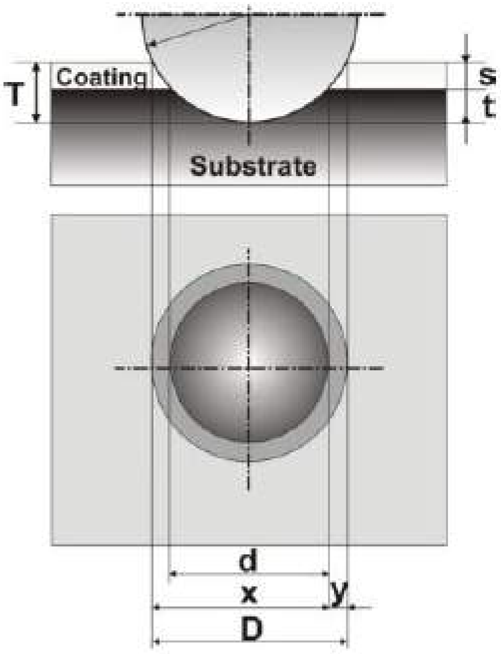

Figure 101: Calotest measurement scheme; s - coating thickness; t - substrate penetration depth; T - total penetration depth; d - inner diameter of the crater; D - outer diameter of the crater; x,y - parameters [42]

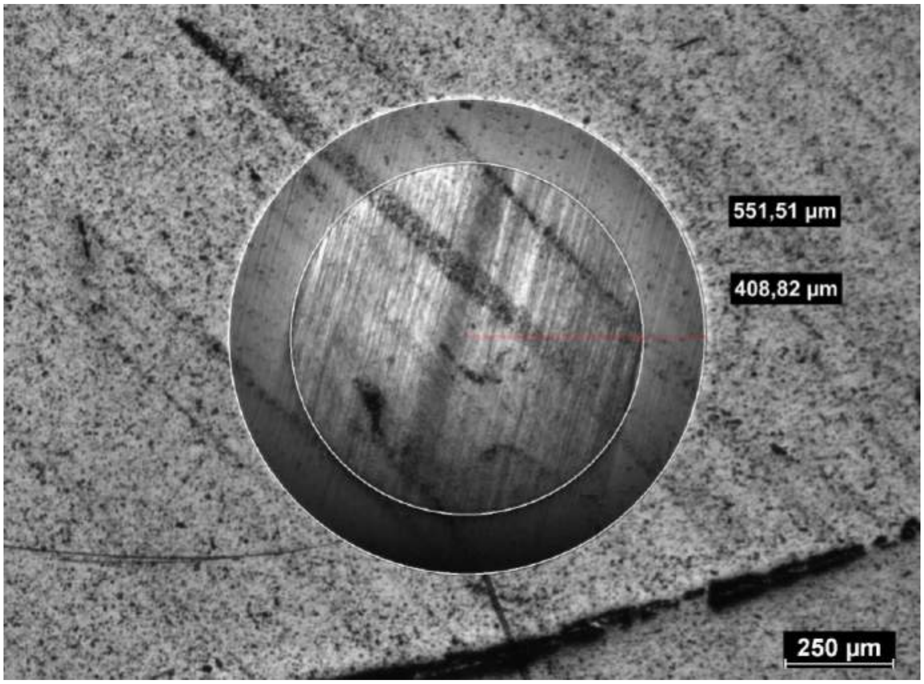

Figure 102: CrAlN coating with exposed substrate after calotest measurement

By measuring parameters x and y from Figure 101 and using the geometry of the measurement, one can obtain simple equation for coating thickness 7, where D_2 is a diameter of used steel ball. This equation can be further arranged using x = R+r and y = R-r, where R and r are the outer and inner radius of the crater, respectively, gaining equation 8.

$$s = \frac{xy}{D_2} \tag{7}$$

$$s = \frac{R^2 - r^2}{D_2} = \frac{D^2 - d^2}{4D_2} \tag{8}$$

Results from the thickness measurements are displayed in Table 7.

Table 7: Approximate values of nitride coating thickness (d)

Material	d [µm]
CrWN	4.4
ZrN	1.4
CrAlN	4.5
CrN	2.6
Cr_2N	2.2
WN	2.3

As can be seen, all coatings were prepared at desired thickness, with the exception of ZrN, which is slightly thinner, but that should not be critical in terms of permeation.

Adhesion was determined by results of a scratch test, performed at ICDAM as well. CSM Revetest express+ device was used, with a diamond stylus with a tip radius of 0.2 mm. The load was set to linear increase from 1 N to 100 N along the path of 10 mm. The lower critical load (L_C) was determined as the smallest load at which significant coating damage occured, according to [88]. Examples of a cluster starting point determination from [88] are in Figures 103 and 104. In our measurements, the reference point was acquired using SEM observation of the scratch. Photos of the reference point and a detail of the damaged area are in Figures 105 and 106.

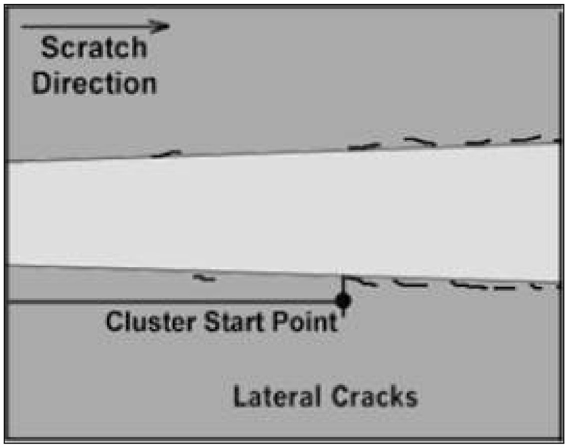

Figure 103: Determination of a cluster starting point, lateral cracks [88]

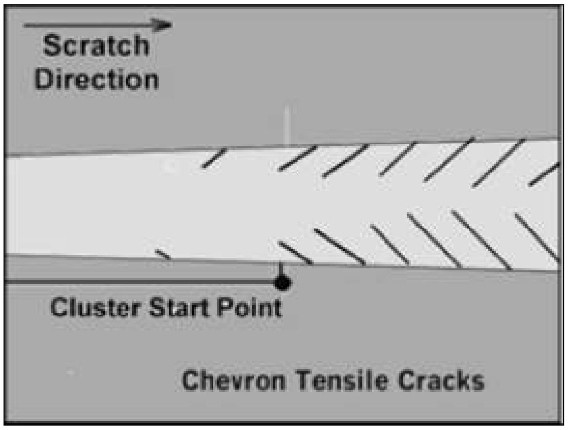

Figure 104: Determination of a cluster starting point, tensile cracks [88]

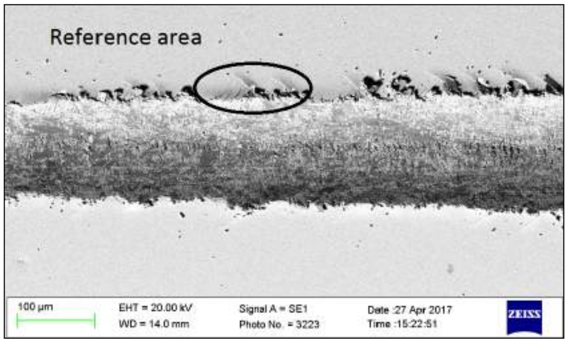

Figure 105: Cluster starting point, WN coating

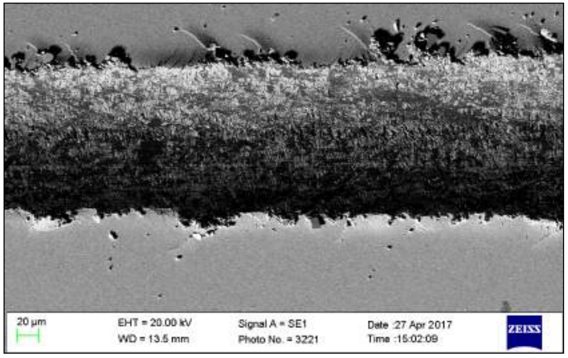

Figure 106: Detailed photo of cracks, WN coating

Results of the scratch tests are displayed in Table 8. Considering limited amount of EUROFER substrate, all coatings for the auxilliary characterization (SEM surface observation, XRD measurements, scratch test, calotest) were deposited on P91 steel, a variant of P92 steel with almost identical composition (see Figure 95). During the deposition of samples for permeation measurements, invasive characterization (calotest, scratch test) was planned on dedicated samples on P91 substrates and, if there are some unused samples left, on the EUROFER ones as well. However, due to unexpected issues, unused samples deposited on EUROFER were not available for all coatings for the scratch test. And because the results show lower adhesion on EUROFER, compared to P91, it may not be reliable to compare the adhesion before and after the permeation measurements for all coating (namely possible only for Cr_2N, CrN and WN).

Table 8: Scratch test results, L_C - lower critical load

Substrate	Coating	Permeation measurement	L_C [N]
P91	CrWN	NO	29
P91	ZrN	NO	32
P91	CrAlN	NO	4
P91	WN	NO	16
P91	CrN	NO	47
P91	Cr_2N	NO	60
EUROFER	WN	NO	13
EUROFER	CrN	NO	33
EUROFER	Cr_2N	NO	33
EUROFER	WN	YES	12
EUROFER	CrN	YES	5
EUROFER	Cr_2N	YES	16
EUROFER	CrWN	YES	15
EUROFER	ZrN	YES	24
EUROFER	CrAlN	YES	14

The results indicate that regarding P91 substrate, Cr_2N has the highest adhesion. CrN, WN and ZrN have also rather higher adhesion, WN and CrAlN have the lowest adhesion, one can say that CrAlN has extremely low adhesion. Measurements on EUROFER substrate before the permeation measurements yielded lower values, for Cr_2N of about one half lower, for CrN about one third. Adhesion for WN is also lowered, but not so dramatically as for the previous coatings. That supports a theory, that comparing P91 samples without permeation with EUROFER samples after permeation may not be reliable. However, for the abovementioned coatings, the effect of exposure to hydrogen can be determined, and according to the table, another decrease in adhesion appeared. For WN, the drop was minimal, but for Cr_2N and mainly CrN, the decrease was significant. For other coatings, we do not have direct comparison, but with the exception of CrAlN, the values are lower that these for P91 substrate. Therefore it can be concluded, that under the conditions described in section 5.2.4, coating adhesion might be negatively affected.

5.2.4 Permeation measurements

The setup of a typical facility for permeation measurements is displayed in Figure 107. It is assembled from all-metal UHV components and consists of accumulation, analytical and calibrating chamber, vacuum gauges, turbo-molecular pump for both upstream and downstream side, hydrogen container and quadrupole mass spectrometer.

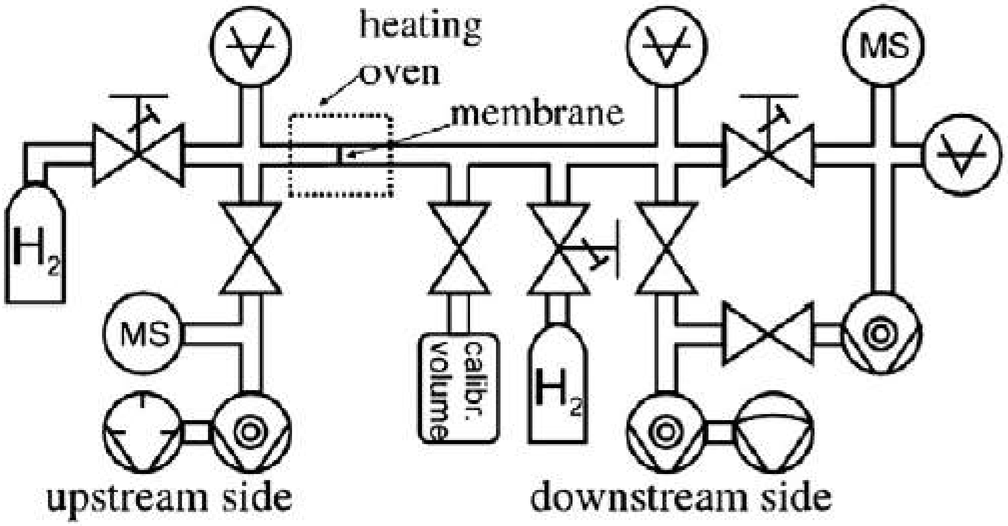

Figure 107: Experimental setup of the permeation facility [54]

During common routine for permeation measurements, the sample is mounted into a special cell dividing the upstream and downstream side, secured by the flanges and Au gasket, which determines the hydrogen exposed area (ca. 8.4 cm^2). The furnace with the sample is then heated to 400 °C and maintained for approximately 24 hours to reach sufficiently low background outgassing rate. After this period, hydrogen is introduced into the upstream side at defined pressure - usually 1 bar - and the permeated flux is detected. Permeation reduction factor (PRF) is derived afterwards. It is also possible to record temperature or pressure dependence of PRF. Further details can be found in [54] or [57].

5.2.5 Permeation results

The initial plan for permeation measurements expected measurements of 6 different coatings. Due to some unexpected results, 8 measurements were performed in the end. Overall results, expressed by the PRF are summarized in Table 9. Below the Table, performance of each samples is described and results of post-permeation examination are presented.

Table 9: Approximate values of PRF measured in IJS facility, UDF - undefined, below the detection limit

Sample	Material	PRF [-]
1	CrWN	UDF
2	CrWN	100
3	ZrN	34,000
4	ZrN	4,600
5	CrAlN	350
6	CrN	117
7	Cr_2N	236
8	WN	38

The first sample, CrWN, was measured double coated; the sample was fixed into the cell, baked-out at 160 °C for several hours, then heated up to 400 °C and 1 bar hydrogen was introduced. After 20-hour-measurement, still no significant permeation flux was recorded and the sample was thus declared highly impermeable with the current setting of the facility. In the particular setup, detection limit was considered as 5% above the background outgassing rate of hydrogen, PRF $\sim 10^5$. Due to double-sided sample, hydrogen that permeated through the upstream coating may not continue through the downstream coating, but was probably lost at sides. This may contribute to extremely low hydrogen flux recorded and therefore extremely high PRF. The decision was made to remove one side coating from the second CrWN sample with ALAP damage to the substrate and the latter side coating and to repeat the measurement. For the procedure, the sample was sent back to Prague, where the modification was performed, and then back to Slovenia.

The second CrWN sample was measured after the coating removal from one side, using the same procedure as stated above. The sample was exposed to 1290 ± 2 mbar H_2 and PRF was determined two times with results 99.6 and 99.7. This measurement, as well as sample 3 measurement, was affected by an air leak caused by imperfection of a gold gasket (defining the effective permeation area).

During the measurements of sample 3, the background outgassing rate could not be suppressed to such ultimate value as during the previous measurements. It was presumed that small air leak developed during the heating. Therefore, the discrimination of the permeation fluxes was difficult. Nevertheless, the PRF was finally estimated as $\sim$ 34,000. After the measurements, the sample was examined and on the downstream, small groove was identified, which was created probably during the handling and which may have caused the leak, unable to be prevented by the gold gasket. This may be the cause for surprisingly high PRF value.

Due to extremely high PRF values recorded on the first ZrN sample, the measurement was repeated on a second ZrN sample. The background outgassing rate was higher as well as with sample 3, but no air leak was detected this time. Repeated measurement did not confirm such extreme PRF value, however, the sample exhibited PRF $\sim$ 4,600, which is high value as well.

During the measurement of sample 5, the outgassing rate returned to values similar to those during the measurements of samples 1 and 2, indicating that the higher values might be connected to the properties of ZrN. PRF of CrAlN coating exposed to 1.1 bar H_2 was estimated $\sim$ 350.

Measurement of sample 6 was regular, the outgassing rate was rather higher, but the leak testing gained no signal. The PRF value was determined from 3 exposures at various pressure. The highest PRF, 117, was recorded for the lowest pressure, 0.732 bar. At higher pressures, PRF reached 58 and 74. With each exposure, the film was becoming less and less permeable. However, this phenomenon was not explained, as it was not observed before.

During the measurements of Cr_2N sample, the outgassing rate was low again and no signal from leak testing was detected. The PRF was again determined from multiple measurements, in this case two. At pressure of 0.968 bar and 0.938 bar, PRF reached 236 and 212, respectively.

During the measurement of WN sample, the background outgassing rate was again rather high and this time, weak leak testing signal was detected. The measurement was carried out anyway, reaching PRF of 26 and 38, respectively.

6 SUMMARY

6.1 Alumina coatings and remelting experiments

Based on the previous study [89] and literature review conducted, the goal of the current experiments was to reach successful remelting of Al_2O_3 layer, eliminating the surface defects, especially cracks, and reaching homogenous remelted layer, as thick as possible. In total 41 samples were remelted. Moderate success was reached, smooth surface with low amount of defects and sufficient thickness of the remelted layer was obtained in 20 samples, however non-negligible amount of cracks still remained. Remelting of complete deposited layer was not achieved, however regarding eventual function as a permeation barrier, unremelted layer beneath homogenous defect-free layer of sufficient thickness (reached during the study) should not constitute a serious threat. Several dependencies between the remelting parameters and the resulting surface state were observed:

- increasing of remelting current, number of beam passes and frequency (separately) promoted the remelting

  Samples remelted with higher current or perpendicular frequency of the beam (for electron beam characteristics, see section 5.1.3) or treated with more beam passes usually showed smoother surface and thicker remelted layer. The effect can be suppressed by high velocity of the samples.

- decreasing of the sample velocity affected the surface smoothness and remelted thickness beneficially

  Samples remelted using lower velocity (e.g. 20 mm/s compared to 100 mm/s) showed usually smoother surface and thicker remelted layer. However, at lower velocities and higher powers, samples exhibited slight overmelting and the risk of substrate revealing increased.

- current lower than 5 mA, velocity higher than 100 mm/s and frequency lower than 100 Hz proved to be unsuitable for successful remelting

  Low remelting current and high velocity of the sample resulted in low level of remelting, most samples treated with these values preserved the structure of plasma sprayed coatings: rough surface consisting of individual splats, showing high level of porosity on the cross section. Beam frequency of 100 Hz resulted in jagged pattern on the sample: unaffected areas alternating with traces, partly revealing the substrate (see Figure 49).

- thicker coating act as a thermal barrier during the remelting

  Samples with thicker as-sprayed coating, remelted with identical parameters as thinner samples, exhibited better surface conditions, e.g. smoother surface, lower amount of defects, and thicker remelted layer. The coating apparently act as a thermal barrier, preventing heat conduction from the surface and promoting the remelting. However, the use of higher power might easily lead to overmelting and degradation of the coating.

6.2 Nitride coatings and permeation experiments

In total 12 samples of 6 nitrides were deposited on the RAFM steel EUROFER97. Initial characterization of the coatings was performed by various means. Smooth, defect-free surface essential for permeation measurements was confirmed by SEM observations. Chemical composition of the coatings was confirmed by EDS measurements - all coatings were deposited with desired composition. XRD measurements showed uniform phase composition, with the exception of CrAlN and WN - CrAlN showed presence of CrN and AlN, WN showed WN and W phases. XRD measurements also showed that all coatings contained compressive residual strain. Thickness of the coating was determined by the calotest and varied from 1.4 to 4.5 µm, which is in the desired range. Adhesion of the coatings was measured by the scratch test. The results indicated a drop in adhesion after permeation measurements in most cases; the highest adhesion was reached by ZrN coating. In total 8 permeation measurements were conducted, at 400 °C and 1 bar H_2. All coatings exhibited stability during the measurements and did not suffer any damage. The lowest PRF recorded was 38 for WN, chromium-based nitrides exhibited PRF from 100 to 350. Very high PRF values were reached by ZrN, approximately 34,000 during the first measurement and 4,600 during the second measurement. Value derived from the first measurement however may not be reliable, as during post investigation, small groove in the sample was identified, causing a leak which may have affected the observed value. Nevertheless, ZrN coating showed the best performance from the tested samples. In addition, ZrN coating was deposited with the lowest thickness (1.4 µm) and reached the best results in adhesion testing as well. Although the coating contained moderate residual strain, higher than WN or CrWN, the overall results present ZrN coating as very promising.

References

[1] Eurofer-97 technical specification. [online], www.uni-lj.si/mma/1-F4E-2008-GRT-010.%20Technical%20Specification/2013070115554947/, 11.2.2017.

[2] Stellarator. [online], http://www.grs.de/sites/default/files/images/stellaratorI.jpg, 14.10.2016.

[3] Tokamak principle. [online], https://www.euro-fusion.org/2011/09/tokamak-principle-2/, 14.10.2016.

[4] Plasma spray-coating. [online], http://sciencelearn.org.nz/Contexts/Gases-and-Plasmas/Looking-Closer/Plasma-spray-coating, 14.3.2017.

[5] IPP CAS - Key Technologies. [online], http://www.ipp.cas.cz/vedecka_struktura_ufp/ materialove_inzenyrstvi/Klicove_technologie/index.html, 16.3.2017.

[6] NETME centre. [online], http://netme.cz/electron-beam/, 16.3.2017.

[7] ProjectSoft - Plasmatron WSP-H 500. [online], http://www.projectsoft.cz/plazma-system-nastriku.php, 16.3.2017.

[8] Sodick - wire EDM technology. [online], http://www.sodick.com/technology/wireedmtech, 16.3.2017.

[9] Carburising. [online], http://www.twi-global.com/technical-knowledge/faqs/process-faqs/faq-what-is-carburising-carbonitriding/, 19.10.2016.

[10] Carburising. [online], http://www.uk-finishing.org.uk/N-COAT70/carburising.htm, 19.10.2016.

[11] Comparing and contrasting: carbonitriding and nitrocarburizing. [online], http://www.industrialheating.com/articles/92958-comparing-and-contrasting-carbonitriding-and-nitrocarburizing, 19.10.2016.

[12] Nitrocarburizing. [online], http://www.bodycote.com/en/services/heat-treatment/case-hardening-without-subsequent-hardening-operation/nitrocarburising.aspx, 19.10.2016.

[13] Active screen plasma nitriding. [online], http://web.ald-vt.de/cms/vakuum-technologie/technologien/vacuum-heat-treatment/aspn-active-screen-plasma-nitriding/, 2.4.2017.

[14] Pack carburizing. [online], http://4mechtech.blogspot.cz/2013/11/case-hardening-process-pack-carburizing.html, 2.4.2017.

[15] Anders A. Cathodic arc plasma deposition. Vacuum technology and coating, vol. 3 no. 7:p. 27–35, 2002.

[16] Bethe H. A. Energy production in stars. Physical Review, vol. 55:p. 434–456, Mar 1939.

[17] Causey R.A.; Karnesky R.A.; San Marchi Ch. Tritium barriers and tritium diffusion in fusion reactors. Sandia National Laboratories, 2009.

[18] Glasbrenner H.; Perujo A.; Serra E. Hydrogen permeation behaviour of hot-dip aluminized MANET steel. Fusion Technology, vol. 28:p. 1159–1164, 1995.

[19] Abdou M. et al. Blanket/first wall challenges and required RD on the pathway to DEMO. Fusion Engineering and Design, vol. 100:p. 2–43, 2015.

[20] Abe F. et al. Influence of forming conditions on the titanium model in rapid prototyping with the selective laser melting process. Journal of Mechanical Engineering Science, vol. 217:p. 119–126, 2003.

[21] Aiello A. et al. Hydrogen isotopes permeability in EUROFER 97 martensitic steel. Fusion Science and Technology, vol. 41:p. 872–876, 2002.

[22] Benamati G. et al. Mechanical and corrossion behaviour of EUROFER 97 steel exposed to Pb-17Li. Journal of Nuclear Materials, vol. 307-311:p. 1391–1395, 2002.

[23] Causey R. A. et al. Hydrogen diffusion and solubility in silicon carbide. Journal of the American Ceramic Society, vol. 61:p. 221–225, 1978.

[24] Causey R. A. et al. Tritium migration in vapor-deposited β-silicon carbide. Journal of Nuclear Materials, vol. 203:p. 196–205, 1993.

[25] Checchetto R. et al. Analysis of the hydrogen permeation properties of TiN-TiC bilayers deposited on martensitic stainless steel. Surface and Coating Technology, vol. 83:p. 40–44, 1996.

[26] Chikada T. et al. Thermal influence on erbium oxide coating for tritium permeation barrier. Fusion science and technology, vol. 56:p. 309–313, 2009.

[27] Chikada T. et al. Modelling of tritium permeation through erbium oxide coatings. Fusion science and technology, vol. 60:p. 389–393, 2011.

[28] Chikada T. et al. Deuterium permeation through erbium oxide coatings on RAFM steels by a dip-coating technique. Journal of Nuclear Materials, vol. 442:p. 533–537, 2013.

[29] Conrad R. et al. Irradiation of liquid breeder material Pb-17Li with in situ tritium release measurements in the LIBRETTO-2 experiment. Journal of Nuclear Materials, vol. 179:p. 875–878, 1991.

[30] Conrad R. et al. LIBRETTO-3 - performance of tritium permeation barriers under irradiation at the HFR Petten. Journal of Nuclear Materials, vol. 215:p. 998–1002, 1994.

[31] Demange D. et al. Tritium management and anti-permeation strategies for three different breeding blanket options foreseen for the european powerplant physics and technology demonstration reactor study. Fusion Engineering and Design, vol. 89:p. 1219–1222, 2014.

[32] Elleman T. S. et al. Hydrogen diffusion and permeation in ceramic materials. Proceedings of the 3rd Topical Meeting on Techniques of Controlled Nuclear Fusion, vol. 2:p. 763–766, 1978.

[33] Esteban G. A. et al. Hydrogen transport and trapping in ODS-EUROFER. Fusion Engineering and Design, vol. 80:p. 2634–2640, 2007.

[34] Farabolini W. et al. Tritium control modelling for a helium cooled lithium-lead blanket of a fusion power reactor. Fusion Engineering and Design, vol. 81:p. 753–762, 2006.

[35] Federici G. et al. Overview of EU DEMO design and RD activities. Fusion Engineering and Design, vol. 89:p. 882–889, 2014.

[36] Fedorov A.V. et al. Tritium permeation and desorption in reduced activation martensitic steels studied in EXOTIC-9/1 irradiation experiment. Journal of Nuclear Materials, vol. 442:p. S723–S725, 2013.

[37] Forcey K.S. et al. The formation of tritium permeation barriers by CVD. Journal of Nuclear Materials, vol. 200:p. 417–420, 1993.

[38] Futerrer M.A. et al. Further improvements of the water-cooled Pb-17Li blanket. Fusion Engineering and Design, vol. 58-59:p. 523–527, 2001.

[39] Gauthier E. et al. Boronization in Tore Supra. Journal of Nuclear Materials, vol. 196-198:p. 637–641, 1992.

[40] Giroux P.F. et al. Mechanical and microtructural stability of P92 steel under unaxial tension at high temperature. Materials Science and Engineering, vol. A 527:p. 3984–3993, 2010.

[41] Greenwald M. et al. H mode confinement in Alcator C-Mod. Nuclear Fusion, vol. 37:p. 793–809, 1997.

[42] Hernandez L.C. et al. Nanohardness and residual stress in TiN coatings. Materials, vol. 4:p. 929–940, 2011.

[43] Higashijima S. et al. Impurity and particle recycling reduction by boronization in JT-60U. Journal of Nuclear Materials, vol. 220-222:p. 375–379, 1995.

[44] Ihli T. et al. Review of blanket designs for advanced fusion reactors. Fusion Engineering and Design, vol. 83:p. 912–919, 2008.

[45] Jackson G.L. et al. Boronization in DIII-D. Journal of Nuclear Materials, vol. 196-198:p. 236–240, 1992.

[46] Koch F. et al. Crystallization behavior of arc-deposited ceramic barrier coatings. Journal of Nuclear Materials, vol. 329:p. 1403–1406, 2004.

[47] Konys J. et al. Corrossion behaviour of EUROFER steel in flowing eutectic Pb-17Li alloy. Journal of Nuclear Materials, vol. 329-333:p. 1379–1383, 2004.

[48] Konys J. et al. Comparison of corrossion behaviour of bare and hot-dip coated EUROFER steel in flowing Pb-17Li. Journal of Nuclear Materials, vol. 367-370:p. 1144–1149, 2007.

[49] Konys J. et al. Compatibility behaviour of EUROFER steel in flowing Pb-17Li. Journal of Nuclear Materials, vol. 386-388:p. 678–681, 2009.

[50] Krauss W. et al. Al-based anti-corrossion and T-permeation barrier development for future DEMO blankets. Journal of Nuclear Materials, vol. 417:p. 1233–1236, 2011.

[51] Leuders S. et al. On the mechanical behaviour of titanium alloy TiAl6V4 manufactured by selective laser melting: fatigue resistance and crack growth performance. International Journal of Fatigue, vol. 48:p. 300–307, 2013.

[52] Levchuk D. et al. Deuterium permeation through EUROFER and α alumina coated EUROFER. Journal of Nuclear materials, vol. 328:p. 103–106, 2004.

[53] Maeda Y. et al. Solubility, diffusivity and isotopic exchange rate of hydrogen isotopes in Li-Pb. Fusion Science and Technology, vol. 54:p. 131–134, 2008.

[54] McGuiness P.J. et al. Hydrogen permeation through TiAlN-coated Eurofer 97 steel. Surface and Coating Technology, vol. 205:p. 2709–2713, 2011.

[55] Morono A. et al. Radiation enhanced deuterium absorption for Al_2O_3 and macor ceramics. Fusion Engineering and Design, vol. 88:p. 2488–2491, 2013.

[56] Nakamichi M; Nakamura H; Hayashi K et al. Impact of ceramic coating deposition on the tritium permeation in the japanese ITER-TBM. Journal of Nuclear Materials, vol. 386-388:p. 692–695, 2009.

[57] Nemanič V. et al. Hydrogen permeation through disordered nanostructured tungsten films. Journal of Nuclear Materials, vol. 429:p. 92–98, 2012.

[58] Noda N. et al. Boronization in future devices - protecting layer against tritium and energetic neutrals. Journal of Nuclear Materials, vol. 266-269:p. 234–239, 1999.

[59] Perujo A. et al. Low aluminium content permeation barrier coatings for DIN 1.4914 martensitic steel MANET. Fusion Technology, vol. 28:p. 1256–1261, 1995.

[60] Perujo A. et al. Hydrogen permeation rate reduction by post-oxidation of aluminide coatings on DIN 1.4914 martensitic steel (MANET). Journal of Nuclear Materials, vol. 233-237:p. 1102–1106, 1996.

[61] Pint B.A. et al. Investigation of Pb-Li compatibility issues for the dual coolant blanket concept. Journal of Nuclear Materials, vol. 367-370:p. 1150–1154, 2007.

[62] Proust E. et al. Preiminary interpretation of the LIBRETTO-2 experimental results in terms of tritium permeation barrier efficiency. Journal of Nuclear Materials, vol. 191:p. 186–189, 1992.

[63] Racault C. et al. Formation of permeation barriers on ceramic SiC/SiC composites. Journal of nuclear materials, vol. 233-237:p. 1262–1265, 1996.

[64] Salavy J.-F. et al. The HCLL test blanket module system: Present reference design system integration in ITER and RD needs. Fusion Engineering and Design, vol. 83:p. 1157–1162, 2008.

[65] Sample T. et al. The hydrogen permeation behaviour of aluminised coated martensitic steels under gaseous hydrogen, liquid Pb-17Li/hydrogen and cyclic thermal loads. Journal of Nuclear Materials, vol. 283-287:p. 1272–1276, 2000.

[66] Serra E. et al. Alumina sputtered on MANET as an effective deuterium permeation barrier. Journal of Nuclear Materials, vol. 257:p. 194–198, 1998.

[67] Serra E. et al. Hot-dip aluminium deposit as a permeation barrier for MANET steel. Fusion Engineering and Design, vol. 41:p. 149–155, 1998.

[68] Shan C. et al. The behaviour of diffusion and permeation of tritium through 316L stainless steel with coating of TiC and TiN+TiC. Journal of Nuclear Materials, vol. 191-194:p. 221–225, 1992.

[69] Shirasu Y. et al. Hydrogen solubility in boron-carbide. Journal of Alloys and Compounds, vol. 190:p. 87–90, 1992.

[70] Tamura M. et al. Characteristic change of hydrogen permeation in stainless steel plate by BN coating. Surface and Coatings Technology, vol. 260:p. 148–154, 2014.

[71] Tazhibaeva I.L. et al. Hydrogen permeation through steels and alloys with different protective coatings. Fusion Engineering and Design, vol. 51-52:p. 199–205, 2000.

[72] Wang J. et al. Performances of AlN coatings as hydrogen isotopes permeation barriers. Fusion Engineering and Design, vol. 102:p. 94–98, 2016.

[73] Welzel U. et al. Stress analysis of polycrystalline thin films and surface regions by x-ray diffraction. Journal of Applied Crystallograhy, vol. 38:p. 1–29, 2005.

[74] Winter J. et al. Boronization in Textor. Journal of Nuclear Materials, vol. 162-164:p. 713–723, 1989.

[75] Xiang X. et al. Preparation technique and alloying effect of aluminide coatings as tritium permeation barriers: A review. International Journal of Hydrogen Energy, vol. 40:p. 3697–3707, 2015.

[76] Yao Z. et al. The permeation of tritium through 316L stainless steel with multiple coatings. Journal of Nuclear Materials, vol. 283-287:p. 1287–1291, 2000.

[77] Yao Z. et al. Hydrogen permeation through MANET II steel with hot dipping aluminized coating. Chinese Journal of Nuclear Science and Engineering, vol. 22:p. 36–42, 2003.

[78] Yao Z. et al. SiC coating by RF sputtering as tritium permeation barrier for fusion blanket. Fusion Science and Technology, vol. 52:p. 865–869, 2007.

[79] Yoshida H.; et al. ITER RD auxiliary systems: Tritium systems. Fusion Engineering and Design, vol. 55:p. 313–323, 2001.

[80] Gastaldi O.; Ghirelli N.; Gabriel F.; Giancarli L.; Salavy J. F. Tritium transfers and main operating parameters impact for DEMO lithium lead breeding blanket. Fusion Engineering and Design, vol. 83:p. 1340–1347, 2008.

[81] Reiter F. Solubility and diffusivity of hydrogen isotopes in liquid Pb17Li. Fusion Engineering and Design, vol. 14:p. 207–211, 1991.

[82] Aiello A.; Ciampichetti A.; Benamati G. An overview on tritium permeation barrier development for WCLL blanket concept. Journal of Nuclear Materials, 2004.

[83] Aiello A.; Ciampichetti A.; Benamati G. Determination of hydrogen solubility in lead lithium using SOLE device. Fusion Engineering and Design, vol. 81:p. 639–644, 2006.

[84] Schnarr K.; Munzel H. Release of tritium from boron-carbide. Journal of the Chemical Society-Faraday Transactions, vol. 86:p. 651–656, 1990.

[85] Schnarr K.; Munzel H. Release of tritium from boron-carbide irradiated with reactor neutrons. Journal of Nuclear Materials, vol. 170:p. 253–260, 1990.

[86] IAEA. ITER EDA agreement and protocol 1. ITER EDA Documentation Series No. 1, Vienna 1992.

[87] IAEA. ITER technical basis. ITER EDA Documentation Series No. 24, Vienna 2002.

[88] ASTM International. Standard test method for adhesion strength and mechanical failure modes of ceramic coatings by quantitative single point scratch testing, astm c1624-05(2015). 2015.

[89] Veverka J. Materials for permeation barriers. Czech Technical University in Prague, 2016.

[90] Almeida E.A.S; Costa C.E.; Milan J.C.G. Study of the nitrided layer obtained by different nitriding methods. Revista Matéria, vol. 20 n. 2:p. 460–465, 2015.

[91] Dmitri Kopeliovich. Electroplating. [online], http://www.substech.com/dokuwiki/doku.php?id=electroplating, 14.3.2017.

[92] Perujo A.; Forcey K.S. Tritium permeation barriers for fusion technology. Fusion Engineering and Design, vol. 28:p. 252–257, 1995.

[93] He D.; Li S.; Liu X.; Zhang Ch.; Yu O.; Wang S.; Jiang L. Preparation of Cr2O3 film by MOCVD as hydrogen permeation barrier. Fusion Engineering and Design, vol. 89:p. 35–39, 2014.

[94] Al-Borno A. Liskiewicz T. DLC coating in oil and gas production - slideshow. [online], http://www.slideshare.net/TomaszLiskiewicz/dlc-coatings-in-oil-and-gas-production, 2.2.2017.

[95] Jones A.H. Luo Q. High-precision deretmination of residual stress of polycrystalline coatings using optimised XRD-$\sin^2\psi$ technique. Surface & Coatings Technology, vol. 205:p. 1403–1408, 2010.

[96] Giancarli L.M.; Abdou M.; Campbell D.J.; Chuyanov V.A.; Ahn M.Y.; Enoeda M.; Pan C.; Poitevin Y.; Rajendra Kumar E.; Ricapito I.; Strebkov Y.; Suzuki S.; Wong P.C.; Zmitko M. Overview of the ITER TBM program. Fusion Engineering and Design, vol. 87:p. 395–402, 2012.

[97] Osakada S.; Shiomi M. Flexible manufacturing of metallic products by selective laser melting of powder. International Journal of Machine Tools and Manufacture, vol. 46:p. 1188–1193, 2006.

[98] Wikimedia Commons Shared media repository. Principle of eds. [online], https://upload.wikimedia.org/wikipedia/commons/9/9f/EDX-scheme.svg, 28.4.2017.

[99] Baskes M.I. DIFFUSE 83, SAND-83-8231. Sandia National Laboratories, Livermore, 1983.

[100] Australian microscopy and microanalysis research facility. Myscope - training for advanced research. [online], http://www.ammrf.org.au/myscope/analysis/eds/, 28.4.2017.

[101] Matejicek J.; Chraska P. Development of advanced coatings for ITER and future fusion devices. Advances in Science and Technology, vol. 66:p. 47–65, 2010.

[102] Causey R. A.; Wampler W. R. The use of silicon carbide as a tritium permeation barrier. Journal of Nuclear Materials, vol. 220-222:p. 823–826, 1995.

[103] Cheng X.; Ma X.; Jiang K.; Chen L.; Huang K.; Liu S. Thermal hydraulic design and analysis of a water-cooled ceramic breeder blanket with superheated steam for CFETR. Plasma Science and Technology, vol. 17:p. 787–791, 2015.

[104] Eddington A. S. The internal constitution of stars. The Observatory, vol. 43:p. 341–358, 1920.

[105] Santucci A.; Ciampichetti A.; Demange D.; Franza F.; Tosti S. Tritium migration in HCLL and WCLL blankets: Impact of tritium solubility in liquid Pb-17Li. IEEE Transactions on plasma science, vol. 42:p. 1053–1056, 2014.

[106] Patel T. Chemical vapour deposition and physical vapour deposition techniques - slideshow. [online], http://www.slideshare.net/Tapan7777/chemical-vaour-deposition-physical-vapour-deposition-techniques, 2.2.2017.

[107] Tanabe T. Tritium handling issues in fusion reactor materials. Journal of Nuclear Materials, vol. 417:p. 545–550, 2011.

[108] Terai T. Research and development on ceramic coatings for fusion reactor liquid blankets. Journal of Nuclear Materials, vol. 248:p. 153–158, 1997.

[109] Wong C.P.C; Salawy J.-F.; Kim Y.; Kirillov I.; Rajendra Kumar E.; Morley N.B.; Tanaka S.; Wu Y.C. Overview of liquid metal TBM concepts and programs. Fusion Engineering and Design, vol. 83:p. 850–857, 2008.